ELSEVIER

Coordination Chemistry Reviews
197 (2000) 335–395

COORDINATION CHEMISTRY REVIEWS

www.elsevier.com/locate/ccr

The impact of multi-NMR spectroscopy on the development of noble-gas chemistry☆

Michael Gerken, Gary J. Schrobilgen *

Department of Chemistry, McMaster University, Hamilton, Ont., Canada L8S 4M1

Received 14 April 1999; accepted 25 May 1999

Contents

☆ Dedicated to Professor Ronald J. Gillespie, on the occasion of his 75th birthday and in appreciation of the exemplary high standards in basic research and scholarship he has provided us with over the years.

* Corresponding author. Tel.: +1-905-525-9140 ext. 23306; fax: +1-905-525-2509.
E-mail address: schrobil@mcmail.cis.mcmaster.ca (G.J. Schrobilgen)

PII: S0010-8545(99)00188-5

Abstract

The role of nuclear magnetic resonance spectroscopy in the structural studies of xenon and krypton species has been essential to the development of noble-gas chemistry since the early ^{19}F-NMR studies carried out in Ronald J. Gillespie's laboratory at McMaster University in the late 1960's and early 1970's. These early investigations of noble-gas species in strong acid media and subsequent multi-nuclear magnetic resonance (multi-NMR) studies utilizing ^{1}H, ^{13}C, ^{14}N, ^{15}N, ^{17}O, ^{77}Se, ^{125}Te, ^{129}Xe, and ^{131}Xe as the observed nuclides have made possible numerous important advances of noble-gas chemistry, contributing to our knowledge and understanding of the fluoride ion donor–acceptor behavior of noble-gas fluorides and oxide fluorides, Lewis acid properties of noble-gas species and the structures of compounds containing novel Xe–C, Xe–N, Xe–O, Kr–N, and Kr–O bonds. Trends among NMR parameters have also proven useful in assessing the formal oxidation state of xenon and the relative covalent characters of noble gas–ligand bonds.

Keywords: Noble-gas chemistry; Xenon; Krypton; Fluorine; Multi-NMR; VSEPR

1. Introduction

The intense interest in the preparative and structural main-group chemistry and in superacidic solvent media in Professor Ronald J. Gillespie's laboratory during the late 1960s and early to mid-1970s, provided the research background that led to the syntheses and characterization of a significant number of novel noble-gas species in his laboratory at that time. A significant driving force behind the syntheses of new noble-gas species at McMaster University lay in the desire to confirm their geometries based on the valence shell electron repulsion (VSEPR)

rules. This interest was expressed shortly after the discovery of noble-gas reactivity by Neil Bartlett [1], when Ron Gillespie [2] applied the VSEPR rules to the prediction of the molecular geometries of then known and unknown xenon fluorides and oxide fluorides. Conditional on acceptance of an offer to join the McMaster Chemistry Department in 1958 from University College, London, where he was a Lecturer, Ron Gillespie had stipulated that a commercial NMR spectrometer capable of running ^{19}F and ^{1}H spectra be purchased for his use at McMaster. The instrument, a Varian HR-60, operating at 56.4 MHz for ^{19}F, and equipped with a 'hot-wire' plotter, was one of the first commercial NMR spectrometers in Canada and was installed during the summer of 1959. While being installed in the basement of the McMaster Engineering Building, the 2-ton electromagnet was dropped outside the building, creating a sizable indentation in the concrete pavement. Despite its early trauma, the instrument performed to specifications until 1967 when it was upgraded to a Varian DP-60 with flux stabilization, and was used by G.J. Schrobilgen, a graduate student in Ron Gillespie's group, for early ^{19}F-NMR studies of noble-gas species from 1971–1973. The instrument was finally decommissioned in 1978. Almost simultaneous with the arrival of the Chemistry Department's first NMR spectrometer, Ron Gillespie offered the first NMR course at McMaster in the fall of 1959 and continued to do so in subsequent years. His early dedication to the use of ^{19}F-NMR spectroscopy for the characterization of fluoro-species in superacids provided a ready-made means for the structural characterization of noble-gas species and, in particular, noble-gas fluoride and oxide fluoride cations in strong acid media.

Following on these early studies, and with the availability of commercial multi-NMR spectrometers, multi-NMR spectroscopy became an extremely powerful tool in the structural characterization of xenon and krypton species in solution and remains so today. The material treated in this review is concerned with the application and impact of NMR spectroscopy on the development of noble-gas chemistry and mainly chronicles the early research performed in Professor R.J. Gillespie's laboratory and the continuing work in the field at McMaster University by his former Ph.D. student, Professor G.J. Schrobilgen. All multi-NMR spectroscopic data cited in this review are summarized in a comprehensive table at the end of this review (Table 2).

Besides the indisputable importance of the ^{129}Xe nucleus for NMR spectroscopic characterization of xenon species, the role of other nuclei, e.g. ^{19}F, ^{17}O, ^{15}N, ^{14}N, ^{13}C, and ^{1}H, in the elucidation of the solution structures of noble-gas species needs to be emphasized. Among these nuclei, ^{19}F is by far the most important since the majority of noble-gas species are derived from fluorides or oxide fluorides. Before the widespread availability of commercial FT multi-NMR spectrometers, ^{19}F, because of its high receptivity[1], was the only nucleus available for the routine

[1] ^{19}F chemical shifts prior to 1976 were reported using the old sign convention and must be multiplied by -1 to conform to the current IUPAC convention (Pure Appl. Chem. 29 (1972) 627; 45 (1976) 217). Some confusion in chemical shift referencing also arises from the use of ^{129}Xe references other than the commonly accepted reference, $XeOF_4(l)$ ($\Xi = 27.810184$ MHz) at 24°C.

characterization of xenon fluorides and oxide fluorides on CW instruments. The NMR spectroscopic study of krypton species is limited to the observation of NMR-active nuclei of atoms directly or indirectly attached to the krypton center, since ^{83}Kr, the only spin-active Kr nuclide, is quadrupolar and exhibits fast relaxation in asymmetric environments found in all currently known chemically bound krypton species. Hence, ^{19}F-NMR spectroscopy is usually the only practical means to characterize krypton species in solution.

The following comprehensive reviews of ^{129}Xe-NMR spectroscopy should also be consulted: 'NMR and the Periodic Table' in the chapter by Schrobilgen [3], 'Multinuclear NMR' in the chapter by Jameson [4], 'The Encyclopedia of Nuclear Magnetic Resonance' in the chapter by Schrobilgen [5] and 'Annual Reports on NMR Spectroscopy' in the chapter by Ratcliffe [6], and cover the field up to and not inclusive of the years 1979, 1987, 1996, and 1998, respectively. ^{19}F-NMR spectroscopy of noble-gas species is covered in '^{19}F-NMR-Spektroskopie', volume 4 of the series 'NMR-Spektroskopie von Nichtmetallen' by Berger, Braun, and Kalinowski [7], up to 1993 inclusively. The chemistry of compounds containing Xe^{II}–N bonds, including aspects of their characterization by multi-NMR spectroscopy, has been reviewed in 'Synthetic Fluorine Chemistry' in the chapter by Schrobilgen [8].

2. Early NMR studies of noble-gas species

In the late 1960's, noble-gas chemistry, especially the solution chemistry of Xe^{II} species in acid media, became a new focus of research in Ron Gillespie's laboratory at McMaster University. The method of choice for the characterization of solutions containing neutral xenon(II) species and xenon(II) cations generated and stabilized in strong acid solutions was ^{19}F-NMR spectroscopy, which had not, up until that time, been extensively exploited for the study of noble-gas species in solution. The only prior NMR spectroscopic studies included the observation of the ^{19}F resonances of solid XeF_2, XeF_4, XeF_6, and $XeOF_4$ and of molten XeF_6 and liquid $XeOF_4$ [9]. ^{19}F-NMR spectra of XeF_2, XeF_4, XeF_6, and $XeOF_4$ in HF solvent were obtained and, with the exception of XeF_6 (see Section 3.5), displayed ^{129}Xe satellites ($I=\frac{1}{2}$, 26.44% natural abundance), providing the first measurements of $^{129}Xe-^{19}F$ spin–spin coupling constants [9,10]. Early spin-tickling experiments provided the ^{129}Xe chemical shifts of XeF_2, XeF_4, and $XeOF_4$ [10,11].

In 1966, Peacock and Cohen [12] characterized solutions of XeF_2 and XeF_4 in SbF_5. The observation of a single resonance with ^{129}Xe satellites for XeF_2 in SbF_5 solvent appeared to support the previously proposed structure for the solid adduct, $XeF_2{\cdot}2SbF_5$, a covalent structure containing two Sb–F···Xe fluorine bridges, $F_5SbF{\cdots}Xe{\cdots}FSbF_5$ [13]. However, in 1969, Peacock [14] and co-workers reported the X-ray crystal structure of $XeF_2{\cdot}2SbF_5$ and showed that the adduct contained the dinuclear $Sb_2F_{11}^-$ anion with a single short contact between the XeF^+ cation and anion by means of an Sb–F···Xe bridge. The ^{19}F-NMR spectrum of XeF_4 in SbF_5 solvent was reported to include two triplets and sets of smaller poorly

resolved peaks which were interpreted as ^{129}Xe satellites. The spectrum was incorrectly assigned, by analogy with the SbF_5 solution spectrum of $XeF_2 \cdot 2SbF_5$, to the two terminal and two bridging fluorine atoms bonded to xenon in $F_5SbF\cdots XeF_2\cdots FSbF_5$ [13] (the structural assignment was subsequently shown to be incorrect; see Section 3.2). From the scarce experimental data then available, Frame [15] found a smooth curve correlating the ^{19}F chemical shifts and the one-bond $^{129}Xe-^{19}F$ coupling constants of $XeF^+SbF_6^-$ (XeF_2 in SbF_5),[2] XeF_2, XeF_4, $XeOF_4$, XeO_2F_2, and XeF_6. Extensive further work, much of it at McMaster [16,17], has shown that this empirical correlation holds for all known compounds studied (see Section 5.1.2).

3. Structural studies of noble-gas species by solution multi-NMR spectroscopy

3.1. Xenon(II) species

The earliest solution ^{19}F-NMR studies of noble-gas compounds at McMaster University dealt with the solvolytic behaviors of XeF_2, $FXeSO_3F$, and $Xe(SO_3F)_2$ in anhydrous HF and HSO_3F solvents [16] (Eqs. (1)–(4)). The X-ray crystal structure

$$XeF_2 + HSO_3F \xrightarrow{HSO_3F} FXeSO_3F + HF \quad (1)$$

$$FXeSO_3F + HSO_3F \xrightarrow{HSO_3F} Xe(SO_3F)_2 + HF \quad (2)$$

$$Xe(SO_3F)_2 + HF \xrightarrow{HF} FXeSO_3F + HSO_3F \quad (3)$$

$$FXeSO_3F + HF \overset{HF}{\rightleftharpoons} XeF_2 + HSO_3F \quad (4)$$

of $FXeSO_3F$ had been previously determined and was found to be a covalent molecule with a linear F–Xe–O bonding arrangement, consistent with an AX_2E_3 VSEPR arrangement [18] of a double bond pair and three lone pair domains about xenon as in XeF_2 [19,20].

Solutions of $XeF^+AsF_6^-$, $XeF^+SbF_6^-$, and $XeF^+Sb_2F_{11}^-$ in HSO_3F exhibited singlets with ^{129}Xe satellites in their ^{19}F-NMR spectra [16]. A near-linear variation in ^{19}F chemical shift and $^{129}Xe-^{19}F$ coupling constant was observed for solutions of XeF_2 in SbF_5 and HSO_3F solvents, ranging from -245.5 ppm and 6710 Hz in pure HSO_3F to -290.2 ppm and 7230 Hz in pure SbF_5. The $^{129}Xe-^{19}F$ coupling of XeF^+ in SbF_5 solvent is the largest known spin–spin coupling to xenon. The fluorosulfuric acid solvent is presumably coordinated to XeF^+ and is replaced by the more weakly basic $Sb_2F_{11}^-$, $SbF_5(SO_3F)^-$, and $[Sb_2F_{10}(\mu\text{-}SO_2F)]^-$ anions as the SbF_5 concentration increases, which are, in turn, replaced by still more weakly basic oligomeric fluorine bridged $Sb_nF_{5n+1}^-$ anions at higher SbF_5 concentrations and exclusively by long chain oligomeric $Sb_nF_{5n+1}^-$ anions in pure SbF_5 (Eq. (5)) (see Section 4.1.5):

[2] The wrong $\delta(^{19}F)$ value for XeF_2 in SbF_5 (ca. 578 ppm with the present chemical shift convention) was taken by Frame in his $\delta(^{19}F)/^1J(^{129}Xe-^{19}F)$ correlation and resulted in a curved relationship.

$$XeF_2 + nSbF_5 \xrightarrow{SbF_5} XeF^+Sb_nF_{5n+1}^- \quad (5)$$

A 2:1 adduct between XeF_2 and AsF_5 has been prepared, isolated, and characterized in the solid state by X-ray crystallography and shown to consist of AsF_6^- anions and V-shaped $Xe_2F_3^+$ cations having two terminal fluorines and one bridging fluorine [21,22]. The first evidence for the $Xe_2F_3^+$ cation in solution was obtained by ^{19}F-NMR spectroscopy of $Xe_2F_3^+AsF_6^-$ in BrF_5 at -62°C and consisted of an AX_2 spin system with ^{129}Xe satellites symmetrically disposed about the doublet and triplet (-184.7 (A) and -252.0 ppm (X), $^2J(^{19}F_A-^{19}F_X) = 308$ Hz, $^1J(^{129}Xe-^{19}F_A) = 4865$ Hz, and $^1J(^{129}Xe-^{19}F_X) = 6740$ Hz) [16]. The solvolysis of the $Xe_2F_3^+$ cation in HSO_3F solvent was studied by ^{19}F-NMR spectroscopy and shown to give rise to the $(FXe)_2SO_3F^+$ cation (Eq. (6)) [23], which had been

$$Xe_2F_3^+ + HSO_3F \rightarrow (FXe)_2SO_3F^+ + HF \quad (6)$$

independently prepared by Bartlett et al. [24], and characterized by Raman spectroscopy. The ^{19}F-NMR spectrum of $(FXe)_2SO_3F^+AsF_6^-$ in HSO_3F consists of a singlet at 44.6 ppm in the F-on-S region and a singlet with ^{129}Xe satellites at -220.7 ppm with $^1J(^{129}Xe-^{19}F_t) = 6330$ Hz (HSO_3F, -91°C), which is intermediate between the coupling found in $FXeSO_3F$ (6021 Hz) and XeF^+ (6615 Hz) in HSO_3F solution. A subsequent X-ray crystal structure confirmed that the fluorosulfate group is in the bridging position [25].

3.2. The XeF_3^+ and XeF_5^+ cations

Peacock and Cohen's [12] inconclusive report of the ^{19}F-NMR spectrum of XeF_4 in SbF_5 solvent (see Section 2) inspired the reinvestigation of XeF_4 in SbF_5 solvent as well as in HSO_3F solvent. The use of impure XeF_4 contaminated with XeF_6 initially led to the ^{19}F-NMR spectroscopic study of the XeF_5^+ cation. In HSO_3F solution, these mixtures gave rise to an AX_4 spin coupling pattern with accompanying ^{129}Xe satellites which was assigned to the XeF_5^+ cation (Fig. 1), confirming the expected square pyramidal VSEPR geometry [18] for XeF_5^+ in solution. The structure of XeF_5^+ has been determined in the solid state in the crystal structures of $XeF_5^+PtF_6^-$ [26,27], $XeF_5^+RuF_6^-$ [28], $XeF_5^+PdF_6^-$ [29], and $XeF_5^+AsF_6^-$ [22]. Subsequent work with pure XeF_6 provided the ^{19}F-NMR spectra of $XeF_5^+Sb_nF_{5n+1}^-$ in SbF_5, $XeF_5^+Sb_2F_{11}^-$ in BrF_5 and HSO_3F, and $XeF_5^+SbF_6^-$, XeF_5^+ AsF_6^-, and $XeF_5^+BF_4^-$ in HF solvents [30]. The ^{129}Xe–^{19}F coupling constants of the XeF_5^+ cation displayed large solvent and temperature dependencies, resulting from varying degrees of cation solvation, paralleling similar behavior for the XeF^+ cation (see Section 3.1). A double resonance experiment established that the ^{129}Xe–^{19}F axial and ^{19}F–^{19}F coupling constants have the same sign and they are assumed to be positive (see Section 5.1.2). The reaction of XeF_6 with excess HSO_3F was shown to yield ionic F_5XeSO_3F (Eq. (7)), which was also

$$XeF_6 + HSO_3F \rightarrow F_5XeSO_3F + HF \quad (7)$$

independently prepared and isolated by DesMarteau and Eisenberg [31].

The ^{19}F-NMR spectra of a solution of pure XeF_4 in SbF_5 solvent at 26°C showed an AB_2 spin pattern with ^{129}Xe satellites at 23.0 and 38.7 ppm with a $^2J(^{19}F-^{19}F)$ coupling of 174 Hz (Fig. 2), which is consistent with the T-shaped (C_{2v}) geometry of the XeF_3^+ cation predicted for an AX_3E_2 VSEPR arrangement (Eq. (8)) [18,32,33]. The subsequent crystal structure determinations of $XeF_3^+SbF_6^-$ [34]

$$XeF_4 + nSbF_5 \xrightarrow{SbF_5} XeF_3^+Sb_nF_{5n+1}^- \quad (8)$$

and $XeF_3^+Sb_2F_{11}^-$ [35,36] confirmed the T-shaped geometry of the XeF_3^+ cation, which is valence isoelectronic with the halogen trifluorides, ClF_3, BrF_3, and IF_3.

3.3. The $XeOF_3^+$ and XeO_2F^+ cations

The xenon(VI) oxide fluorides, $XeOF_4$ and XeO_2F_2, were shown to act as fluoride ion donors towards SbF_5 solvent giving rise to the $XeOF_3^+$ and XeO_2F^+ cations, respectively (Eqs. (9) and (10)) [33,37]. The fluorine spectrum of the $XeOF_3^+$ cation

$$XeOF_4 + nSbF_5 \xrightarrow{SbF_5} XeOF_3^+Sb_nF_{5n+1}^- \quad (9)$$

$$XeO_2F_2 + nSbF_5 \xrightarrow{SbF_5} XeO_2F^+Sb_nF_{5n+1}^- \quad (10)$$

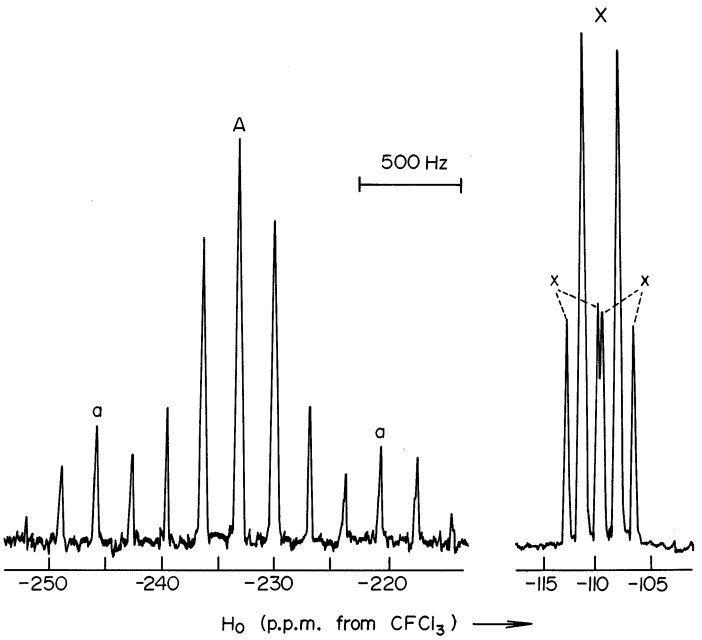

Fig. 1. ^{19}F-NMR spectrum (56.4 MHz, 26°C) of the XeF_5^+ cation (4.87 M $XeF_5^+SbF_6^-$ in HF solution): (A) axial fluorine and (a) ^{129}Xe satellites; (X) equatorial fluorines and (x) ^{129}Xe satellites [30]. The chemical shift scale must be multiplied by -1 to conform with the present IUPAC convention.

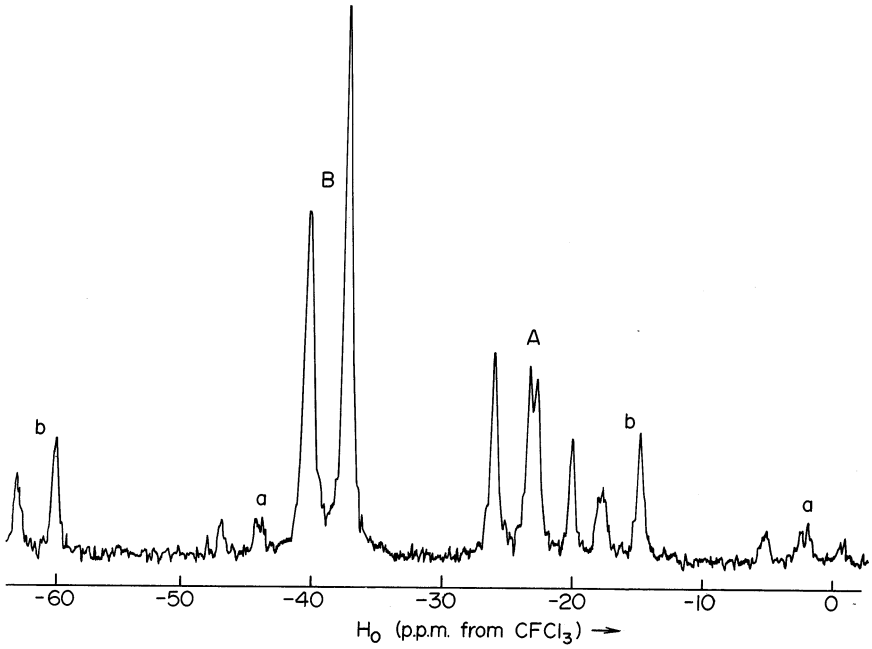

Fig. 2. ^{19}F-NMR spectrum (56.4 MHz, 26°C) of the XeF_3^+ cation (0.20 M XeF_4 and 0.50 M XeF_2 in SbF_5 solution): (A) axial fluorines and (a) ^{129}Xe satellites; (B) equatorial fluorine and (b) ^{129}Xe satellites [33]. The chemical shift scale must be multiplied by -1 to conform with the present IUPAC convention.

in SbF_5 solvent at 5°C consists of an AX_2 spin system with ^{129}Xe satellites at 195.1 (A) and 147.1 ppm (X) (Fig. 3), which is in accordance with the expected VSEPR geometry [18] based on a trigonal bipyramid with the lone pair, the oxygen, and one fluorine in the equatorial position and two fluorines in axial positions. The ^{129}Xe chemical shift of the $XeOF_3^+$ cation in SbF_5 (25°C) at 238 ppm was subsequently reported and more recently the study was completed with the NMR spectroscopic study of ^{17,18}O enriched $XeOF_3^+SbF_6^-$ in HF at 30°C, yielding a ^{17}O chemical shift of 333.7 ppm, $^1J(^{129}Xe-^{17}O)$ coupling constant of 619 Hz, and a secondary isotopic shift in the ^{129}Xe spectrum of -0.69 ppm for $^1\Delta^{129}Xe(^{18,16}O)$ (Fig. 4) [38]. The crystal structure was also obtained in the latter study, verifying the geometry predicted by the VSEPR rules and that deduced from earlier ^{19}F and ^{129}Xe-NMR spectroscopic studies. The ^{19}F-NMR spectrum of the XeO_2F^+ cation in SbF_5 solvent consisted of a singlet with ^{129}Xe satellites at 199.7 ppm and $^1J(^{129}Xe-^{19}F)$ of 80 Hz [33,37]. The $^1J(^{129}Xe-^{19}F)$ coupling of XeO_2F^+ represents the smallest one-bond xenon–fluorine coupling measured to date. The free XeO_2F^+ cation is expected to have a trigonal pyramidal geometry based on an AX_3E arrangement [18] of three bond pair domains and an electron lone pair domain.

An earlier empirical correlation between the $^{129}Xe-^{19}F$ coupling constant and the ^{19}F chemical shift of xenon fluorides and oxide fluorides could now be extended to the xenon(IV) and xenon(VI) fluoro- and oxofluoro-cations XeF_3^+, XeF_5^+,

$XeOF_3^+$, and XeO_2F^+ [30]. The relationship accounts for the small size of $^{129}Xe-^{19}F$ in the XeO_2F^+ cation and suggests that the $^1J(^{129}Xe-^{19}F_{ax})$ and $^1J(^{129}Xe-^{19}F_{eq})$ coupling constants in XeF_5^+ and $XeOF_3^+$, respectivley, are of opposite signs to all previously observed Xe–F coupling constants and are probably positive (see Section 5.1).

3.4. The krypton(II) fluoro-cations, KrF^+ and $Kr_2F_3^+$ and the BrF_6^+ cation

Following on the characterization of the xenon fluoride and oxide fluoride cations, the focus in Professor Gillespie's laboratory shifted to the investigation of the cation chemistry of KrF_2 in anhydrous HF and BrF_5 solvent media. Krypton difluoride is an aggressive fluorinating agent and is a better low-temperature source of fluorine atoms than F_2 with a mean thermochemical bond energy for KrF_2 of only 50 kJ mol^{-1} [39], which is substantially less than the bond dissociation energy of F_2 at 157.7 $\pm$0.4 kJ mol^{-1} [40]. Prior to these studies, KrF_2 had been characterized by ^{19}F-NMR spectroscopy in anhydrous HF solution [41]. The ^{19}F-NMR spectrum of $KrF^+SbF_6^-$ in HF at -40°C comprised a singlet at -22.6 ppm, shifted to a lower frequency with respect to its parent compound KrF_2 (55.6 ppm; HF solvent, 26°C) [43], as observed for the analogous xenon species [16]. Bromine pentafluoride solutions of $Kr_2F_3^+AsF_6^-$ and $Kr_2F_3^+SbF_6^-$ gave AX_2

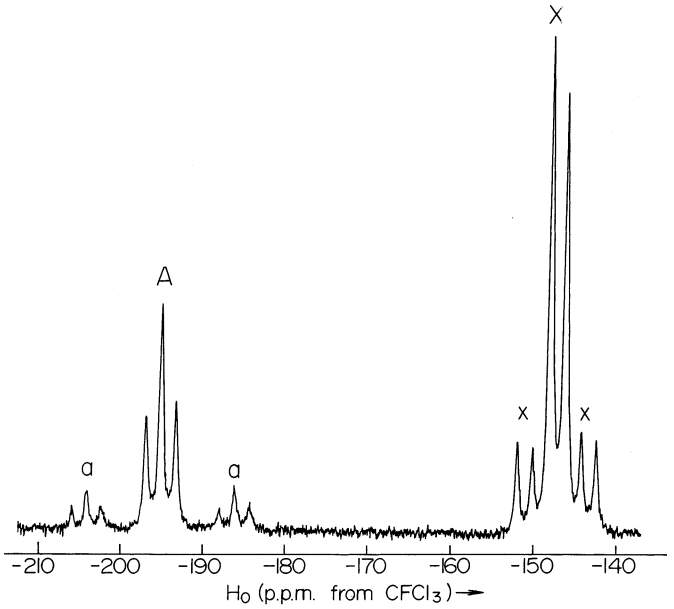

Fig. 3. ^{19}F-NMR spectrum (56.4 MHz, 5°C) of the $XeOF_3^+$ cation (0.70 M $XeOF_3^+Sb_2F_{11}^-$ and 1.10 M XeF_2 in SbF_5 solution): (A) equatorial fluorine and (a) ^{129}Xe satellites; (X) axial fluorines and (x) ^{129}Xe satellites [33]. The chemical shift scale must be multiplied by -1 to conform with the present IUPAC convention.

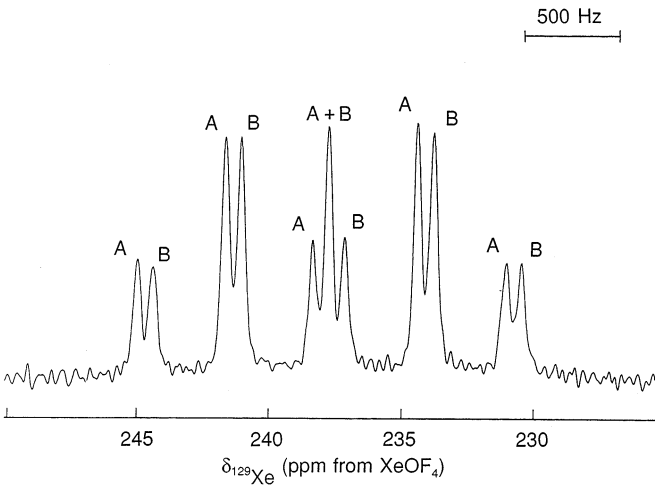

Fig. 4. ^{129}Xe-NMR spectrum (139.051 MHz, 30°C) of ^{17}O- (26.5%) and ^{18}O-enriched (37.0%) $XeOF_3^+$ SbF_6^- (0.33 M) and XeF_2 (1.7 M) dissolved in SbF_5 solvent; resolution enhanced spectrum obtained by Fourier transformation of the free induction decay using a Gaussian fit: (A) $Xe^{16}OF_3^+$, (B) $Xe^{18}OF_3^+$ [38].

spectra at low temperatures (Fig. 5) which were unambiguously assigned to a V-shaped, fluorine-bridged structure similar to that previously established for $Xe_2F_3^+$ by X-ray crystallography [21,22]. However, in contrast with $Xe_2F_3^+$, the terminal resonance of $Kr_2F_3^+$ occurs at a higher frequency than the bridging fluorine.

Although ClF_6^+ [44–46] and IF_6^+ [47] were known at the time, the BrF_6^+ cation was absent from the hexafluorohalogenate series. The tendency for bromine to be unstable in its highest oxidation state, +7, is typical for the late fourth-row main-group elements. It was found necessary to use the powerful oxidizing agents, $Kr_2F_3^+$ and KrF^+, to oxidatively fluorinate BrF_5 to the octahedral $Br^{VII}F_6^+$ cation (Eq. (11)) [42,48], only the third and the last bromine(VII) species to be

$$KrF^+AsF_6^- + BrF_5 \rightarrow BrF_6^+AsF_6^- + Kr \quad (11)$$

prepared after BrO_4^- [49] and BrO_3F [50]. The KrF^+ and BrF_6^+ cations are the strongest and third strongest known oxidative fluorinators, respectively, in the absolute oxidizer strength scale [51], and both oxidize O_2 to O_2^+ and Xe to XeF^+ at ambient temperatures [43]. The ^{19}F-NMR spectrum of BrF_6^+ displays well-resolved spin–spin couplings between ^{19}F and the quadrupolar nuclei ^{79}Br ($I = 3/2$, 50.54%) and ^{81}Br ($I = 3/2$, 49.46%) (Fig. 6), which were observed for the first time, providing definitive proof for the octahedral geometry of the BrF_6^+ cation [48].

A previous report [52] on the preparation of $XeOF_5^+$ by the oxidative fluorination of $XeOF_4$ with $KrF^+Sb_2F_{11}^-$ was reinvestigated and shown by ^{19}F-NMR spectroscopy to yield $XeOF_4 \cdot XeF_5^+SbF_6^-$ instead [53].

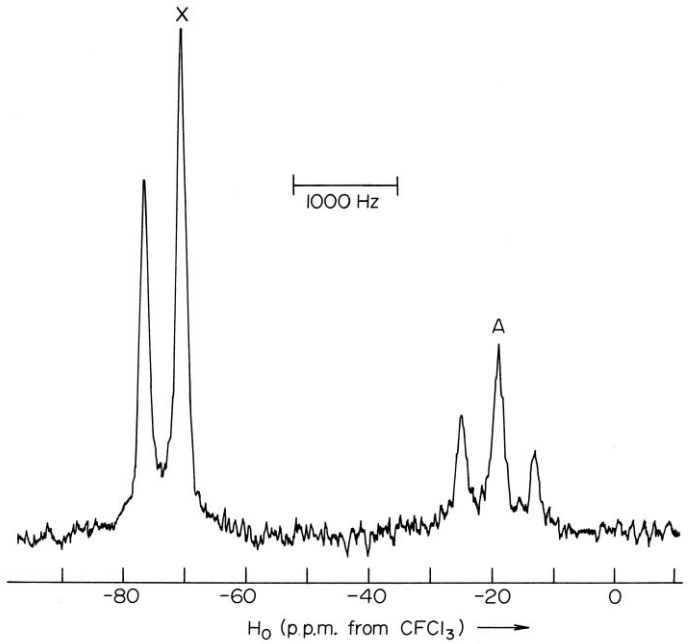

Fig. 5. ^{19}F-NMR spectrum (58.3 MHz, -66°C) of the $Kr_2F_3^+$ cation (~ 0.5 M $Kr_2F_3^+SbF_6^-$ in BrF_5 solvent): (A) bridging fluorine; (X) terminal fluorines [43]. The chemical shift scale must be multiplied by -1 to conform with the present IUPAC convention.

3.5. *^{129}Xe-NMR spectroscopy*

In 1978, 15 years after spin-tickling experiments had afforded the first measurements of ^{129}Xe chemical shifts [10,11], the availability of commercial FT-NMR spectrometers made the direct observation of ^{129}Xe ($I=\frac{1}{2}$, 26.44% natural abun-

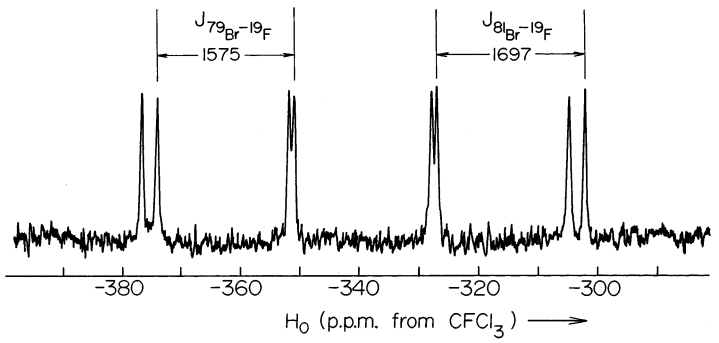

Fig. 6. ^{19}F-NMR spectrum (58.3 MHz, 26°C) of the BrF_6^+ cation in HF solvent [48]. The chemical shift scale must be multiplied by -1 to conform with the present IUPAC convention.

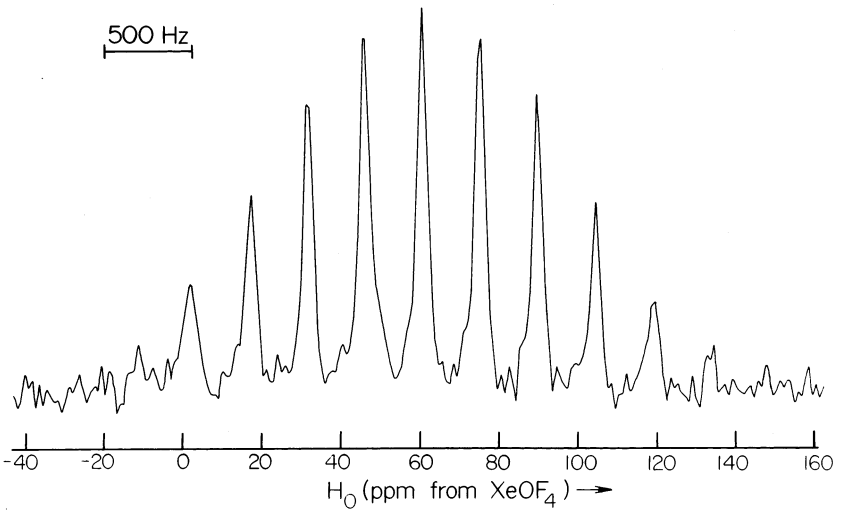

Fig. 7. ^{129}Xe-NMR spectrum (22.63 MHz, −145°C) of the XeF_6 tetramer (1.44 M XeF_6 in 50 mol% SO_2ClF/50 mol% CF_2Cl_2) [55].

dance) in a variety of xenon species routine [54,55], significantly extending the number of directly observed ^{129}Xe chemical shifts [56,57]. The direct observation of the ^{129}Xe nucleus also provided a ready means to establish the number of chemically equivalent fluorines coupled to xenon from their multiplicity patterns in the ^{129}Xe-NMR spectrum. This is exemplified by XeF_6, which represents a special case. The ^{129}Xe-NMR spectrum of XeF_6 shows a multiplet of at least 11 lines at −118 and −145°C in F_5SOSF_5 [58] and a mixture of 50 mol% SO_2ClF and 50 mol% CF_2Cl_2 (Fig. 7) [55], respectively, which collapse into a single broad line at −75°C, instead of the septet expected for a fluxional monomeric XeF_6 molecule with six equivalent fluorines and a stereochemically-active lone electron pair. In the ^{19}F-NMR spectrum of natural abundance XeF_6 and of XeF_6 enriched with ^{129}Xe to 60.1 [55] and 62.5% [58], seven and nine lines were observed, respectively, instead of the singlet with ^{129}Xe satellites expected for a fluxional mononuclear species. The multiplicities and relative intensities are consistent with the fluorine-bridged tetramer, $(XeF_6)_4$, in which the four xenon atoms and all 24 fluorine atoms are rendered chemically equivalent by their rapid intramolecular exchange on the NMR time scale, presumably by means of their fluorine bridges. The exchange could not be sufficiently slowed even at temperatures as low as −145°C in 50 mol% SO_2ClF and 50 mol% CF_2Cl_2 to observe the limiting spectrum. The ^{19}F-NMR spectrum of the fluxional tetramer is the result of the superposition of a statistically weighted singlet corresponding to Xe'_4F_{24} (singlet) and four binomial multiplets arising from the ^{129}Xe–^{19}F spin-coupled isotopomers $^{129}XeXe'_3F_{24}$ (doublet), $^{129}Xe_2Xe'_2F_{24}$ (triplet), $^{129}Xe_3Xe'F_{24}$ (quartet), and $^{129}Xe_4F_{24}$ (quintet), where Xe′ represents the spin-inactive isotopes of xenon and includes ^{131}Xe ($I = 3/2$, 21.18%), which does not result in splitting of the ^{19}F signal because of fast quadrupolar relaxation. Although

only 11 of the 25 lines in the binomial multiplet in the ^{129}Xe-NMR spectrum could be observed, the number n in the molecular formula, $(XeF_6)_n$, was graphically determined from plots of outer line intensity:central line intensity ratios of the ^{129}Xe-NMR multiplet for various values of n versus the number of fluorines in the formula unit (Fig. 8) [55]. The intensities were determined by measuring the peak heights and the areas, resulting in a mean value for the total number of equivalent spin–spin coupled fluorines, $6n$, of 23 ± 2 or $n = 4$.

3.6. The interaction of KrF_2 and XeF_2 with weak fluoride ion acceptors

Xenon difluoride reacts with strong Lewis acids such as AsF_5 and SbF_5, yielding $XeF^+AsF_6^-$ [59], $XeF^+SbF_6^-$ [60], and $XeF^+Sb_2F_{11}^-$ [14] which contain fluorine bridge contacts between the XeF^+ cation and the anion in the solid state. In solution, these anion–cation contacts are labile on the NMR time scale, resulting in

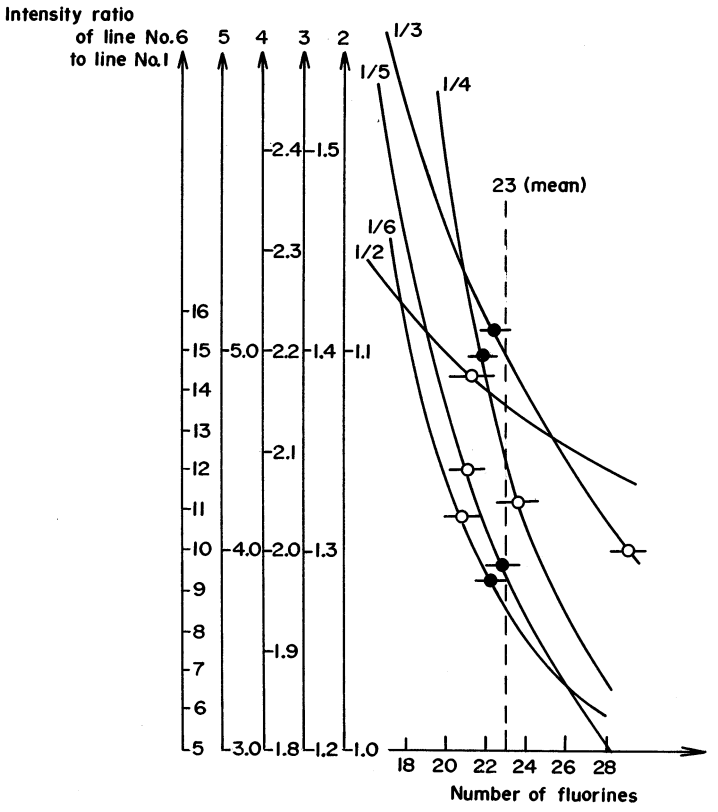

Fig. 8. Graphical determination of n in $(XeF_6)_n$. Plots of outer line intensities:central line intensity for the ^{129}Xe-NMR multiplet of $(XeF_6)_n$ vs. the total number of equivalent fluorines ($6n$) spin coupled to ^{129}Xe (●, relative area by weighing, ○, relative peak height). The mean value of $6n$ determined graphically is 23 ± 2 or $n = 4$ [55].

a singlet in the ^{19}F-NMR spectrum and a doublet in the ^{129}Xe-NMR spectrum of the cation [16]. Solid XeF_2 adducts with the weak fluoride ion acceptors WOF_4 and $MoOF_4$ were shown to possess the stoichiometries $XeF_2{\cdot}MOF_4$ and $XeF_2{\cdot}2MOF_4$ (M = Mo or W) [61,62]. All four adducts show two different environments for fluorine on xenon in the low-temperature ^{19}F-NMR spectra in BrF_5 (supercooled to -62 and to -84°C) and SO_2ClF (-124°C) solvents and comprise a doublet for the terminal fluorine atoms and a doublet for the bridging fluorine atom. The ^{129}Xe-NMR resonance of each adduct consists of a doublet of doublets, and likewise establishes that each structure contains a Xe–F···M bridge which is nonlabile on the NMR time scale at low temperatures. The X-ray crystal structure of $XeF_2{\cdot}WOF_4$ confirms the NMR spectroscopic findings [63]. Equilibria leading to the higher chain-length species $XeF_2{\cdot}nMOF_4$ ($n = 1$–4) were observed at low temperatures in SO_2ClF solution [61,62]. The relative degree of covalent character in the terminal Xe–F bonds of the adduct species, as well as the relative fluoride ion acceptor strengths of $MoOF_4$ and WOF_4 and their polymeric chains, were assessed on the basis of the observed ^{19}F and ^{129}Xe-NMR complexation shifts. The Lewis acid, WOF_4 and its polymeric chains, are stronger fluoride ion acceptors relative to XeF_2 than their $MoOF_4$ analogues. Isomerization between oxygen- and fluorine-bridged XeF groups, which had not been previously observed in noble-gas chemistry, was observed in the tungsten adducts $XeF_2{\cdot}nWOF_4$ ($n = 2$ and 3), but does not occur with either the $MoOF_4$ analogues or with $XeF_2{\cdot}WOF_4$. The isomerization equilibrium constant between the oxygen- and fluorine-bridged species was shown to increase with increasing n. Solvolysis of $XeF_2{\cdot}MOF_4$ (M = Mo, W) in HSO_3F solvent (Eq. (12)) led to a new class of fluorosulfate-bridged species,

$$FXeFMOF_4 + HSO_3F \rightarrow FXeO(F)S(=O)OMOF_4 + HF \quad (12)$$

$FXeO(F)S(=O)OMOF_4$, which were characterized by ^{19}F- and ^{129}Xe-NMR spectroscopy.

The first KrF_2–transition metal oxide fluoride adducts were prepared by reaction of KrF_2 with MOF_4 (M = Mo, W) in SO_2ClF solution at low temperatures [64]. The ^{19}F-NMR spectra of $KrF_2{\cdot}nMoOF_4$ ($n = 1$–3) and $KrF_2{\cdot}WOF_4$ in solution showed that they were best formulated as essentially covalent structures containing Kr–F···M bridges and mononuclear or polynuclear metal oxide fluoride moieties. As in $Kr_2F_3^+$, the bridging resonances of the (μ-F)-$KrF_2{\cdot}nMoOF_4$ species occur at lower frequencies than their terminal fluorine-on-krypton resonances, which is opposite to the trend displayed by $Xe_2F_3^+$, (μ-F)-$XeF_2{\cdot}nWOF_4$, and (μ-F)-$XeF_2{\cdot}nMoOF_4$. While the $KrF_2{\cdot}nMoOF_4$ ($n = 1$–3) adducts are stable up to room temperature (r.t.) in SO_2ClF solution, solutions of KrF_2 and WOF_4 in SO_2ClF spontaneously decompose above -100°C to Kr, O_2, and WF_6 with no evidence for a stable (μ-F)-$KrF_2{\cdot}nWOF_4$ adduct when $n > 1$. The marked difference in oxidizability of $MoOF_4$ and WOF_4 by KrF_2 is attributed to bond isomerization between fluorine- and oxygen-bridged KrF groups in $KrF_2{\cdot}nWOF_4$ for $n > 1$, analogous to the Xe–F → Xe–O bond isomerization observed for $XeF_2{\cdot}nWOF_4$, and to the intrinsic instabilities of Kr–O bonds, which was subsequently illustrated by attempts to prepare $Kr(OTeF_5)_2$ [65] (see Section 3.11).

3.7. Xenon species containing the $OTeF_5$ ligand

The $OTeF_5$ ligand is highly electronegative and is capable of stabilizing the +2, +4, and +6 oxidation states of xenon. The solution NMR characterization of xenon derivatives of the $OTeF_5$ group is facilitated by the observation of ^{129}Xe, ^{125}Te[3] ($I=\frac{1}{2}$, 6.99% natural abundance), and ^{19}F. The ^{19}F-NMR spectra of $OTeF_5$ groups give rise to second order AB_4 spin coupling patterns which make their interpretation somewhat less straightforward. Even the use of a modern NMR instrument with a proton frequency of 500 MHz (471 MHz for ^{19}F) does not result in first order conditions in the majority of the cases.

The $XeOTeF_5^+$ cation, the $OTeF_5$ analogue of XeF^+, had previously been prepared and isolated as its AsF_6^- salt according to Eq. (13) [66]. The absence of

$$FXeOTeF_5 + AsF_5 \rightarrow XeOTeF_5^+ AsF_6^- \quad (13)$$

evidence for the discrete nature of the $XeOTeF_5^+$ cation in solution sparked the solution NMR spectroscopic investigation of the $XeOTeF_5^+$ cation. Dissolution of $XeOTeF_5^+ AsF_6^-$ in SbF_5 led to stable yellow–orange solutions of the $XeOTeF_5^+$ cation and displacement of AsF_5 (Eq. (14)). The r.t. ^{19}F- and ^{125}Te-NMR spectra of

$$XeOTeF_5^+ AsF_6^- + nSbF_5 \xrightarrow{SbF_5} XeOTeF_5^+ Sb_nF_{5n+1}^- + AsF_5 \quad (14)$$

$XeOTeF_5^+$ in SbF_5 solvent were found to consist of an AB_4 spin pattern with ^{125}Te satellites and a doublet of quintets, respectively [67]. The coupling between xenon and the four equatorial fluorines on the tellurium was observed in the ^{129}Xe-NMR spectrum resulting in a quintet; because of its small magnitude, the coupling between xenon and the axial fluorine could not be resolved in either the ^{129}Xe or the ^{19}F-NMR spectrum. The solvolysis of $XeOTeF_5^+ AsF_6^-$ in BrF_5 for 1 min. at r.t. was shown to yield the fluorine-bridged cations $FXeFXeOTeF_5^+$ and $FXeF\cdots BrOF_2^+$ according to Eqs. (15)–(17). The $FXeF\cdots BrOF_2^+$ cation was isolated as its AsF_6^- salt and was also characterized in the solid state by low-temperature Raman spectroscopy. The ^{129}Xe-NMR spectrum of $FXeF\cdots BrOF_2^+ AsF_6^-$ in BrF_5 solvent shows a triplet, indicating rapid intramolecular exchange between the two fluorines of the XeF_2 molecule weakly coordinated to the $BrOF_2^+$ cation. The ^{129}Xe chemical shift of $FXeF\cdots BrOF_2^+$ at −1358 ppm (−59°C) is significantly

$$2XeOTeF_5^+ AsF_6^- + BrF_5 \rightarrow TeF_6 + FXeFXeOTeF_5^+ AsF_6^- + BrOF_2^+ AsF_6^- \quad (15)$$

$$FXeFXeOTeF_5^+ AsF_6^- + BrF_5 \rightarrow TeF_6 + Xe_2F_3^+ AsF_6^- + BrOF_3 \quad (16)$$

$$Xe_2F_3^+ AsF_6^- + BrOF_3 + BrOF_2^+ AsF_6^- \rightarrow 2FXeF\cdots BrOF_2^+ AsF_6^- \quad (17)$$

[3] Tellurium has two spin-active isotopes, ^{125}Te (6.99% natural abundance, $I=\frac{1}{2}$) and ^{123}Te (0.87% natural abundance, $I=\frac{1}{2}$). ^{123}Te is rarely used as an NMR nuclide because of its low natural abundance, however, ^{123}Te satellites are frequently observed in the ^{19}F-NMR spectra of $OTeF_5$ derivatives.

different from that of XeF_2 in BrF_5 (-1708 ppm, -40°C), but is very similar to those of the weakly fluorine-bridged adducts, $FXeFWOF_4$ and $FXeFMoOF_4$ (-1331, -66°C and -1383 ppm, -80°C, respectively) in BrF_5. Dissolution of $XeOTeF_5^+AsF_6^-$ in HSO_3F, a stronger protic acid than $HOTeF_5$, resulted in displacement of $HOTeF_5$ and ^{129}Xe- and ^{19}F-NMR spectroscopic evidence for the $XeOSO_2F^+$ cation.

It has been argued that the $OTeF_5$ group possesses a higher electronegativity than fluorine on the basis of the square-based pyramidal structure of $FI(OTeF_5)_4$ in which the fluorine occupies the axial position [68]. The argument stems from the VSEPR rule [18] that the less electronegative ligand occupies the axial position, a generalization that was shown to be true for the trigonal bipyramid. In order to more reliably assess the relative group electronegativities of F and $OTeF_5$, series of $OTeF_5$ compounds were studied by multi-NMR spectroscopy [69]. Differences between ^{129}Xe chemical shifts for the F and $OTeF_5$ analogues consistently showed that the $OTeF_5$ group is significantly more shielding towards the central xenon nucleus than F. A related Mössbauer experiment in which ^{129}Xe quadrupole splittings were correlated with electronegativities gave values of 3.87 and 3.98 (Pauling scale [70]) for $OTeF_5$ and F, respectively, in excellent agreement with the value of 3.88 obtained earlier for $OTeF_5$ utilizing a correlation of the ^{1}H chemical shift difference between the methyl and methylene protons in CH_3CH_2X with the electronegativity of X (X = F, Cl, Br, I) [71,72].

The reactions of XeF_4, XeO_2F_2, and $XeOF_4$ with $B(OTeF_5)_3$ result in fluorine substitution by $OTeF_5$ groups as exemplified in Eq. (18) [73]. The use of excess

$$3XeO_2F_2 + 2B(OTeF_5)_3 \rightarrow 3O_2Xe(OTeF_5)_2 + BF_3 \quad (18)$$

fluoride or oxide fluoride yields mixtures of $XeF_{4-n}(OTeF_5)_n$, $XeO_2F_{2-n}(OTeF_5)_n$, and $XeOF_{4-n}(OTeF_5)_n$, resulting from rapid ligand redistribution of F and $OTeF_5$ groups at r.t. In the mixed $F/OTeF_5$ species, the magnitudes of $^1J(^{129}Xe-^{19}F)$ couplings range from 3503 to 3817 Hz for Xe^{IV} and from 931 to 1213 Hz for Xe^{VI}. The coupling between xenon and the equatorial fluorines of the $OTeF_5$ groups, $^3J(^{129}Xe-^{19}F_{eq})$, ranges between 34 and 71 Hz, giving rise to splitting patterns in the ^{129}Xe-NMR spectrum that allow for unambiguous structural assignments (Fig. 9). In contrast, the $^3J(^{129}Xe-^{19}F_{ax})$ couplings are small (0–4 Hz) (see Section 5.3) and are usually not resolved. The ^{129}Xe chemical shifts are found to be additive, yielding chemical shift changes of 207 ppm (XeX_2), 211 ppm (XeX_4), 44 ppm ($XeOX_4$), and 20 ppm (O_2XeX_2) per substituted $OTeF_5$ group (see Section 4.1.3). The two-bond $^{129}Xe-^{125}Te$ coupling was found to decrease as n increases in $XeF_{4-n}(OTeF_5)_n$, $XeO_2F_{2-n}(OTeF_5)_n$, and $XeOF_{4-n}(OTeF_5)_n$. The increase in ^{129}Xe shielding and the decrease in the $^1J(^{129}Xe-^{19}F)$ coupling constant with higher $OTeF_5$ substitution are consistent with a greater covalency for the Xe–$OTeF_5$ bond when compared with the Xe–F bond. Increasing the number of Xe–$OTeF_5$ bonds in a compound also results in a decrease in $^2J(^{129}Xe-^{125}Te)$, consistent with a decrease in average Xe–O bond order. The solvolysis reactions of $Xe(OTeF_5)_4$ and $O{=}Xe(OTeF_5)_4$ in the strong $F/OTeF_5$ acceptor solvent SbF_5, leads to $OTeF_5/F$ ligand redistribution and formation of two series of novel, mixed xenon cations, $F_nXe(OTeF_5)_{3-n}^+$ and $O{=}Xe_n(OTeF_5)_{3-n}^+$ ($n = 0$–2) [74]. The observation of slow gas evolution in both

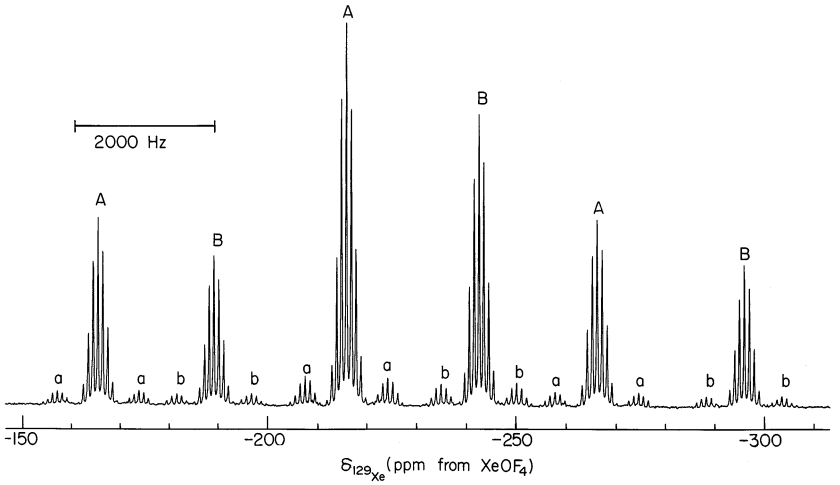

Fig. 9. ^{129}Xe-NMR spectra (69.561 MHz, 24°C) of *cis*-$XeF_2(OTeF_5)_2$ (A) and *trans*-$XeF_2(OTeF_5)_2$ (B) and accompanying ^{125}Te satellites a and b in $CFCl_3$ solvent [73].

systems at 5°C, as well as the presence of TeF_6, XeF^+, $XeOTeF_5{}^+$, O_2XeF^+, and the novel $O_2XeOTeF_5{}^+$ cation, are consistent with the decomposition reactions represented by Eqs. (19)–(22). In all cases, except that of $O_2XeOTeF_5{}^+$, no

$$O{=}XeF_2OTeF_5{}^+ \rightarrow O_2XeF^+ + TeF_6 \quad (19)$$

$$O{=}XeF(OTeF_5)_2{}^+ \rightarrow O_2XeOTeF_5{}^+ + TeF_6 \quad (20)$$

$$O_2XeF^+ \rightarrow XeF^+ + O_2 \quad (21)$$

$$O_2XeOTeF_5{}^+ \rightarrow XeOTeF_5{}^+ + O_2 \quad (22)$$

$^3J(^{129}Xe-{}^{19}F)$ coupling could be resolved because of the viscosity of the SbF_5 solvent. As in the case of the neutral mixed $F/OTeF_5$ series, the ^{129}Xe chemical shifts were found to be additive, yielding average chemical shift changes of 182 and 91 ppm per $OTeF_5$ group for $F_nXe(OTeF_5)_{3-n}^+$ and $O{=}Xe_n(OTeF_5)_{3-n}^+$, respectively.

3.8. Xenon–nitrogen bonds

In the quest for new ligands bonded to xenon, DesMarteau and LeBlond [75] prepared and isolated $FXeN(SO_2F)_2$, the first example of a Xe–N bond, according to Eq. (23) and reported the ^{19}F-NMR spectrum in BrF_5 solvent showing

$$XeF_2 + HN(SO_2F)_2 \rightarrow FXeN(SO_2F)_2 + HF \quad (23)$$

two resonances, each exhibiting a coupling to ^{129}Xe in the form of ^{129}Xe satellites. The low-frequency signal corresponded to fluorine on xenon(II) with a $^1J(^{129}Xe-{}^{19}F)$ coupling and a signal in the fluorine-on-sulfur(VI) region with

a $^{3}J(^{129}Xe-^{19}F)$ coupling. Subsequent Raman, multi-NMR spectroscopic and X-ray crystallographic studies at McMaster University [76,77] provided a full characterization of this compound confirming Xe–N bond formation. NMR and Raman spectroscopic studies were also carried out on ^{15}N-enriched (30%) $FXeN(SO_2F)_2$. The ^{129}Xe-NMR spectrum of the ^{15}N-enriched compound consisted of a doublet with ^{15}N satellites and represented the first example of a directly bonded $^{129}Xe-^{15}N$ coupling (305 Hz). A second mole of $HN(SO_2F)_2$ reacts with $FXeN(SO_2F)_2$, upon HF elimination, to yield $Xe[N(SO_2F)_2]_2$. The ^{129}Xe-NMR spectrum of ^{15}N enriched (30%) $Xe[N(SO_2F)_2]_2$ gave a multi-line spectrum which is the superposition of subspectra of the three different isotopomers with no, one, and two ^{15}N atoms coupling to ^{129}Xe (Fig. 10).

DesMarteau [78] and Schrobilgen et al. [79,80] showed that $FXeN(SO_2F)_2$ acts as a fluoride ion donor towards AsF_5 at low temperature, forming $XeN(SO_2F)_2^+$-AsF_6^- (Eq. (24)). However, $XeN(SO_2F)_2^+AsF_6^-$ decomposes under dynamic vacuum at 22°C to the 2:1 adduct $F[XeN(SO_2F)_2]_2^+$ (Eq. (25)) which, like $Xe_2F_3^+$,

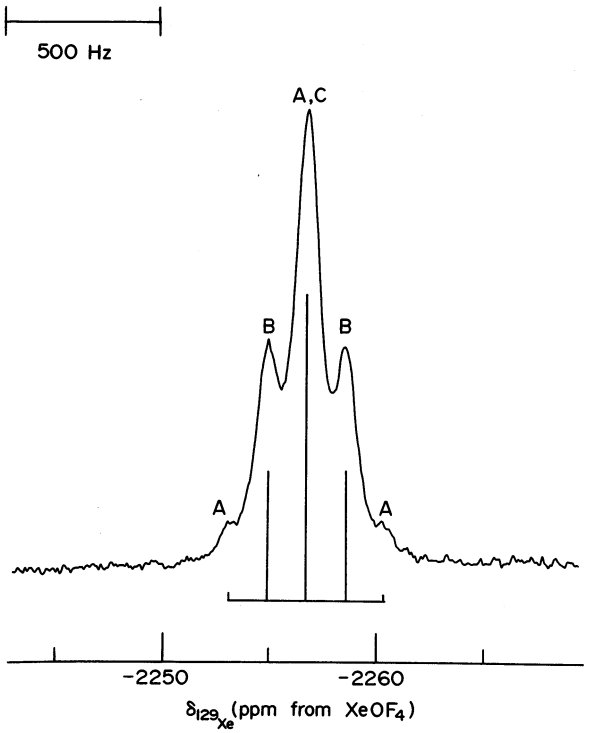

Fig. 10. ^{129}Xe-NMR spectrum (69.20 MHz, −40°C) of 30% ^{15}N-enriched $Xe[N(SO_2F)_2]_2$ recorded in SO_2ClF solvent. Individual multiplet lines are assigned to the following isotopic isomers: (A) $(FO_2S)_2{}^{15}NXe^{15}N(SO_2F)_2$ (triplet); (B) $(FO_2S)_2{}^{14}NXe^{15}N(SO_2F)_2$ (doublet); (C) $(FO_2S)_2{}^{14}NXe^{14}N$-$(SO_2F)_2$ (singlet). The sum of the calculated singlet, doublet and triplet intensities is represented by the stick diagram [78].

$$FXeN(SO_2F)_2 + AsF_5 \rightarrow XeN(SO_2F)_2{}^+AsF_6{}^- \quad (24)$$

$$2XeN(SO_2F)_2{}^+AsF_6{}^- \rightarrow F[XeN(SO_2F)_2]_2{}^+AsF_6{}^- + AsF_5 \quad (25)$$

contains a fluorine bridge. In contrast to the $Xe_2F_3{}^+$ cation, no bridging fluorine could be observed in the ^{19}F-NMR spectrum of $F[XeN(SO_2F)_2]_2{}^+$ in BrF_5 at $-45°C$ which was attributed to rapid fluorine exchange. The measurements of ^{129}Xe and ^{15}N-NMR spectra using the ^{15}N enriched $HN(SO_2F)_2$ in BrF_5 and SO_2ClF supported rapid chemical exchange processes among $F[XeN(SO_2F)_2]_2{}^+$, $FXeN(SO_2F)_2$, XeF_2, XeF^+, and $Xe_2F_3{}^+$ [79]. Dissolution of $F[XeN(SO_2F)_2]_2{}^+$-$AsF_6{}^-$ in SbF_5 solvent resulted in the displacement of the weaker fluoride ion acceptor, AsF_5, yielding a solution of $XeN(SO_2F)_2{}^+Sb_nF_{5n+1}^-$ from which $XeN(SO_2F)_2{}^+Sb_3F_{16}^-$ crystallized [80]. The crystal structure of $XeN(SO_2F)_2{}^+$ $Sb_3F_{16}^-$ consists of the $XeN(SO_2F)_2{}^+$ cation fluorine-bridged to an $Sb_3F_{16}^-$ anion.

Examples of xenon nitrogen bonds were significantly extended by the synthesis of XeF^+ adducts with a number of neutral organic nitrogen bases that are stable towards oxidation by XeF^+. Nitrogen bases having first ionization potentials greater than 10.9 eV, the electron affinity of XeF^+, were chosen to react with $XeF^+AsF_6{}^-$ or $Xe_2F_3{}^+AsF_6{}^-$. Representative bases include, HCN, CH_3CN, C_5F_5N, and s-$C_3F_3N_3$ which have first adiabatic ionization potentials of 13.80, 12.194 ± 0.005, 10.08 ± 0.05, and 10.07 ± 0.05 eV, respectively [8]. Nitrile–XeF^+ adducts were obtained from HF solutions of equimolar amounts of $XeF^+AsF_6{}^-$ and the nitrile (Eq. (26)) [81]. The use of $Xe_2F_3^+AsF_6{}^-$ instead of $XeF^+AsF_6{}^-$ yielded an equimolar amount of XeF_2 in addition to the XeF^+ adduct (Eq. (27)).

$$XeF^+AsF_6{}^- + RC{\equiv}N \xrightarrow{HF} RC{\equiv}NXeF^+AsF_6{}^- \quad (26)$$

$$Xe_2F_3{}^+AsF_6{}^- + RC{\equiv}N \xrightarrow{HF} RC{\equiv}NXeF^+AsF_6{}^- + XeF_2 \quad (27)$$

Adducts with perfluoropyridines were obtained in a similar way from HF solution and by reaction of equimolar amounts of XeF_2 and protonated perfluoropyridinium salts of the $AsF_6{}^-$ anion in BrF_5 according to Eq. (28) [82]. The inter-

$$XeF_2 + C_5F_5NH^+AsF_6{}^- \xrightarrow{BrF_5} C_5F_5NXeF^+AsF_6{}^- + HF \quad (28)$$

action of liquid s-$C_3F_3N_3$ with $XeF^+AsF_6{}^-$ at r.t. followed by removal of excess s-$C_3F_3N_3$ yielded the s-$C_3F_3N_2NXeF^+$ cation according to Eq. (29) [83]. It is not necessary to ^{15}N enrich the nitrile adducts in order to observe xenon-nitrogen

$$XeF^+AsF_6{}^- + \text{xs } s\text{-}C_3F_3N_3 \rightarrow s\text{-}C_3F_3N_2NXeF^+AsF_6{}^- \quad (29)$$

coupling because the high axial symmetry about nitrogen affords a low electric field gradient (efg) at the ^{14}N nucleus. The low efg and low viscosity of the HF solvent lead to sufficiently slow quadrupolar relaxation to permit observation of the $^1J(^{129}Xe-^{14}N)$ coupling. One-bond $^{129}Xe-^{19}F$ couplings have also been observed for the $C_5F_5NXeF^+$ and s-$C_3F_3N_2NXeF^+$ cations in HF but are quadrupole collapsed at low temperatures in the higher viscosity solvent, BrF_5. In principle, every atom in these adduct cations has one observable spin-active isotope, making

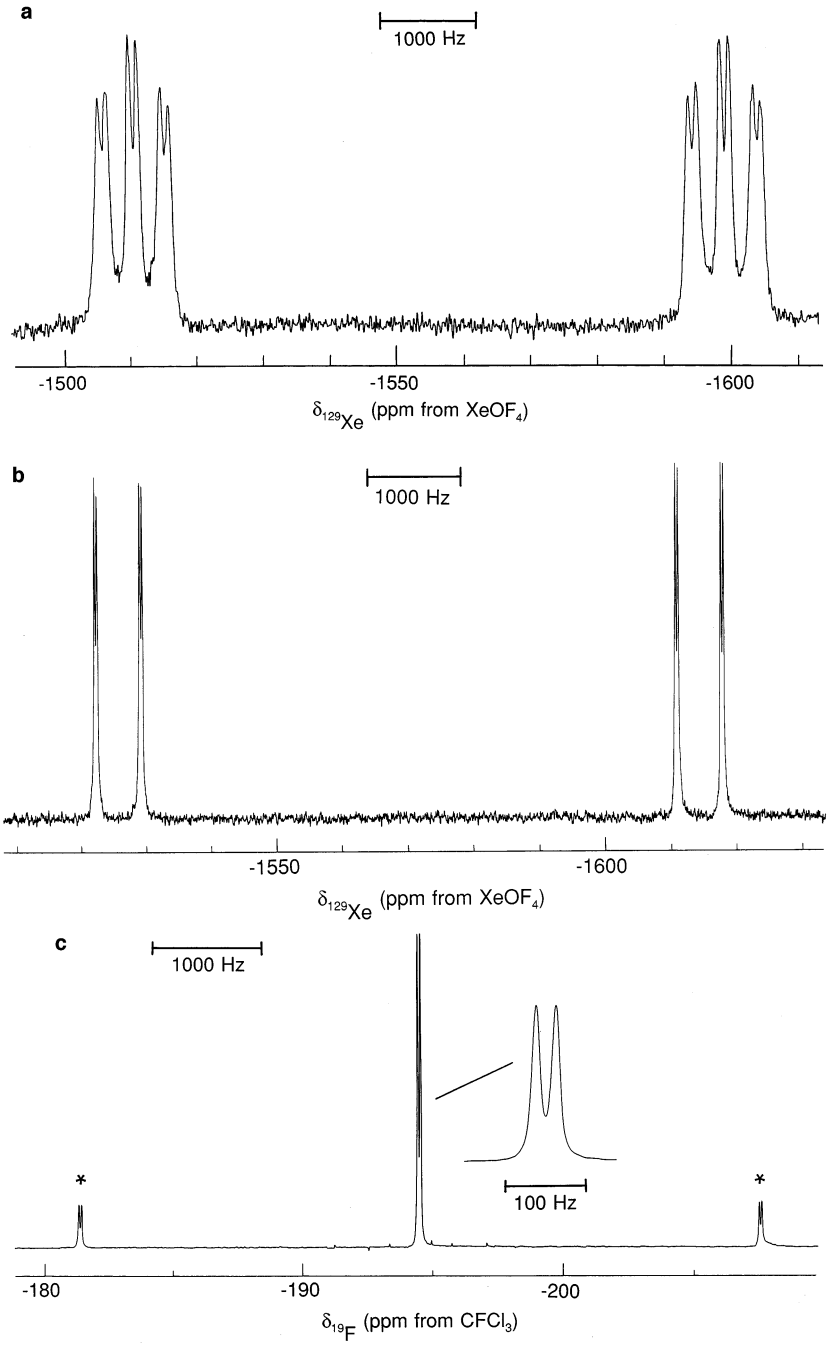
a
1000 Hz
-1500
-1550
-1600
δ_{129}Xe (ppm from $XeOF_4$)
b
1000 Hz
-1550
-1600
δ_{129}Xe (ppm from $XeOF_4$)
c
1000 Hz
100 Hz
*
*
-180
-190
-200
δ_{19}F (ppm from $CFCl_3$)

Fig. 11.

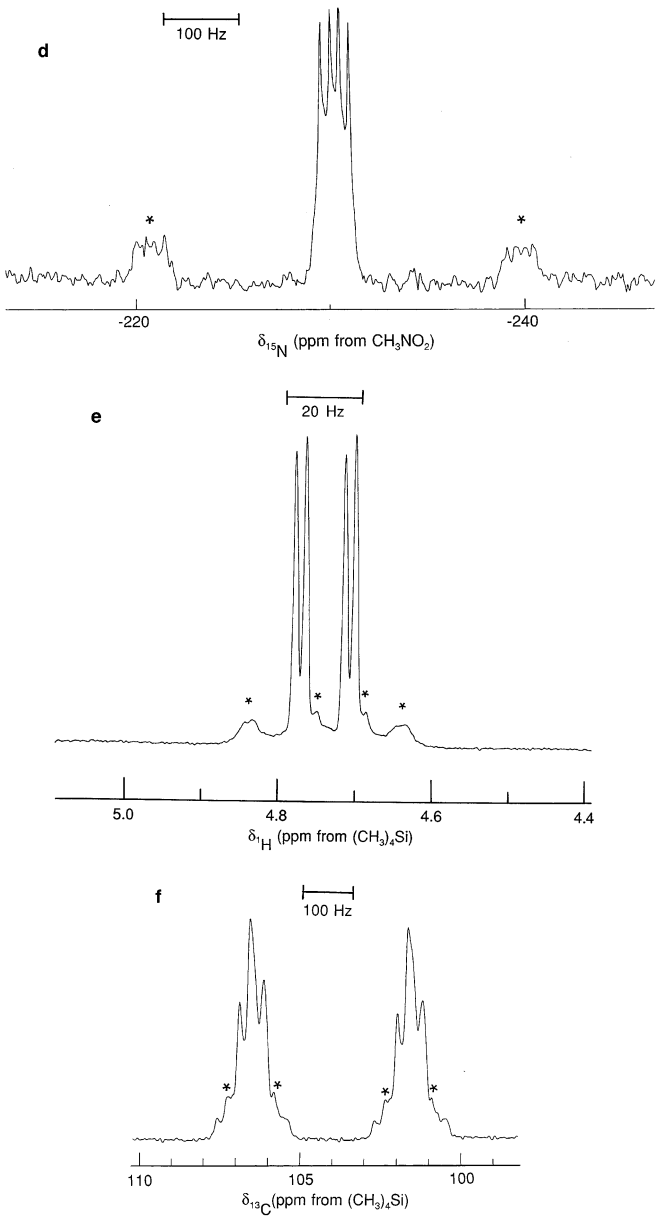

Fig. 11. NMR spectra of $HC{\equiv}NXeF^{+}AsF_6^{-}$: (a) ^{129}Xe-NMR spectrum (69.563 MHz, −10°C) of 99.2% ^{13}C-enriched sample recorded in HF solvent. (b) ^{129}Xe-NMR spectrum (69.563 MHz, −50°C) of 99.5% ^{15}N-enriched sample recorded in BrF_5. (c) ^{19}F-NMR spectrum (235.361 MHz, −50°C) of 99.5% ^{15}N-enriched sample recorded in BrF_5 solvent. (d) ^{15}N-NMR spectrum (25.347 MHz, −50°C) of 99.5% ^{15}N-enriched sample recorded in BrF_5 solvent. (e) ^{1}H-NMR spectrum (200.133 MHz, −50°C) of 99.5% ^{15}N-enriched sample recorded in BrF_5. (f) ^{13}C-NMR spectrum (62.915 MHz, −10°C) of 99.2% ^{13}C-enriched sample recorded in HF solvent. Asterisks denote ^{129}Xe satellites [84].

multi-NMR spectroscopy an ideal structural probe for their study. The $HC{\equiv}NXeF^+$ cation is illustrative of this point in that all possible chemical shifts and coupling constants have been extracted for the natural abundance and ^{15}N-enriched $HC{\equiv}NXeF^+$ cations (Structure (1) and Fig. 11) [84]. The ^{129}Xe chemical shifts have served as a particularly sensitive probe for the ionicities of the xenon–nitrogen bonds over the series of nitrogen base adducts of XeF^+ [8] (see Section 4.1.6).

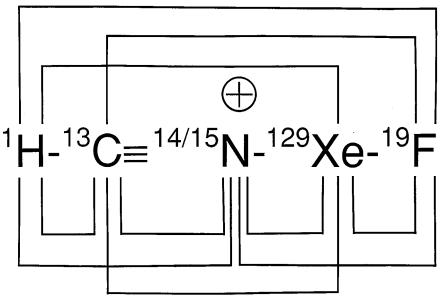

Structure 1.

The potential ambident ligand, $CF_3C(O)NH_2$, reacts as the protonated $CF_3C(OH)NH_2{}^+AsF_6{}^-$ salt with XeF_2 in BrF_5 solvent to give the xenon–oxygen bonded $CF_3C(OXeF)NH_2{}^+$ cation and an equimolar amount of HF [85]. The Xe–O bond of the $CF_3C(OXeF)NH_2{}^+$ cation was interpreted as having substantial covalent character on the basis of trends among ^{129}Xe and ^{19}F chemical shifts, $^1J(^{129}Xe$–$^{19}F)$ couplings and Xe–F stretching frequencies for related xenon(II) species.

Xenon–nitrogen cations result from the reaction of the XeF^+ cation with the inorganic bases, F_5TeNH_2 [8,86] and $N{\equiv}SF_3$ [8,87] and are formed in BrF_5 at -50°C according to Eqs. (30) and (31). In addition, $F_5TeN(H)Xe^+$ is obtained in HF solvent in equilibrium with $F_5TeNH_3^+$ (Eq. (32)). Two consecutive additions of

$$F_5TeNH_3{}^+AsF_6{}^- + XeF_2 \xrightarrow{BrF_5} F_5TeN(H)\text{–}Xe^+AsF_6{}^- + 2HF \quad (30)$$

$$F_3S{\equiv}N + XeF^+AsF_6{}^- \xrightarrow{BrF_5} F_3S{\equiv}N\text{–}XeF^+AsF_6{}^- \quad (31)$$

$$F_5TeNH_3{}^+AsF_6{}^- + XeF_2 \overset{HF}{\rightleftharpoons} F_5TeN(H)\text{–}Xe^+AsF_6{}^- + HF \quad (32)$$

HF across the sulfur–nitrogen bond of the $F_3S{\equiv}N\text{–}XeF^+$ cation in anhydrous HF followed by HF elimination yield $F_4S{=}N\text{–}Xe^+$ and $F_5S\text{–}N(H)\text{–}Xe^+$ (Eqs. (33) and (34)) [8,86]. In addition to nitrogen base adducts of XeF^+, adducts of $XeOMF_5{}^+$

$$F_3S{\equiv}N\text{–}XeF^+AsF_6{}^- + HF \rightarrow [F_4S{=}N(H)\text{–}XeF^+AsF_6{}^-] \rightarrow F_4S{=}N\text{–}Xe^+AsF_6{}^- + HF \quad (33)$$

$$F_4S{=}N\text{–}Xe^+AsF_6{}^- + HF \rightarrow F_5S\text{–}N(H)\text{–}Xe^+AsF_6{}^- \quad (34)$$

(M = Se, Te) have been prepared and characterized by multi-NMR spectroscopy, i.e. $CH_3C{\equiv}N\text{–}XeOTeF_5{}^+$, $C_5F_5N\text{–}XeOTeF_5{}^+$, $s\text{-}C_3F_3N_2N\text{–}OTeF_5{}^+$, and $F_3S{\equiv}N\text{–}XeOSeF_5{}^+$, and comprise the first examples of O–Xe–N linkages [8,87].

3.9. Krypton–nitrogen bonds

The choice of nitrogen bases that are stable to oxidation by KrF^+ is much more limited than for XeF^+ [83,88]. The KrF^+ cation has an estimated electron affinity of 13.2 eV. In order to prepare KrF^+ adducts with nitrogen donors that are analogous to those of XeF^+, the weaker oxidizer KrF_2 was utilized instead of KrF^+ itself. This was accomplished by allowing KrF_2 to react with the protonated nitrogen base salt at low temperature and is illustrated by the reaction of KrF_2 with $HC{\equiv}NH^+$-AsF_6^- in BrF_5 or HF yielding the $HC{\equiv}NKrF^+$ cation (Eq. (35)), providing the

$$HC{\equiv}NH^+AsF_6^- + KrF_2 \xrightarrow{BrF_5 \text{ or } HF} HC{\equiv}NKrF^+AsF_6^- + HF \quad (35)$$

first example of krypton bonded to an element other than fluorine, as well as the first example of a krypton–nitrogen bond [88]. Protonation of the nitrogen base also served to prevent attack by the aggressive oxidizer-solvent, BrF_5. The reaction was allowed to proceed at ca. -60°C in HF and also resulted in the formation of $HC{\equiv}NKrF^+AsF_6^-$ which has, in contrast to BrF_5 solvent, a low solubility in HF. Warming of the reaction mixture in HF to -50°C resulted in rapid gas evolution that was accompanied by a violent detonation. The behavior of the HF solvent system contrasts with the reaction between $HC{\equiv}NH^+AsF_6^-$ and KrF_2 in BrF_5 solvent which yielded a solution of $HC{\equiv}NKrF^+AsF_6^-$ that was stable to at least -55°C with only slight decomposition. The ^{19}F-NMR spectrum of the ^{15}N enriched (99.5%) $HC{\equiv}NKrF^+$ cation in BrF_5 displayed $^2J(^{19}F-^{15}N)$ and $^4J(^{19}F-^1H)$ spin–spin couplings as well as the krypton secondary isotopic shifts (see Section 6 and Fig. 12). The krypton nitrogen series was extended to adducts with the perfluorinated nitriles $R_FC{\equiv}N$ ($R_F = CF_3$, C_2F_5, and n-C_3F_7) by reaction of $R_FC{\equiv}N{-}AsF_5$ with KrF_2 at -57 to -61°C in BrF_5 solvent (Eq. (36)) [83]. The

$$R_FC{\equiv}N{-}AsF_5 + KrF_2 \xrightarrow{BrF_5} R_FC{\equiv}N{-}KrF^+AsF_6^- \quad (36)$$

secondary isotopic shifts arising from ^{82}Kr, ^{84}Kr, and ^{86}Kr could be resolved for the ^{19}F-on-Kr resonances of $HC{\equiv}NKrF^+$ and $F_3CC{\equiv}NKrF^+$. Secondary isotopic splittings for ^{78}Kr, ^{80}Kr, ^{82}Kr, ^{84}Kr, and ^{86}Kr, have also been observed in the ^{19}F-NMR spectrum of KrF_2 (Fig. 13) [89]. The signals corresponding to fluorine bonded to ^{83}Kr in $HC{\equiv}NKrF^+$, $CF_3C{\equiv}NKrF^+$, and KrF_2 were collapsed into the spectral baselines as a result of quadrupolar relaxation of the $^1J(^{83}Kr-^{19}F)$ spin–spin coupling (11.55% ^{83}Kr, $I = 9/2$). The ^{19}F-NMR spectrum of XeF_2 (Fig. 13) also showed secondary isotopic splittings arising from fluorine bonded to ^{128}Xe, ^{130}Xe, ^{132}Xe, ^{134}Xe, and ^{136}Xe. The line corresponding to the quadrupolar nucleus ^{131}Xe (21.18%, $I = 3/2$) was not detectable, again, owing to quadrupolar line broadening and collapse of ^{131}Xe–^{19}F coupling into the spectral baseline.

3.10. The $OIOF_4$ ligand

In addition to the simple binary fluoride XeF_2, a number of ligands are known to form covalent derivatives with Xe^{II}. Included in this list of ligands are $-OSO_2F$,

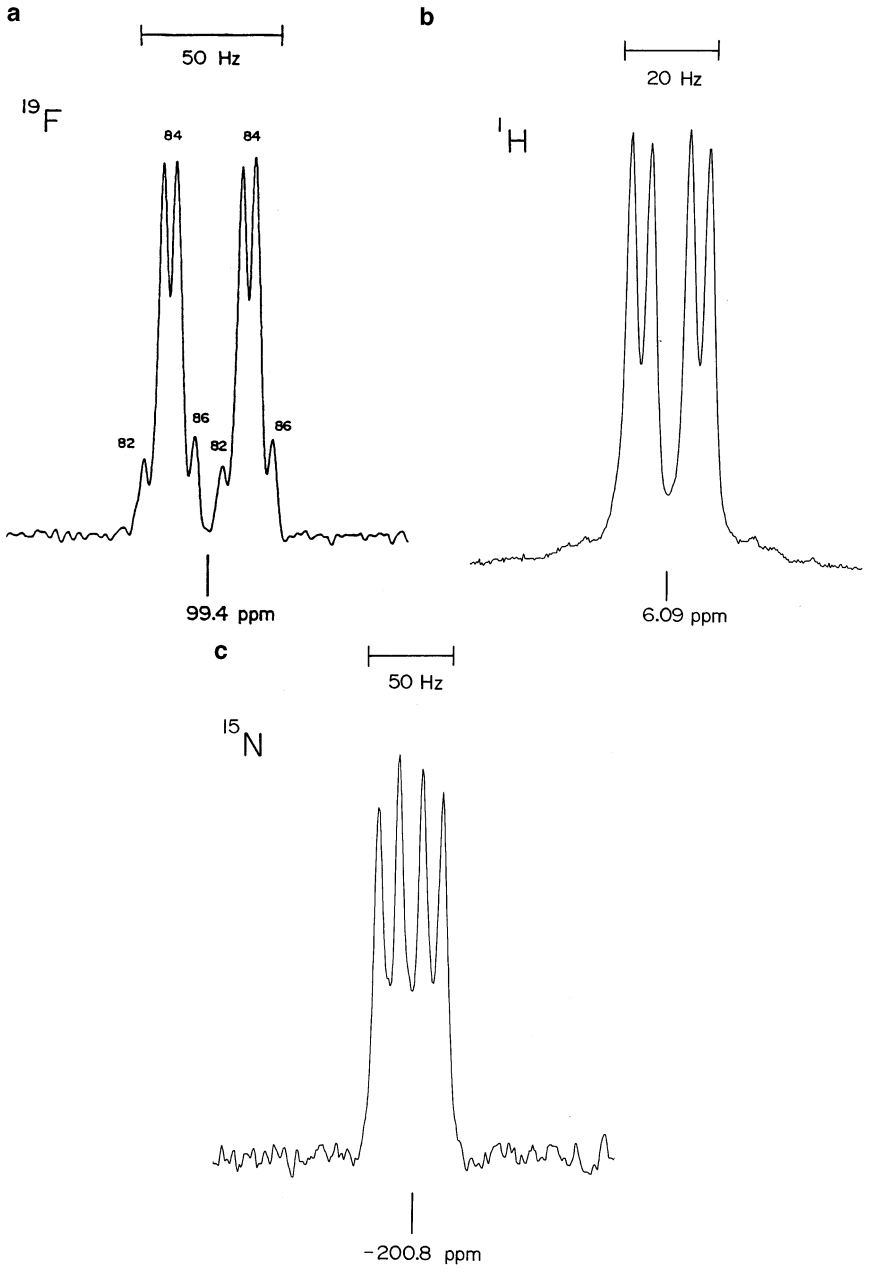

Fig. 12. NMR spectra of the HC≡N–Kr–F^+ cation enriched to 99.5% ^{15}N, recorded in BrF_5 solvent at −57°C. (a) ^{19}F-NMR spectrum (235.36 MHz) depicting $^2J(^{19}F?^{15}N)$ and $^4J(^{19}F?^1H)$ and krypton isotope shifts. Lines assigned to fluorine bonded to ^{82}Kr (11.56%), ^{84}Kr (56.90%), and ^{86}Kr (17.37%) are denoted by the krypton mass number. The innermost lines of the ^{87}Kr and ^{86}Kr doublets overlap their corresponding ^{84}Kr doublets. The isotopic shift arising from ^{83}Kr (11.53%) is not observed because of quadrupolar collapse of the $^1J(^{83}Kr–^{19}F)$ coupling; those of ^{78}Kr (0.35%) and ^{80}Kr (2.27%) are too weak to be observed. (b) ^1H-NMR spectrum (80.02 MHz) depicting $^2J(^{15}N?^1H)$ and $^4J(^{19}F?^1H)$. (c) ^{15}N-NMR spectrum (50.70 MHz) depicting $^2J(^{19}F?^{15}N)$ and $^2J(^{15}N?^1H)$ [88].

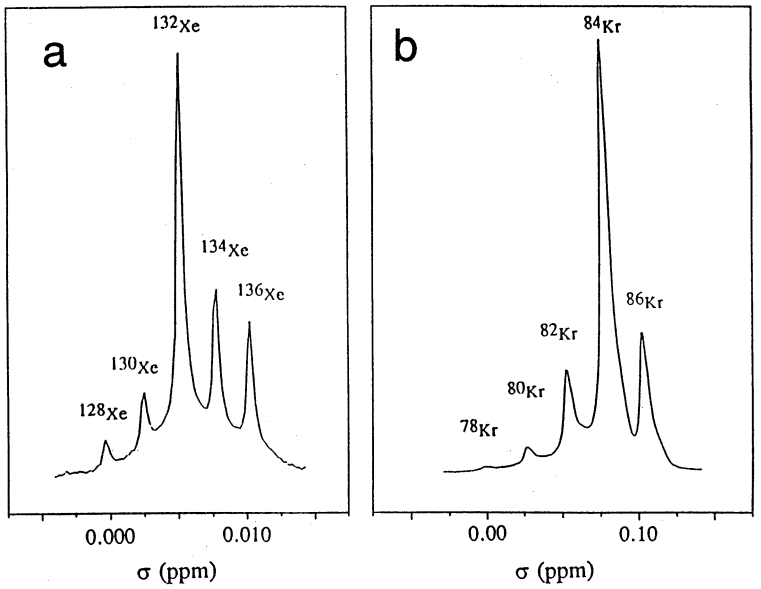

Fig. 13. High-resolution ^{19}F-NMR spectra showing the secondary isotope effect of the noble gas on the (a) ^{19}F-NMR spectrum (376.153 MHz, −15.8°C) of XeF_2 dissolved in acetonitrile-d_3. The ^{129}Xe satellites used to obtain the ^{19}F chemical shift and the ^{129}Xe–^{19}F spin–spin coupling in the $^{129}XeF_2$ isotopomer are not shown. (b) ^{19}F-NMR spectrum (470.599 MHz, −15.8°C) of KrF_2 dissolved in SO_2ClF [89]. Lines assigned to individual krypton and xenon isotopes are denoted by the mass number of the isotope.

–$OTeF_5$, –$OPOF_2$, –$OSeF_5$, –$OClO_3$, –$OCOCF_3$, –ONO_2, –$N(SO_2F)_2$, and –$N(SO_2CF_3)_2$ which all satisfy the same set of criteria for a ligand sufficiently electronegative and resistant to oxidation to stabilize Xe^{II}; namely, they form moderate to strong monoprotic acids, positive chlorine derivatives, and stable alkali-metal salts [90]. The –$OIOF_4$ ligand also fulfills these criteria and several xenon(II) derivatives have been prepared [91,92]. Iodine dioxide trifluoride inserts into the Xe–F bond of XeF_2 to give *cis*- and *trans*-$OIOF_4$ oxygen-bonded derivatives of xenon(II) according to Eqs. (37) and (38). Pure solid $Xe(OIOF_4)_2$ was obtained by displacement of $HOTeF_5$ from $Xe(OTeF_5)_2$ at 0°C using $HOIOF_4$ according to Eq. (39) as a neat mixture of the two reactants or, alternatively, in

$$IO_2F_3 + XeF_2 \rightleftharpoons FXeOIOF_4 \quad (37)$$

$$IO_2F_3 + FXeOIOF_4 \rightleftharpoons Xe(OIOF_4)_2 \quad (38)$$

$$Xe(OTeF_5)_2 + 2HOIOF_4 \rightleftharpoons Xe(OIOF_4)_2 + 2HOTeF_5 \quad (39)$$

$CFCl_3$ solvent. Equilibrium (Eq. (39)) is driven to the right by pumping off the more volatile $HOTeF_5$ at 0°C. Xenon bonded to a *trans*-$OIOF_4$ group couples to four equivalent fluorines resulting in a quintet splitting in the ^{129}Xe-NMR spectrum, while xenon bonded to a *cis*-$OIOF_4$ group couples to four fluorines in three

magnetically non-equivalent environments resulting in a multiplet splitting which has not been fully resolved. Besides the three possible $Xe(OIOF_4)_2$ isomers and the two possible $FXeOIOF_4$ isomers resulting from *cis–trans* isomerization, fluorosulfate derivatives were observed in SO_2ClF solutions and resulted from Eqs. (40) and (41). A comparison of ^{129}Xe-NMR chemical shifts among Xe(II) compounds,

$$SO_2ClF + FXeOIOF_4 \rightarrow FXeOSO_2F + IOF_3 + [ClF] \quad (40)$$

$$FXeOSO_2F + IO_2F_3 \rightarrow F_4OIOXeOSO_2F \quad (41)$$

including the mixed derivatives $F_4OIOXeOSO_2F$ and $F_4OIOXeOTeF_5$, indicates the effective group electronegativity order is $-F > -OSO_2F >$ *trans*-$OIOF_4 >$ *cis*-$OIOF_4 > -OTeF_5$.

3.11. $Kr(OTeF_5)_2$

An earlier attempt to obtain $Kr(OTeF_5)_2$ from KrF_2 and $B(OTeF_5)_3$ in ClO_3F at -100°C yielded $F_5TeOOTeF_5$ [93] and a subsequent attempt to conduct this reaction in SO_2ClF at -78°C gave similar results [65]. However, maintenance of the latter reaction mixture below -110°C resulted in a new AB_4 pattern in the ^{19}F-NMR spectrum in addition to the AB_4 pattern of the decomposition product, $F_5TeOOTeF_5$, which is believed to form according to Eq. (43) and is analogous to the thermolysis reaction of $Xe(OTeF_5)_2$ at 160°C [65]. The new AB_4 pattern was assigned to unstable $Kr(OTeF_5)_2$ formed according to Eq. (42) and provided the

$$3KrF_2 + 2B(OTeF_5)_3 \rightarrow 3Kr(OTeF_5)_2 + BF_3 \quad (42)$$

$$Kr(OTeF_5)_2 \rightarrow Kr + F_5TeOOTeF_5 \quad (43)$$

first example of a species containing a krypton–oxygen bond. The ^{17}O-NMR spectrum of ^{17}O enriched $Kr(OTeF_5)_2$ was also obtained.

3.12. The XeF_5^- and $XeOF_5^-$ anions

The preparation of anhydrous $N(CH_3)_4^+F^-$ by Christe et al. [94] sparked new interest in the synthesis of xenon fluoride and xenon oxide fluoride anions, whose $N(CH_3)_4^+$ salts are, in most cases soluble in CH_3CN, rendering solution NMR spectroscopic studies and crystal growth for X-ray structure determination possible. The reaction of XeF_4 or $XeOF_4$ with anhydrous $N(CH_3)_4^+F^-$ in CH_3CN yielded the XeF_5^- [95] and $XeOF_5^-$ [96] anions, respectively (Eq. (44)). The ^{129}Xe-NMR

$$N(CH_3)_4^+F^- + XeF_4 \rightarrow N(CH_3)_4^+XeF_5^- \quad (44)$$

spectrum of $N(CH_3)_4^+XeF_5^-$ in CH_3CN (Fig. 14) shows a sextet which is consistent with the novel AX_5E_2 VSEPR geometry [18] containing five equivalent fluorines in a pentagonal plane. The crystal structure of the $N(CH_3)_4^+XeF_5^-$ verified the pentagonal planar geometry of the anion. A previous investigation of the fluoride ion acceptor properties of $XeOF_4$ [97] resulted in the preparation of the 3:1 adduct, $Cs^+[F(XeOF_4)_3]^-$, and its X-ray crystal structure showed three $XeOF_4$

moieties equivalently bridged to one central fluorine atom. Raman spectra of $Xe^{16}OF_5^-$ and $Xe^{18}OF_5^-$ in $Cs^+XeOF_5^-$ were consistent with a stereochemically active lone pair. The highly explosive salt, $N(CH_3)_4^+XeOF_5^-$, was subsequently prepared and gave rise to a broad ^{129}Xe-NMR signal at -357.9 ppm with no couplings to fluorine resolved and a ^{17}O-NMR signal (^{17}O enrichment, 21.9%) with ^{129}Xe satellites. The broadening of the ^{129}Xe-NMR resonance and lack of ^{129}Xe satellites in the ^{19}F-NMR spectrum are attributed to intermolecular fluorine exchange, which has been observed, although to a much lesser extent, in the structurally related XeF_5^- anion. Vibrational spectroscopic studies in conjunction with density functional theory calculations were consistent with a pentagonal–bipyramidal geometry with the oxygen and the stereochemically active lone pair in the axial positions. The geometry was subsequently verified by the crystal structure of $NO^+XeOF_5^-$ [98].

3.13. NMR spectroscopic study of the Xe^{VIII} species, XeO_4 and XeO_3F_2

Recent progress in xenon(VIII) chemistry at McMaster University has included the characterization of highly explosive XeO_4 by ^{129}Xe- and ^{131}Xe-NMR spectroscopy [99]. Xenon tetroxide was prepared according to Eqs. (45)–(47) [100–102]. The reaction of ca. 100 mg of Na_4XeO_6 with 100% H_2SO_4 according to Eq. (47)

$$XeF_6 + 3H_2O \xrightarrow{H_2O} XeO_3 + 6HF \quad (45)$$

$$NaHXeO_4 + O_3 + 3NaOH \xrightarrow{H_2O} Na_4XeO_6 + O_2 + 2H_2O \quad (46)$$

$$Na_4XeO_6 + 2H_2SO_4 \rightarrow XeO_4 + 2H_2O + 2Na_2SO_4 \quad (47)$$

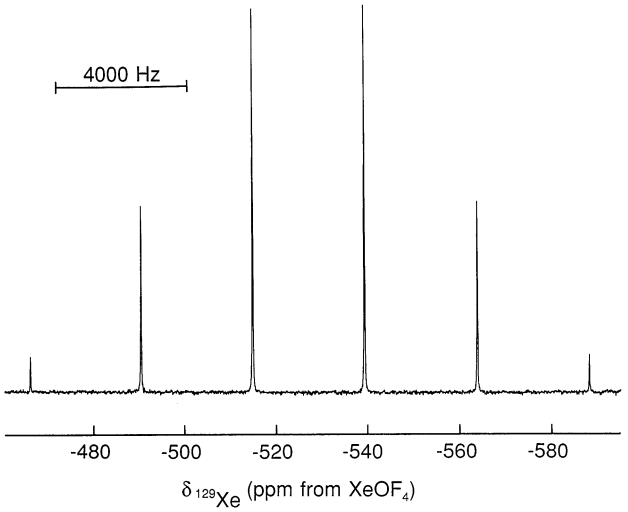

Fig. 14. ^{129}Xe-NMR spectrum (139.05 MHz, 24°C) of a saturated solution of $N(CH_3)_4^+XeF_5^-$ in CH_3CN containing an equimolar amount of $N(CH_3)_4^+F^-$ [95].

leads to the formation of ca. 30 mg of XeO_4 which is isolated by condensation under dynamic vacuum at -196°C. The ^{129}Xe-NMR spectra of XeO_4 in HF, SO_2ClF, and BrF_5 solutions comprise singlets at -85.8, -92.9, and -94.7 ppm, respectively. The tetrahedral geometry of XeO_4 has made possible the observation of the first ^{131}Xe-NMR signal ($\Delta\nu_{1/2} = 43$ Hz; SO_2ClF at -79°C) arising from a chemical species. The extreme deshielding of the ^{129}Xe resonance of XeO_4 in CH_3CN solution (224.9 ppm) and the absence of a ^{131}Xe resonance in this solvent are consistent with the formation of an adduct, which is presumed to be $O_4Xe{-}N{\equiv}CCH_3$, representing the first example of a Xe^{VIII}–N bond. The high-frequency shift found for $O_4Xe{-}N{\equiv}CCH_3$ (224.9 ppm) with respect to XeO_4 in SO_2ClF (-92.9 ppm) is paralleled by the xenon deshieldings observed for the xenon(VI) oxide (XeO_3 in H_2O, 217.0 ppm[4]) and oxide fluorides (XeO_2F_2 in HF, 171.0 ppm; $XeOF_4$, neat, 0 ppm) upon CH_3CN coordination ($XeO_3{\cdot}CH_3CN$, 218.1 ppm; $XeO_2F_2{\cdot}CH_3CN$, 263.0 ppm; $XeOF_4{\cdot}CH_3CN$, 164.7 ppm). The series of Xe^{VI} acetonitrile adducts represents the first examples of Xe^{VI}–N bonds. Section 6 should be consulted for an explanation of their structural characterization using oxygen secondary isotope effects [103]. The reaction of XeO_4 with XeF_6 in solution yielded XeO_3F_2 (Eq. (48)) in low concentrations, which was identified for the first time

$$XeO_4 + XeF_6 \rightarrow XeO_3F_2 + XeOF_4 \tag{48}$$

in solution by its ^{19}F- and ^{129}Xe-NMR spectra, and consisted of a singlet, with ^{129}Xe satellites, and a triplet, respectively [99].

4. Chemical shift trends

4.1. ^{129}Xe-NMR chemical shifts

4.1.1. Theoretical considerations

Theoretical approximations have been developed to represent the shielding of a nucleus such as ^{129}Xe by the local terms, σ^{d}_{Xe} and σ^{p}_{Xe}, which are calculated by Ramsey's theory applied to the electrons on Xe only [104]. Ramsey [105] used second-order perturbation theory to express the nuclear magnetic shielding as a sum of the first-order term, the diamagnetic term σ^{d}, which is analogous to the Lamb formula for an isolated atom or ion, and a second-order term, the paramagnetic term σ^{p}. Because ^{129}Xe exhibits a large dynamic chemical shift range (-5460 to 704.3 ppm), σ^{d}_{Xe} is assumed to differ little from the free-atom value so that chemical shift trends are largely ascribable to variations in the σ^{p}_{Xe} term. Jameson and Gutowsky [106] used this approach in an early theoretical study to show that ^{129}Xe chemical shifts can be calculated with considerable accuracy in the limited number of cases then known by application of Eq. (49):

[4] The ^{129}Xe chemical shift of XeO_3 has only been measured in H_2O and CH_3CN solvents. In both cases, strong donor–acceptor interactions between XeO_3 and the Lewis base solvents are assumed.

$$\sigma^{p} \simeq (-\mu_0/4\pi)(4\mu_B^2/\Delta E)[\langle r^{-3}\rangle_{np} P_i + \langle r^{-3}\rangle_{nd} D_i] \quad (49)$$

where P_i and D_i represent the imbalance of the valence electrons in the p and d orbitals centered on the atom in question. These calculations showed that a localized description of the bonding employing d hybridization, provides a more satisfactory description than a delocalized description without d hybridization. Moreover, the approach showed that ΔE, $\langle r^{-3}\rangle_{5p}$ and $\langle r^{-3}\rangle_{5d}$ can be regarded as essentially constant over the entire range of $\delta(^{129}Xe)$ so that P_i and D_i determine variations in $\delta(^{129}Xe)$.

^{129}Xe chemical shifts exhibit large dependencies on the formal oxidation state, the number of oxygen ligands, the charge of the species, and the ionic character of the Xe–L bond where L is F, O, or a polyatomic ligand bonded to Xe through O, N, or C.

4.1.2. Formal oxidation state of xenon

In general, the ^{129}Xe chemical shift range increases with increasing formal oxidation state of xenon:

$\delta(^{129}Xe^{0}) = -5460$ (Xe gas at infinite dilution) to -5331 (Xe in n-C_6H_{14}) ppm,

$\delta(^{129}Xe^{II}) = -3967.5$ ($C_6F_5Xe^+$) to -574 (XeF^+) ppm,

$\delta(^{129}Xe^{IV}) = -662.8$ ($Xe(OTeF_5)_4$) to 595 (XeF_3^+) ppm,

$\delta(^{129}Xe^{VI}) = -357.9$ ($XeOF_5^-$) to 704.3 (XeO_2F^+) ppm,

$\delta(^{129}Xe^{VIII}) = -748$ (XeO_6^{4-}) to 224.9 ($XeO_4\cdot CH_3CN$) ppm.

For the higher oxidation states, Xe^{IV}, Xe^{VI}, and Xe^{VIII}, the ^{129}Xe chemical shift ranges overlap considerably. The observed $\delta(^{129}Xe)$ trend is, however, in agreement with the deshielding trend calculated by Jameson and Gutowsky [104] for $XeF_4 > XeOF_4 > XeF_6 > XeF_2$. The lower shielding for xenon in XeF_4 (166.1 to 335.3 ppm) and in XeF_3^+ (595 ppm) is in marked contrast with the corresponding $\delta(^{19}F)$ trends, which vary monotonically with oxidation state, i.e. with deshielding increasing with increasing xenon oxidation state (see Section 4.2.1).

4.1.3. Variations of ^{129}Xe chemical shift with oxygen content

A monotonic increase in the chemical shift of the central atom for the series $(XeF_6)_4$ (-35 to -60.8 ppm) $< XeOF_4$ (-29.9 to 23.7 ppm) $< XeO_2F_2$ (171.0 to 173.2 ppm) $< XeO_3$ (217.0 ppm), XeF_5^+ (-23.9 to 12.7 ppm) $< XeOF_3^+$ (200.4 to 242.8 ppm) $< XeO_2F^+$ (600–704.3 ppm), and XeO_3F_2 (-414.5 to -412.9) $< XeO_4$ (-94.7 to -85.8 ppm) is observed with increasing oxygen substitution, and may be attributed to contributions of the sort $Xe{=}O \leftrightarrow Xe^+{-}O^-$, which serve to increase P_i and D_i in Eq. (27), decreasing the σ^{p}_{Xe} term (see Section 4.1.1). The opposite effect is observed upon increasing oxygen substitution in the homologous series of mixed $F/OTeF_5$ derivatives of Xe^{II}, Xe^{IV}, and Xe^{VI}. Within each of the neutral series $XeF_{2-n}(OTeF_5)_n$, $XeF_{4-n}(OTeF_5)_n$, $O{=}XeF_{4-n}(OTeF_5)_n$, and $O_2XeF_{2-n}(OTeF_5)_n$ and the cation series $XeF^+/XeOTeF_5^+$, $O_2XeF^+/O_2XeOTeF_5^+$,

$XeF_{3-n}(OTeF_5)_n^+$, and $O{=}XeF_{3-n}(OTeF_5)_n^+$; the ^{129}Xe chemical shifts are found to be additive. Increased shieldings with an increasing number of $OTeF_5$ groups in all eight series confirm the lower effective electronegativity of the $OTeF_5$ group relative to that of fluorine [73,74]:

$$\delta[^{129}XeF_{2-n}(OTeF_5)_n] = -207n - 1890$$

$$\delta[^{129}XeF_{4-n}(OTeF_5)_n] = -211n + 195.0$$

$$\delta[^{129}XeOF_{4-n}(OTeF_5)_n] = -43.9n - 26.1$$

$$\delta[^{129}XeO_2F_{2-n}(OTeF_5)_n] = -20.0n - 172.0$$

and:

$$\delta[^{129}XeF_{3-n}(OTeF_5)_n^+] = -182.2n + 198.3$$

$$\delta[^{129}XeOF_{3-n}(OTeF_5)_n^+] = -91.1n + 232.7$$

where n = number of $OTeF_5$ groups.

4.1.4. Cations and anions

For all xenon oxidation states, the xenon nucleus of a cation having one less F or $OTeF_5$ group is deshielded relative to that of the neutral parent molecule, i.e. $\delta(^{129}Xe)$: $XeL_n < XeL_{n-1}^+$ and $O_mXeL_n < O_mXeF_{n-1}^+$ (Table 1). ^{129}Xe-NMR spectra have been recorded for only three fluoride and oxide fluoride xenon anions, XeF_5^-, XeF_7^-, and $XeOF_5^-$. The ^{129}Xe nucleus of the anion is, as anticipated, significantly more shielded than that of the neutral parent fluoride or oxide fluoride (Table 1).

4.1.5. Nature of Xe^{II}–L bonds

The majority of known xenon compounds contain xenon in the +2 oxidation state and have been extensively studied by ^{129}Xe-NMR spectroscopy. The xenon chemical shifts of Xe^{II} species follow the trend $\delta(^{129}Xe)$: $XeL_2 < FXeL < (LXe)_2F^+ < XeL^+$, where L = F, $OTeF_5$, $OSeF_5$, OSO_2F, $OIOF_4$, and $N(SO_2F)_2$, and is found to hold without exception. NMR studies of xenon(II) derivatives containing XeF groups have established trends among ^{19}F and ^{129}Xe chemical shifts and $^1J(^{129}Xe-^{19}F)$ couplings (vide infra) that are of importance in assessing the relative covalent characters of Xe–L and Xe–F bonds in compounds of the type F–Xe–L and F–Xe–L^+, where L is a terminal fluorine, bridging fluorine or a ligand bonded to Xe^{II} through oxygen or nitrogen. In general, as the ionic character of the Xe–L bond increases, the covalent character of the terminal Xe–F bond increases, increasing the formal charge on xenon and deshielding the xenon nucleus and vice versa [8]. This trend is also paralleled by increasing values of $^1J(^{129}Xe-^{19}F)$ and decreasing values of $\delta(^{19}F)$ for the terminal XeF group (see Section 5.1.2). The patterns observed in the ^{19}F- and ^{129}Xe-NMR spectra are corroborated by Xe–F stretching frequencies provided by Raman spectroscopy and by Xe–F bond lengths determined from X-ray crystal structures. Bonding models for XeF_2 indicate a high degree of ionic character in the Xe–F bond. The charge distribution, represented as

$F^{-1/2}Xe^{+}F^{-1/2}$, has been predicted by theoretical treatments and is arrived at using either a three-center-two-electron bonding model or a valence bond description [107]. A simple valence bond description satisfactorily accounts for qualitative trends in xenon shieldings, $^{1}J(^{129}Xe^{II}-^{19}F)$ couplings (vide infra), Xe–F bond lengths, and Xe–F stretching frequencies in Xe^{II} species [8]. The bonding in neutral XeL_2, XeL^{+}, and in the adduct cations $LXeF^{+}$ (L = nitrogen- or oxygen-bonded ligand, or fluorine) may be represented by valence bond schemes (I) and (II), respectively, where structures $[L^{-}Xe^{2+}F^{-}]$

$$L^{-}Xe^{2+}F^{-} \leftrightarrow L\text{–}Xe^{+}F^{-} \leftrightarrow L^{-}Xe\text{–}F^{+} \quad \text{I}$$

$$L\ Xe^{2+}F^{-} \leftrightarrow L\text{–}Xe^{2+}F^{-} \leftrightarrow L\ Xe\text{–}F^{+} \quad \text{II}$$

and $[L\ Xe^{2+}F^{-}]$ are the least important contributing structures when L is not fluorine. Accordingly, structures $[L\text{–}Xe^{+}F^{-}]$ and $[L^{-}Xe\text{–}F^{+}]$ apply to formally neutral species so that the XeF_2 molecule has a formal Xe–F bond order of $\frac{1}{2}$, whereas for LXeF, the formal Xe–F bond order is $\geq \frac{1}{2}$ and < 1, approaching 1 in the most weakly coordinated cases of XeF^{+} and $XeOTeF_5^{+}$ in SbF_5 solvent. Because the fluoride ion basicities of the polymeric $Sb_nF_{5n+1}^{-}$ anions are low in solutions of XeF^{+} and $XeOTeF_5^{+}$ in SbF_5, these highly acidic (electron-poor) solutions provide the closest approximations to free XeF^{+} and $XeOTeF_5^{+}$ cations. The formal Xe–F and Xe–O bond orders of both cations approach unity and display ^{129}Xe chemical shifts that are dramatically deshielded relative to those of the parent molecules, i.e. XeF^{+} (-574 ppm, SbF_5 solvent) and XeF_2 (-1592 to -2009 ppm), $XeOTeF_5^{+}$ (-1472 ppm, SbF_5 solvent), $FXeOTeF_5$ (-2051 to -2067 ppm), and $Xe(OTeF_5)_2$ (-2327 to -2447.4 ppm). The chemical shift of XeF^{+} in SbF_5, in fact, represents the most deshielded ^{129}Xe resonance observed for a Xe^{II} species. As the base strength of L increases (group electronegativity decreases), the Xe–L bond becomes progressively more covalent and the shielding of the xenon nucleus increases as illustrated above by XeL_2 and XeL^{+}, where L = F, and/or $OTeF_5$. In cases where both fluorines are replaced by ligands that provide Xe–L bonds of greater covalent character than Xe–F bonds, the ^{129}Xe shieldings increase relative to those of XeF_2 and FXeL. The opposite effect is observed for the ^{19}F shieldings of L–Xe–F and L–Xe–F^{+} species. Plots of the ^{129}Xe chemical shift versus the ^{19}F chemical shift of the terminal fluorine on xenon result in separate linear relationships, one for XeF groups bonded to oxygen and another for XeF groups bonded to bridging fluorines (Fig. 15) [55]. The lines intersect, as expected, in the vicinity of the weakly fluorine-bridged XeF^{+} cation in SbF_5 solvent. The reader is cautioned that, where possible, such comparisons need to be made under the same solvent and temperature conditions because of the large temperature and solvent dependencies of $^{129}Xe^{II}$ and ^{19}F-on-Xe^{II} chemical shifts and $^{1}J(^{129}Xe^{II}-^{19}F)$ couplings.

Table 1
Comparison of ^{129}Xe chemical shifts with the oxidation numbers for selected cationic, neutral, and anionic xenon species

Cation, $\delta(^{129}Xe)$, ppm	Neutral, $\delta(^{129}Xe)$, ppm	Anion, $\delta(^{129}Xe)$, ppm
$Xe^{II}F^+$, −991 to −574	$Xe^{II}F_2$, −2009 to −1592	
$Xe^{IV}F_3^+$, 595	$Xe^{IV}F_4$, 166.1 to 335.3	$Xe^{IV}F_5^-$, −527
$Xe^{VI}F_5^+$, −23.9 to 12.7	$(Xe^{VI}F_6)_4$, −35 to −60.8	$Xe^{VI}F_7^-$, −169.3
	$Xe^{VI}OF_4$, −29.9 to 23.7	$Xe^{VI}OF_5^-$, −357.9
$Xe^{II}OTeF_5^+$, −1608 to −1472	$Xe^{II}(OTeF_5)_2$, −2447.4 to −2327	
$Xe^{IV}(OTeF_5)_3^+$, −341.9	$Xe^{IV}(OTeF_5)_4$, −662.8 to −637	
$Xe^{VI}O(OTeF_5)_3^+$, −1.9	$Xe^{VI}O(OTeF_5)_4$, −211.8 to −204.1	
$Xe^{VI}O_2(OTeF_5)^+$, 543.0	$Xe^{VI}O_2(OTeF_5)_2$, 131	

4.1.6. Nitrogen base adducts of xenon(II)

The ^{129}Xe chemical shifts of nitrogen base adducts of the XeF^+ cation indicate a significant measure of XeL^+ character and have been used to assess the nature of the Xe–N donor–acceptor bond. With corroboration from the vibrational spectra of L–Xe–F^+ cations, the nature of the Xe–N donor–acceptor bond can be rationalized in terms of resonance structures [L Xe–F^+] and [L–$Xe^{2+}F^-$]. For the L–Xe–F^+ cations, resonance structure [L Xe–F^+] is dominant relative to structure [L–$Xe^{2+}F^-$] as a result of the high charge localization on xenon in the latter case. Thus, the Xe–N bonds of L–Xe–F^+ cations are best described as essentially ionic interactions of the ligand, L, and XeF^+ cation, and exhibit deshielded xenon nuclei that are consistent with weakly coordinated XeF^+ cations. In general, this class of Xe^{II} species exhibits trends similar to those of the neutral L–Xe–F species as the electron donor properties of L are varied, i.e. greater *s* contribution to the hybridization of the nitrogen donor atom raises the effective electronegativity of nitrogen, resulting in a more ionic Xe–L bond (greater contribution from structure, L Xe–F^+), greater XeF^+ character and a more deshielded xenon nucleus. This is illustrated by a series of cations containing formally sp-hybridized nitrogen (e.g. $F_3S{\equiv}N{-}XeF^+$, $RC{\equiv}N{-}XeF^+$) in which the xenon nuclei are consistently more deshielded (more ionic Xe–N bonds) than the xenon nuclei in cations containing formally sp^2-hybridized nitrogen (e.g. 4-$CF_3C_5F_4N{-}XeF^+$, $C_5F_5N{-}XeF^+$, *s*-$C_3F_3N_2N{-}XeF^+$).

In the extreme case of a neutral L–Xe–F species where L is strongly electron-donating, valence bond structure [L–Xe^+F^-] dominates to the extent that the Xe–F bond is completely ionized. Such XeL^+ cations are known in which xenon is bonded through strongly electron-donating carbon and nitrogen ligand groups and are typified by $C_6F_5Xe^+$ (−3967.5 ppm), $F_5TeN(H)Xe^+$ (−2903 to −2841 ppm), $F_5SN(H)Xe^+$ (−2886 ppm), and $F_4S{=}NXe^+$ (−2672 ppm) and are classified, on the basis of their ^{129}Xe shieldings, as the most highly covalent bonds formed by xenon. With the exception of elemental xenon, the strong electron-donating properties of the latter four ligands result in the most shielded xenon environments known.

4.2. ^{19}F-NMR chemical shifts

4.2.1. Formal oxidation state of krypton and xenon

Fluorine bonded to krypton(II) is significantly less shielded than in the analogous xenon(II) species with chemical shifts ranging from 93.1 to −22.6 ppm for CF_3CNKrF^+ and KrF^+, respectively. The chemical shift of KrF_2 in BrF_5, unlike that of XeF_2, shows a considerable temperature dependence which has been attributed to equilibria involving $KrF_2 \cdot n BrF_5$ solvates [43]:

$$KrF_2 + n BrF_5 \rightleftharpoons KrF_2 \cdot n BrF_5 \quad (50)$$

The ^{19}F chemical shift of the terminal fluorine bonded to krypton in the fluorine-bridged Kr species, $Kr_2F_3^+$, $FKrFMoOF_4(MoOF_4)_n$ ($n = 0$–2), and $FKrFWOF_4$ [64] was found to occur at a higher frequency than that of the bridging fluorine. This is in marked contrast to the analogous xenon species, where the terminal fluorine is more shielded than the fluorine bridge [62].

The ^{19}F chemical shift for fluorine bonded to xenon increases with increasing oxidation number and follows the anticipated trend of decreasing Xe–F bond polarity with increasing oxidation number. Fluorine bonded to xenon exhibits ^{19}F chemical shift ranges which are non-overlapping for the oxidation states +2 to +6 and serve as important diagnostic aids for determining or confirming the formal oxidation numbers of xenon in its compounds:

$\delta(^{19}F, Xe^{II}) = -294.5$ (XeF^+) to -126.0 ($FXeN(SO_2F)_2$) ppm,

$\delta(^{19}F, Xe^{IV}) = -48.6$ ($XeOF_2$) to 49.3 ($FXe(OTeF_5)_2^+$) ppm,

$\delta(^{19}F, Xe^{VI}) = 92.5$ ($XeOF_4 \cdot CH_3CN$) to 231.7 (XeF_4^+) ppm,

$\delta(^{19}F, Xe^{VIII}) = 223.9$ and 229.5 ppm (XeO_3F_2).

The $^1J(^{129}Xe-^{19}F)$ coupling, which is related to $\delta(^{19}F)$ by an empirical correlation, also displays ranges characteristic of the xenon oxidation states (see Section 5.1.2).

4.2.2. Cations and anions

The KrF^+ cation exhibits a lower ^{19}F chemical shift than its parent compound, KrF_2, and is paralleled by the same trend for XeF^+ and XeF_2. This increase in shielding with increasing covalent character of the Ng–F (Ng = Kr, Xe) bond seems counter intuitive and appears to contradict previous theoretical predictions of Saika and Slichter [108] and Karplus and Das [109] using the mean excitation energy approximation. However, ClF, which is valence isoelectronic with KrF^+ and XeF^+, has also been found to exhibit an extremely low-frequency ^{19}F chemical shift (−419.4 ppm) [110,111]. Cornwell [112] accounted for the unusually large shielding of fluorine in ClF by considering the excitation, $\pi^* \rightarrow \sigma^*$, which corresponds to electron circulation in opposite senses on the two atoms and results in shielding of fluorine and deshielding of chlorine. Low-energy excitations may also be responsible for the greater shieldings of ^{19}F in KrF^+ and XeF^+ relative to their parent difluorides and deshielding of ^{129}Xe in XeF^+ when compared with XeF_2.

The ^{19}F-NMR resonances of the XeF_3^+, XeO_3F^+, XeO_2F^+, and XeF_5^+ cations exhibit high-frequency shifts relative to their neutral parent compounds which are consistent with increases in the covalent characters of Xe–F bonds and with decreases in Xe–F bond lengths observed in the X-ray structures of the cations relative to their neutral parent molecules.

The only ^{19}F chemical shifts reported for xenon fluoride or xenon oxide fluoride anions are those of the XeF_5^- (38.1 ppm) and $XeOF_5^-$ (118.9 ppm) anions. The fluorines of both anions are significantly deshielded with respect to their parent compounds XeF_4 (-20.1 to -15.66 ppm) and $XeOF_4$ (100.3–101.59 ppm). This behavior is somewhat surprising in view of the greater Xe–F bond polarities normally associated with the anions. The anomaly may be related to the congested environments of the fluoride ligands and their short nearest-neighbor F···F contact distances and has also been observed for the IOF_6^- anion [113]. The resonance of the five equatorial fluorines in the pentagonal bipyramidal IOF_6^- anion is deshielded by ca. 100 ppm with respect to the F-*trans*-to-F environments of IOF_5 and *cis*-/*trans*-$IO_2F_4^-$.

4.2.3. Variations of ^{19}F chemical shifts with oxygen content

In contrast to the variations found for ^{129}Xe chemical shifts with oxygen content, the trends in the ^{19}F chemical shift are far less pronounced. The substitution of two fluorine atoms with one oxygen atom has a relatively small deshielding influence on the ^{19}F resonance(s) of the remaining fluorine ligands for the series $XeOF_4$ (100.3 to 101.59 ppm) < XeO_2F_2 (105.1 ppm) and XeF_5^+ (134.4–131.6 ppm, weighted average between F_{eq} and F_{ax}) < $XeOF_3^+$ (163.1–159.1 ppm, weighted average between F_{eq} and F_{ax}) < XeO_2F^+ (199.4 ppm), but is accompanied by a more pronounced deshielding trend in the ^{129}Xe-NMR spectra. Fluorine is, however, more shielded in $XeOF_2$ (-48.6 to -45.2 ppm) than in XeF_4 (-15.66 to -20.1 ppm). Fluorine directly bonded to xenon in the series $XeOF_{2-n}(OTeF_5)_n$, $XeF_{4-n}(OTeF_5)_n$ and $OXeF_{4-n}(OTeF_5)_n$, and in $XeF_2(OTeF_5)^+$ and $XeF(OTeF_5)_2^+$ becomes progressively deshielded with increasing $OTeF_5$ substitution and is consistent with the opposite deshielding trend observed in the ^{129}Xe-NMR spectra (see Section 4.1.3). In the cationic series, $OXeF_{3-n}(OTeF_5)_n^+$, the opposite ^{19}F shielding trend is observed, i.e. the fluorine on xenon becomes more shielded upon $OTeF_5$ substitution, whereas the ^{129}Xe shielding trend is the same as for other mixed $F/OTeF_5$ series (see Section 4.1.3).

4.2.4. Nature of Xe–L bonds

Besides the ^{129}Xe chemical shift and $^1J(^{129}Xe-^{19}F)$ coupling constants, ^{19}F-NMR spectroscopy of the Xe^{II} species, L–Xe–F and L–Xe–F^+, can also be used to assess the relative ionic character of the Xe–L bonds, where L = F, $OTeF_5$, $OSeF_5$, OSO_2F, $OIOF_4$, and $N(SO_2F)_2$ (see Section 4.1.5). The Xe–F bond becomes more ionic with increasing covalent character of the Xe–L bonds, resulting in deshielding of the fluorine nucleus. This trend is exemplified by $\delta(^{19}F)$ for XeF^+ (-294.5 ppm, SbF_5 solvent), with a formal bond order close to 1, and that of XeF_2 (-181.8 ppm, BrF_5 solvent), with a formal bond order of $\frac{1}{2}$ (see Section 4.2.2). The ^{19}F chemical

shifts of L–Xe–F and L–Xe–F^+ range from -213.2 ppm for C_3F_7CN–Xe–F^+, with a rather ionic L–Xe bond, to -126.0 ppm for $(FO_2S)_2N$–Xe–F containing an Xe–N bond which apparently has a higher covalent character than its Xe–F bond.

4.2.5. Nitrogen base adducts of KrF^+ and XeF^+

The nitrogen base adducts, L–Ng–F^+, have been prepared with L = HCN, CF_3CN, C_2F_5CN, and *n*-C_3F_7CN for both krypton and xenon. The ^{19}F resonances occur at higher frequencies (99.4–91.1 ppm) for the L–Kr–F^+ adducts than for KrF_2 (77.7–55.6 ppm), which is in marked contrast with the ^{19}F resonances of L–Xe–F^+. The latter appear at lower frequencies (-213.2 to -182.8 ppm) than XeF_2 (-199.6 to -181.8 ppm) and suggest somewhat greater covalent characters in the Kr–N bonded cations when compared with their xenon analogues.

4.3. ^{17}O-NMR chemical shifts

^{17}O chemical shift data for oxygen bonded to a noble gas are limited to the $OTeF_5$ species, $Kr(OTeF_5)_2$ (95.2 ppm), $Xe(OTeF_5)_2$ (152.1 ppm), $FXeOTeF_5$ (128.8 ppm), and to the xenon oxide fluorides, $XeOF_5^-$ (270.8 ppm), $XeOF_4$ (316.3 ppm), $XeOF_3^+$ (333.7–342 ppm), XeO_2F_2 (302.5 ppm), and $XeOF_2$ (209 ppm). The increase in shielding in the series, $XeOF_3^+ < XeOF_4 < XeOF_5^-$, is in accord with the charge increase and is paralleled by the monotonic increase in shielding of the ^{129}Xe nucleus (see Section 4.1.4). The oxygen directly bonded to xenon becomes less shielded with increasing oxidation number of xenon and is the same trend found for the ^{19}F resonance when fluorine is bonded to xenon (see Section 4.2.1).

5. Spin–spin coupling constant trends

5.1. One-bond ^{129}Xe–^{19}F coupling constants

5.1.1. Theoretical considerations

Relativistic calculations by Pyykkö and Wiesenfeld [114] on selected nuclei revealed that the relativistic term corresponding to the nonrelativistic Fermi contact term almost invariably dominates one-bond spin–spin coupling and concur with the molecular orbital treatment of spin coupling constants by Pople and Santry [115]. The only exceptions found are the coupling constants between two group VI or group VII atoms such as Se–Se or I–I. The Fermi contact term is generally given by Eq. (51) [116]:

$$ {}^nK_{AB} = -(16/9)\pi\mu_0\mu_B^2\left|\Psi_s(0)\right|_A^2\left|\Psi_s(0)\right|_B^2\Pi_{AB} \tag{51}$$

where ${}^nK_{AB}$ is the reduced coupling constant, as defined in Eq. (52), μ_0 and μ_B are the permeability of a vacuum and the Bohr magneton, respectively, and $\left|\Psi_s(0)\right|_A^2$ and $\left|\Psi_s(0)\right|_B^2$ represent the s-electron densities at the spin-coupled nuclei A and B and Π_{AB} is the mutual polarizability. The reduced coupling constant, ${}^nK_{AB}$, is defined with respect to the observed coupling constant, ${}^nJ_{AB}$, by:

$$^{n}J_{AB} = h(\gamma_A/2\pi)(\gamma_B/2\pi)^{n}K_{AB} \quad (52)$$

where γ_A and γ_B are the gyromagnetic ratios of spin-coupled nuclei, and is independent of the nuclear properties of the spin-coupled nuclei. The negative sign of $\gamma(^{129}Xe)$ and positive sign of $\gamma(^{19}F)$ results in opposite signs for $^{n}J(^{129}Xe–^{19}F)$ and $^{n}K(Xe–F)$. Owing to the high nuclear charge of xenon, the spin–spin coupling constants, as well as xenon nuclear shieldings, experience significant relativistic effects because the s-electron density at the nucleus, $|\Psi_s(0)|^2$, appears in the Fermi contact term of the spin–spin coupling and should be evaluated relativistically. For xenon, the estimated ratio of the relativistic coupling to the coupling in the absence of relativistic effects is 1.484 [114,117].

5.1.2. Empirical correlations between $\delta(^{19}F)$ and $^{1}J(^{129}Xe–^{19}F)$

Empirical correlations between ^{19}F chemical shifts and one-bond $^{129}Xe–^{19}F$ coupling constants were introduced by Frame [15] and significantly extended using data obtained at McMaster University [16,17]. An almost linear correlation between the value of $^{1}J(^{129}Xe–^{19}F)$ and $\delta(^{19}F)$ was found for all oxidation states of xenon (Fig. 16). The correlation provides a rationale for the small $^{1}J(^{129}Xe–^{19}F)$ couplings observed for XeO_2F^+, $(XeF_6)_4$, and the equatorial fluorines of XeF_5^+ if

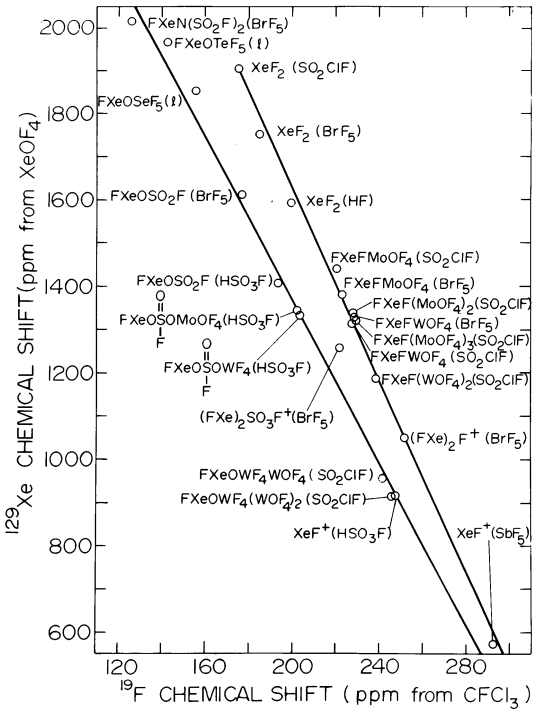

Fig. 15. Empirical plot of the ^{129}Xe chemical shift vs. ^{19}F chemical shift of the terminal fluorine on xenon for some xenon(II) species containing F bridges (lower line) and O bridges (upper line) [55].

a change in the signs of the coupling constants is assumed to occur over the series in the vicinity of these species. The correlation implies that the signs of the equatorial coupling of $XeOF_3^+$, the axial coupling of XeF_5^+ and the couplings in all potential Xe^{VIII} species are likely to be opposite in sign with respect to those of the remaining species. The magnitude of the first $^1J(^{129}Xe-^{19}F)$ coupling of a Xe^{VIII} compound has recently been measured for XeO_3F_2 in HF, SO_2ClF, and BrF_5 solvents [99] and confirms the assumed sign change and the validity of the $\delta(^{19}F)$ versus $^1J(^{129}Xe-^{19}F)$ correlation. Although no absolute sign determinations have been made for any of the couplings to ^{129}Xe, the signs of the reduced couplings, $^1K(Xe-F)$, may be inferred by considering the isoelectronic series of Xe^{IV}–I^{VII} hexafluoro-species. A near-linear relationship is obtained when $^1K(X-F)^{1/2}$ is plotted and no sign change is assumed along the series [118]. Since the signs of $^1K(Sn^{IV}-F)$ and $^1K(Te^{VI}-F)$ couplings have been determined to be negative, and the magnitude of $^1K(X-F)$ increases along the series $SnF_6^{2-} < SbF_6^- < TeF_6 < IF_6^+$, the hypothetical Xe^{VIII} cation, XeF_6^{2+}, would possess the most negative value for the reduced one-bond coupling. The signs of $^1K(Xe-F)$ for all fluoro-Xe^{VIII} species and for XeF_5^+ (F_{ax}) and $XeOF_3^+$ (F_{eq}), and possibly XeO_2F^+, are therefore taken as negative, which is equivalent to a positive sign for their $^1J(^{129}Xe-^{19}F)$ couplings.

5.1.3. Formal oxidation states

The magnitude of the one-bond xenon–fluorine coupling constant can be used as a diagnostic tool to assess the formal oxidation number of a xenon species by virtue of their non-overlapping ranges, where $^1J(^{129}Xe^{VI/VIII}-^{19}F) < {}^1J(^{129}Xe^{IV}-^{19}F) < {}^1J(^{129}Xe^{II}-^{19}F)$:

$$^1J(^{129}Xe^{II}-^{19}F_{terminal}) = -7594\ (XeF^+)\ \text{to}\ -5572\ (FXeN(SO_2F)_2)\ \text{Hz},$$

$$^1J(^{129}Xe^{II}-^{19}F_{bridging}) = -5117\ (FXeFMoOF_4)\ \text{to}\ -4828\ (FXeFXeF^+)\ \text{Hz},$$

$$^1J(^{129}Xe^{IV}-^{19}F) = -3913\ (XeF_4)\ \text{to}\ -2384\ (XeFF_2^+)\ \text{Hz},$$

$$^1J(^{129}Xe^{VI}-^{19}F) = -2724\ (XeF_7^-)\ \text{to}\ 1512\ (XeFF_4^+)\ \text{Hz},$$

$$^1J(^{129}Xe^{VIII}-^{19}F) = 991\ \text{Hz}\ (XeO_3F_2).$$

Although a distinction between Xe^{VI} and Xe^{VIII} is not possible based solely on the magnitude of $^1J(^{129}Xe-^{19}F)$, the overall variation of $^1J(^{129}Xe-^{19}F)$ with the oxidation number is in agreement with trends noted for the dependence of one-bond scalar couplings on the oxidation number [119].

5.2. One-bond $^{129}Xe-^{17}O$ and two-bond $^{129}Xe-^{125}Te$ coupling constants

The only $^1J(^{129}Xe-^{17}O)$ couplings reported to date are those for $XeOF_5^-$ (566 Hz), $XeOF_4$ (692–704 Hz), $XeOF_3^+$ (619 Hz), and XeO_2F_2 (521 Hz). The smaller $^1J(^{129}Xe-^{17}O)$ coupling for $XeOF_5^-$ compared with that for $XeOF_4$ and $XeOF_3^+$ is likely to be a consequence of more polar bonding in the anion.

Pentafluorooxotellurate derivatives of xenon in its +2, +4, and +6 oxidation states exhibit $^2J(^{129}Xe-^{125}Te)$ couplings and have essentially non-overlapping

ranges which can be correlated with the formal oxidation state of xenon, but which vary in a sense opposite to that observed for $^{1}J(^{129}Xe-^{19}F)$:

$$^{2}J(^{129}Xe^{II}-^{125}Te) = 470\ (Xe(OTeF_5)_2)\ \text{to}\ 540\ (XeF(OTeF_5))\ \text{Hz},$$

$$^{2}J(^{129}Xe^{IV}-^{125}Te) = 968\ (OXe(OTeF_5)_2)\ \text{to}\ 1293\ (XeF(OTeF_5)_3)\ \text{Hz},$$

$$^{2}J(^{129}Xe^{VI}-^{125}Te) = 1245\ (XeO(OTeF_5)_3^{+})\ \text{to}\ 1856\ (XeO_2F(OTeF_5))\ \text{Hz}.$$

5.3. Three-bond $^{129}Xe-^{19}F$ coupling constants

While $^{3}J(^{129}Xe^{II}-^{19}F)$ couplings in $OTeF_5$ derivatives are uniformly smaller than in Xe^{IV} and Xe^{VI} derivatives of the $OTeF_5$ group, there is less consistency among three-bond couplings than among one- and two-bond $^{129}Xe-^{19}F$ couplings. The relative magnitudes of three-bond couplings in $XeN{=}SF_4^{+}$, and in $OTeF_5$ and $OSeF_5$ derivatives differ considerably because their coupling paths differ. This is illustrated by xenon coupling to the equatorial fluorines of the $OTeF_5$ groups in the series $O{=}XeF_{4-n}(OTeF_5)_n$ (51–54 Hz) and to the two axial fluorine environments in the $XeN{=}SF_4^{+}$ cation (129 and 202 Hz) which have coupling paths with dihedral angles of 0 or 180°, whereas the xenon couplings to the axial fluorines in $OTeF_5$ groups (0–4 Hz) and to the equatorial fluorines in the $XeN{=}SF_4^{+}$ cation (ca. 0 Hz) have paths with dihedral angles of 90°.

6. Isotopic shifts

The secondary effects of krypton isotopes on the nuclear shielding of ^{19}F have been reported for three krypton compounds, $^{1}\Delta^{19}F(^{m'/m}Kr) = -0.0105$ ppm u^{-1} for KrF_2 [89], -0.0138 ppm u^{-1} for $FKrN{\equiv}CH^{+}$ [88], and -0.0105 ppm u^{-1} for $FKrN{\equiv}CCF_3^{+}$ [83]. Since krypton does not have an observable spin-active nucleus exhibiting spin–spin coupling to ^{19}F, the observation of the secondary krypton isotope shift is an important tool in unambiguously establishing the existence of a Kr–F bond. The only secondary effects of xenon isotopes on the nuclear shielding of ^{19}F have been reported for XeF_2, $^{1}\Delta^{19}F(^{m'/m}Xe) = -0.00118$ ppm u^{-1} [89]. The ^{19}F resonances arising from $^{83}KrF_2$ and $^{131}XeF_2$ are not detectable since the spin couplings of ^{19}F with the quadrupolar nuclides, ^{131}Xe ($I = 3/2$) and ^{83}Kr ($I = 9/2$), are severely broadened and collapsed into the spectral baselines. The first two-bond isotopic effect for a xenon compound has been observed for $^{16/18}O$ in the ^{19}F-NMR spectrum of $XeOF_2$, $^{2}\Delta^{19}F(^{m'/m}O) = -0.007$ ppm u^{-1} [120].

The only secondary isotopic effects on the nuclear shielding of ^{129}Xe that are known arise from oxygen isotopes, i.e. $^{1}\Delta^{129}Xe(^{m'/m}O) = -0.29$ ppm u^{-1} for $XeOF_4$ [73], -0.26 ppm u^{-1} for XeO_2F_2 [73], -0.345 ppm u^{-1} for $XeOF_3^{+}$ [38], -0.215 ppm u^{-1} for $XeO_3{\cdot}CH_3CN$ [103], -0.275 ppm u^{-1} for $XeO_2F_2{\cdot}CH_3CN$ [103], and -0.355 ppm u^{-1} for $XeOF_4{\cdot}CH_3CN$ [103]. The number of directly bonded oxygen ligands was unambiguously determined from the number and the relative intensities of the oxygen isotope splittings in the ^{129}Xe-NMR spectra of

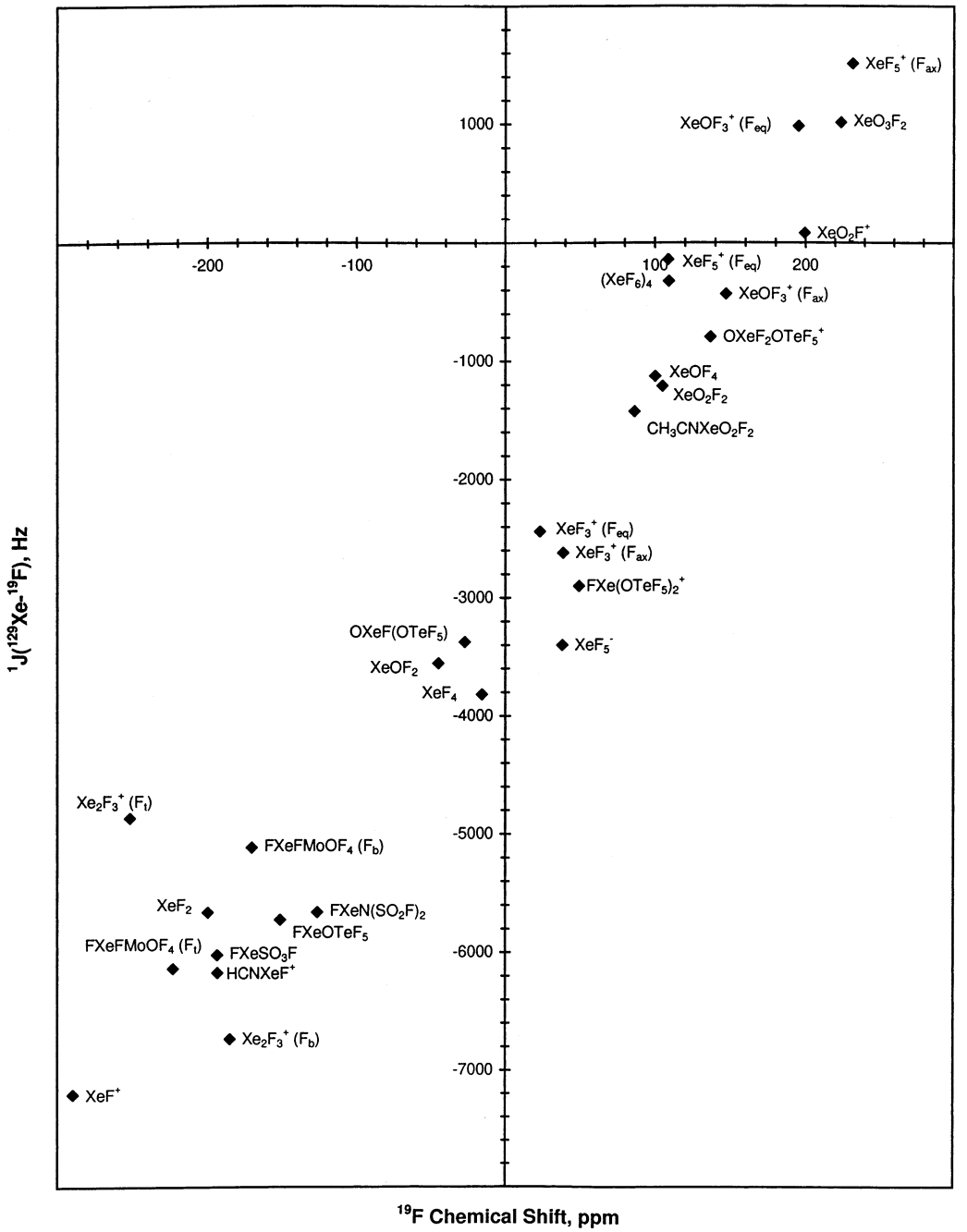

Fig. 16. Empirical correlation of the ^{19}F chemical shift and the $^{1}J(^{129}Xe?^{19}F)$ coupling constant for selected xenon compounds.

Table 2
NMR spectroscopic data of selected noble-gas species

Noble gas species	Solvent	T (°C)	$\delta(^{129}Xe)^{a}$ (ppm)	$\delta(^{19}F)^{a,b}$ (ppm)	$\delta(L)^{a}$ (ppm)	$J(^{129}Xe-^{19}F)^{c}$ (Hz)	$J(^{129}Xe-L)^{c}$ (Hz)	$J(^{19}F\text{-}L)^{c}$ (Hz)	Ref.
Kr(II)									
KrF_2	HF	26		55.6					[43]
KrF_2	BrF_5	27		77.7					[43]
KrF_2	BrF_5	−50		67.9					[43]
KrF^+	HF	−40		−22.6					[43]
$Kr_2F_3^+$ (SbF_6^-)	BrF_5	−65		73.4 (F_t) 18.8 (F_b)				$^2J/^{19}F$ 347	[43]
$Kr_2F_3^+$ (AsF_6^-)	BrF_5	−65		73.8 (F_t) 19.0 (F_b)				$^2J/^{19}F$ 347	[43]
$Kr_2F_3^+$ (SbF_6^-)	BrF_5	−66		73.6(F_t) 19.0 (F_b)				$^2J/^{19}F$ 351	[43]
$Kr(OTeF_5)_2$	SO_2ClF	−90		−42.1 (F_{ax}) −47.2 (F_{eq})	^{17}O 95.2			$^2J/^{19}F$ 181	[65]
$HCNKrF^{+}$ [d]	BrF_5	−57		99.4	^{15}N −200.8 ^{13}C 98.5 ^{1}H 6.09			$^2J/^{15}N$ 26 $^3J/^{13}C$ 25.0 $^4J/^{1}H$ 4.2	[88]
$HCNKrF^+$	HF	−60		81.0					[88]
CF_3CNKrF^+	BrF_5	−58		93.1 (FKr) −53.9 (CF_3)					[83]
$C_2F_5CNKrF^+$	BrF_5	−58		91.1 (FKr) −83.8 (CF_3) −108.6 (CF_2)					[83]
n-$C_3F_7CNKrF^+$	BrF_5	−58		91.9 (FKr) −81.1 (CF_3) −105.7 (CF_2) −125.2 (CF_2CN)					[83]
$FKrFMoOF_4$ [e]	SO_2ClF	−121		70.4 (F_tKr) −12.4 (KrF_b) 148.6 (F_1Mo)				$^2J/^{19}F_b$ 296 $^2J/^{19}F_1$ 44	[64]

Table 2 (Continued)

Noble gas species	Solvent	T (°C)	$\delta(^{129}Xe)^{a}$ (ppm)	$\delta(^{19}F)^{a,b}$ (ppm)	$\delta(L)^{a}$ (ppm)	$J(^{129}Xe-^{19}F)^{c}$ (Hz)	$J(^{129}Xe-L)^{c}$ (Hz)	$J(^{19}F\text{-}L)^{c}$ (Hz)	Ref.
$FKrF(MoOF_4)_2$[e]	SO_2ClF	−121		64.9 (F_tKr) −28.8 (KrF_b) 190.8 (F_1Mo_1) 208.5 (F'_1Mo_1) −34.8 ($Mo_1F'_bMo_2$) 150.1 (F_2Mo_2)				$^2J/^{19}F_b$ 314 $^2J/^{19}F'_b$ 48 $^2J/^{19}F_1$ 44 $^2J/^{19}F'_1$ 52 $^2J/^{19}F'_b$ 92 $^2J/^{19}F'_1$ 100 $^2J/^{19}F'_b$ 110 $^2J/^{19}F_2$ 44	[64]
$FKrF(MoOF_4)_3$[e]	SO_2ClF	−121		65.4 (F_tKr) −31.1 (KrF_b) 0 (F_1Mo_1) 0 (F_1 Mo_1) 14.6 ($Mo_1F'_bMo_2$) 10.8 ($Mo_2F''_bMo_3$) 10.8 (F_3Mo_3)				$^2J/^{19}F_b$ 326	[64]
$FKrFWOF_4$[e]	SO_2ClF	−121		67.7 (F_tKr) −26.1 (KrF_b) 67.9 (F_1W)				$^2J/^{19}F_b$ 311 $^2J/^{19}F_1$ 48	[64]
Xe(0)									
Xe atom			ca. −5460						[4]
Xe	n-C_6F_{14}	25	−5331						[56]
Xe(II)									
$C_6F_5Xe^+$ (AsF_6^-)	HF	−10	−3967.5	−123.08 (F_o) −137.79 (F_p) −151.47 (F_m)		^3J/58.9			[121]
$F_5TeN(H)Xe^+$	HF	−50	−2903						[8,86]
$F_5TeN(H)Xe^+$	HF	−45	−2841				$^1J/^{15}N$ 138		[8,86]
$F_5TeN(H)Xe^+$[f]	HF	−40			^{15}N −268.0		$^1J/^{15}N$ 138		[86]
$F_5TeN(H)Xe^+$	HF	−31.2		−51.6 (F_{ax}) −43.4 (F_{eq})	^{15}N −268.0			$^2J/^{19}F_{eq}$ 166 $^1J/^{125}Te$ 3767	[86]

Table 2 (Continued)

Noble gas species	Solvent	T (°C)	$\delta(^{129}Xe)$[a] (ppm)	$\delta(^{19}F)$[a,b] (ppm)	$\delta(L)$[a] (ppm)	$J(^{129}Xe-^{19}F)$[c] (Hz)	$J(^{129}Xe-L)$[c] (Hz)	$J(^{19}F\text{-}L)$[c] (Hz)	Ref.
$F_5TeN(H)Xe^+$[g]	BrF_5	−45	−2902		^{15}N −266.3		$^1J/^{15}N$ 142		[86]
$F_5TeN(H)Xe^+$	BrF_5	−50			^{125}Te 580				[86]
$F_5TeN(H)Xe^+$	BrF_5	−56			^1H 6.90				[86]
$F_5TeN(H)Xe^+$	BrF_5	−44		−51.9 (F_{ax})				$^2J/^{19}F_{eq}$ 166	[86]
				−43.2 (F_{eq})				$^1J/^{125}Te$ 3767	
$F_5SN(H)Xe^+$	HF	−20	−2886	59.2 (F_{ax})				$^2J/^{19}F_{eq}$ 153	[8,87]
				71.9 (F_{eq})					
$F_4S{=}NXe^+$	HF	−20	−2672	54.0 (F_{eq})				$^2J/^{19}F_{ax}$ 207	[8,87]
								$^2J/^{19}F'_{ax}$ 206	
				64.2 (F_{ax})[h]		^3J/202		$^2J/^{19}F'_{ax}$ 18	
				110.5 (F'_{ax})[h]		^3J/129			
$Xe(OTeF_5)_2$	SO_2ClF	−16		−42.6 (F_{ax})	^{17}O 152.1			$^2J/^{19}F_{eq}$ 183	[65]
				−45.3 (F_{eq})					
$Xe(OTeF_5)_2$	SO_2ClF	−50		−41.9 (F_{ax})				$^2J/^{19}F_{eq}$ 176	[122]
				−45.0 (F_{eq})				$^1J/^{129}Te$ 3649	
$Xe(OTeF_5)_2$	$CFCl_3$	26	−2447.4			^3J/31 (F_{eq})			[69]
$Xe(OTeF_5)_2$	$CFCl_3$	5	−2423.2						[92]
$Xe(OTeF_5)_2$	SO_2ClF	26	−2327			^3J/30 (F_{eq})			[69]
$Xe(OTeF_5)_2$	$CFCl_3$		−2379[i]			^3J/31 (F_{eq})	$^2J/^{125}Te$ 470		[57]
$Xe(OSeF_5)(OTeF_5)$	$CFCl_3$		−2289[i]				$^2J/^{125}Te$ 480		[57]
$Xe(OSeF_5)_2$	$CFCl_3$		−2200[i]			^3J/37 (F_{eq})			[57]
$FXeOTeF_5$	$CFCl_3$		−2067[i]			^1J/5670 (FXe)	$^2J/^{125}Te$ 540		[57]
						^3J/30 (F_{eq})			
$FXeOTeF_5$	SO_2ClF	−16		−40.8 (F_{ax})	^{17}O 128.8			$^2J/^{19}F_{eq}$ 180	[65]
				−46.7 (F_{eq})					
$FXeOTeF_5$	SO_2ClF	26	−2051			^1J/5743 (FXe)			[69]
						^3J/34 ($F_{eq}Te$)			
$FXeOTeF_5$	SO_2ClF	−50		−151 (FXe)		^1J/5729 (FXe)			[122]
				−46.3 ($F_{eq}Te$)				$^1J/^{125}Te$ 3621	
								$^2J/^{19}F_{ax}$ 179	

Table 2 (Continued)

Noble gas species	Solvent	T (°C)	$\delta(^{129}Xe)^{a}$ (ppm)	$\delta(^{19}F)^{a,b}$ (ppm)	$\delta(L)^{a}$ (ppm)	$J(^{129}Xe-^{19}F)^{c}$ (Hz)	$J(^{129}Xe-L)^{c}$ (Hz)	$J(^{19}F\text{-}L)^{c}$ (Hz)	Ref.
$FXeOSeF_5$	$CFCl_3$		−1952[i]			^{1}J/5630 (FXe) ^{3}J/37(F_{eq}Se)			[57]
$C_5F_5NXeOTeF_5^+$	SO_2ClF	−70	−2246	−46.3 (F_{ax}Te) −42.8 (F_{eq}Te)				$^{2}J/^{19}F_{eq}$ ca.181	[8,123]
s-$C_3F_3N_2NXeOTeF_5^+$	SO_2ClF	−50	−2192	−47.1 (F_{ax}Te) *ca.* −42.3 (F_{eq}Te)				$^{2}J/^{19}F_{eq}$ *ca.*187	[8,123]
$CH_3CNXeOTeF_5^+$	SO_2ClF	−50	−2061	−45.8 (F_{ax}Te) −44.0 (F_{eq}Te)				$^{2}J/^{19}F_{eq}$ 181	[8,123]
$F_3SNXeOSeF_5^+$	BrF_5	−60	−1979	53.5 (F_3S) 67.9 (F_{ax}Se) 70.4 (F_{eq}Se)				$^{2}J/^{19}F_{eq}$ 219	[8,87,123]
$Xe[N(SO_2F)_2]_2$	SO_2ClF	−40	−2257	60.2	^{15}N −232.5		$^{1}J/^{15}N$ 259		[79]
$Xe[N(SO_2F)_2]_2$	SO_2ClF	−50	−2248	60.3					[79]
$FXeN(SO_2F)_2$	SO_2ClF	−40	−2009	−126.0 (FXe)	^{15}N −247.9	^{1}J/5664	$^{1}J/^{15}N$ 307		[79]
$FXeN(SO_2F)_2$	BrF_5	−58	−1997	−126.1 (FXe) 57.6 (SO_2F)	^{15}N −250.4 ^{17}O 169.4	^{1}J/5586 ^{3}J/18.7	$^{1}J/^{15}N$ 307.4	$^{2}J/^{15}N$ 39.2	[77]
$FXeN(SO_2F)_2$	BrF_5	−40	−2016			^{1}J/5572 ^{3}J/*ca.* 18			[55]
$XeN(SO_2F)_2^+$	SbF_5	25	−1943	67.9	^{15}N −243.0		$^{1}J/^{15}N$ 91.7		[80]
trans,*trans*-$Xe(IO_2F_4)_2$	SO_2ClF	−5	−1860.7	76.9		^{3}J/38			[92]
trans,*trans*-$Xe(IO_2F_4)_2$	SO_2ClF	−40	−1802.7						[92]
trans,*trans*-$Xe(IO_2F_4)_2$	BrF_5	−40	−1871.4						[92]
trans,*trans*-$Xe(IO_2F_4)_2$	$CFCl_3$	24	−1994.6			^{3}J/38			[92]
cis,*trans*-$Xe(IO_2F_4)_2$	SO_2ClF	−5	−1987.0	76.3 (*trans*-IO_2F_4)		^{3}J/19			[92]
cis,*trans*-$Xe(IO_2F_4)_2$	SO_2ClF	−40	−1929.8						[92]
cis,*trans*-$Xe(IO_2F_4)_2$	BrF_5	−40	−1929.2						[92]
cis,*trans*-$Xe(IO_2F_4)_2$	$CFCl_3$	24	−2120.0	79.2 (*trans*-IO_2F_4)					[92]
cis,*trans*-$Xe(IO_2F_4)_2$	$CFCl_3$	24	−2131.3						[92]
cis,*trans*-$Xe(IO_2F_4)_2$	$CFCl_3$	5	−2119.8						[92]
cis,*cis*-$Xe(IO_2F_4)_2$	SO_2ClF	−5	−2105.8						[92]

Table 2 (Continued)

Noble gas species	Solvent	T (°C)	$\delta(^{129}Xe)$[a] (ppm)	$\delta(^{19}F)$[a,b] (ppm)	$\delta(L)$[a] (ppm)	$J(^{129}Xe-^{19}F)$[c] (Hz)	$J(^{129}Xe-L)$[c] (Hz)	$J(^{19}F\text{-}L)$[c] (Hz)	Ref.
cis,*cis*-$Xe(IO_2F_4)_2$[j]	SO_2ClF	−40	−2076.0	104.7 (F_1I)				$^2J/^{19}F_2$ 274	[92]
								$^2J/^{19}F_3$ 238	
				82.4 (F_2I)				$^2J/^{19}F_3$ 190	
				74.0 (F_3I)					
cis,*cis*-$Xe(IO_2F_4)_2$[j]	BrF_5	−40	−2059.5	102.8 (F_1I)				$^2J/^{19}F_2$ 287	[92]
								$^2J/^{19}F_3$ 241	
				81.9 (F_2I)				$^2J/^{19}F_3$ 191	
				73.6 (F_3I)					
cis,*cis*-$Xe(IO_2F_4)_2$	$CFCl_3$	24	−2235.7						[92]
cis,*cis*-$Xe(IO_2F_4)_2$	$CFCl_3$	5	−2219.5						[92]
trans-$FXeIO_2F_4$	SO_2ClF	−5	−1741.2	−168.4 (FXe)		^1J/5913			[92]
				71.8 (IO_2F_4)		^3J/42			
trans-$FXeIO_2F_4$	SO_2ClF	−40	−1701.5	−168.5 (FXe)		^1J/5893			[92]
				71.3 (IO_4F_4)					
trans-$FXeIO_2F_4$	BrF_5	−40	−1702.8	−170.1 (FXe)		^1J/5868			[92]
				75.1 (IO_2F_4)		^3J/37			
trans-$FXeIO_2F_4$	$CFCl_3$	24	−1853.6	−164.8 (FXe)		^1J/5880			[92]
				79.9 (IO_2F_4)		^3J/43			
trans-$FXeIO_2F_4$	BrF_5	0	−1720.5			^1J/5910			[92]
cis-$FXeIO_2F_4$	SO_2ClF	−5	−1865.0	−158.7 (FXe)		^1J/5870			[92]
cis-$FXeIO_2F_4$[j]	SO_2ClF	−40	−1824.4	−158.5 (FXe)		^1J/5851			[92]
				103.3 (F_1I)				$^2J/F_2$ 284	
								$^2J/F_3$ 240	
				86.6 (F_2I)				$^2J/F_3$ 191	
				70.3 (F_3I)					
cis-$FXeIO_2F_4$[j]	BrF_5	−40	−1798.2	−161.7 (FXe)		^1J/5814			[92]
				101.5 (F_1I)		^3J/41		$^2J/F_2$ 280	
								$^2J/F_3$ 234	
				85.8 (F_2I)				$^2J/F_3$ 193	
				70.4 (F_3I)					
cis-$FXeIO_2F_4$	$CFCl_3$	24	−1962.0	−156.3 (FXe)		^1J/5849			[92]
cis-$FXeIO_2F_4$	BrF_5	0	−1823.5			^1J/5803			[92]

Table 2 (Continued)

Noble gas species	Solvent	T (°C)	$\delta(^{129}Xe)^a$ (ppm)	$\delta(^{19}F)^{a,b}$ (ppm)	$\delta(L)^a$ (ppm)	$J(^{129}Xe-^{19}F)^c$ (Hz)	$J(^{129}Xe-L)^c$ (Hz)	$J(^{19}F\text{-}L)^c$ (Hz)	Ref.
trans-$IO_2F_4XeOTeF_5$	$CFCl_3$	24	−2217.5						[92]
trans-$IO_2F_4XeOTeF_5$	$CFCl_3$	5	−2205.3						[92]
cis-$IO_2F_4XeOTeF_5$	$CFCl_3$	24	−2315.7						[92]
cis-$IO_2F_4XeOTeF_5$	$CFCl_3$	5	−2298.7						[92]
trans-$IO_2F_4XeSO_3F$	SO_2ClF	−5	−1834.2						[92]
cis-$IO_2F_4XeSO_3F$	SO_2ClF	−5	−1956.4						[92]
$C_5F_5NXeF^+$	BrF_5	−30	−1922.5	−139.6 (FXe) −88.0 (F_o) −153.9 (F_m) −110.1 (F_p)		^1J/5926		$^4J/^{19}F_o$ 25.3	[82]
$C_5F_5NXeF^+$	HF	−30	−1871.9	−148.3 (FXe) −89.7 (F_o) −158.0 (F_m) −115.4 (F_p)	^{14}N −208	^1J/5936	$^1J/^{14}N$ 236	$^4J/^{19}F_o$ 24.6 $^4J/^{19}F'_o$ 21.2 $^3J/^{19}F_m$ 17.6 $^3J/^{19}F'_m$ 14.4 $^4J/^{19}F'_m$ 2.0 $^4J/^{19}F_p$ 19.5	[82]
s-$C_3F_3N_2NXeF^+$	BrF_5	−50	−1862.4	−145.6 (FXe) −26.2 (F_o) −8.7 (F_p)		^1J/5932		$^4J/^{19}F_o$ 10.9 $^4J/^{19}F_p$ 13.3	[83]
s-$C_3F_3N_2NXeF^+$	HF	−5	−1807.9	−154.9 (FXe) −27.7 (F_o) −13.5 (F_p)		^1J/5909	$^1J/^{14}N$ 245		[83]
4-$CF_3C_5F_4NXeF^+$	BrF_5	−50	−1853.4	−144.6 (FXe) −86.8 (F_o) −132.6 (F_m) −59.7 (CF_3)		^1J/5963		$^4J/^{19}F_o$ 25.8 $^4J/^{19}F'_o$ 19.9 $^3J/^{19}F_m$ 12.5 $^3J/^{19}F'_m$ 19.3 $^4J/^{19}F'_m$ 2.7 $^4J/^{19}F_{CF_3}$ 20.4	[82]

Table 2 (Continued)

Noble gas species	Solvent	T (°C)	$\delta(^{129}Xe)^{a}$ (ppm)	$\delta(^{19}F)^{a,b}$ (ppm)	$\delta(L)^{a}$ (ppm)	$J(^{129}Xe-^{19}F)^{c}$ (Hz)	$J(^{129}Xe-L)^{c}$ (Hz)	$J(^{19}F\text{-}L)^{c}$ (Hz)	Ref.
$4\text{-}CF_3C_5F_4NXeF^+$	HF	−15	−1802.6	−153.8 (FXe) −88.7 (F_o) −136.2 (F_m) −60.9 (CF_3)		^1J/5977	$^1J/^{14}N$ 238	$^4J/^{19}F_o$ 25.8	[82]
$C_2H_5CNXeF^{+k}$	HF	−10	−1717	−184.6	^{14}N −251.9 ^1H 1.29 ^1H 2.80	^1J/6017	$^1J/^{14}N$ 311		[81]
CH_3CNXeF^{+l}	HF	−10	−1708	−185.5	^{14}N −251.1 ^{13}C 115.3 (CN) ^{13}C 0.6 (CH_3) ^1H 2.41	^1J/6020	$^1J/^{14}N$ 313 $^2J/^{13}C$ 79	$^2J/^{14}N$ 18 $^3J/^{13}C$ 19	[81]
XeF_2	$CFCl_3$	26	−2009			^1J/5579			[69]
XeF_2	SO_2ClF	26	−1913			^1J/5621			[69]
XeF_2	SO_2ClF	25	−1905			^1J/5630			[55]
XeF_2	BrF_5	25	−1750			^1J/5616			[55]
XeF_2	BrF_5	−40	−1708			^1J/5583			[55]
XeF_2	HF	25	−1592			^1J/5652			[55]
XeF_2	HF	−68		−199.6		^1J/5665			[16,43]
XeF_2	BrF_5	26		−181.8		^1J/5645			[43]
XeF_2	BrF_5	−20		−181.8		^1J/5650			[43]
$F_3S{\equiv}NXeF^+$	BrF_5	−60	−1661	−180.5 (FXe) 53.3 (F_3S)		^1J/6248		$^4J/^{19}F$ 15	[8,87]
$F_3S{\equiv}NXeF^+$	HF	−20	−1653	−185.5 (FXe) 51.2 (F_3S)		^1J/6251	$^1J/^{14}N$ 347		[87]
$CH_2ClCNXeF^+$	HF	−10 to −30	−1583	−195.5	^{14}N −236.6	^1J/6147	$^1J/^{14}N$ 331		[8]
$CH_2FCH_2CNXeF^+$	HF	−10 to −30	−1662	−182.8 (FXe) −218.8 (CH_2F)		^1J/6063	$^1J/^{14}N$ 322		[8]
$C_3H_7CNXeF^+$	HF	−10 to −30	−1718	−189.1	^{14}N −249.7	^1J/6020	$^1J/^{14}N$ 309		[8]
$CH_2FC_2H_4CNXeF^+$	HF	−10 to −30	−1663	−187.7 (FXe) −222.7 (CH_2F)		^1J/6065	$^1J/^{14}N$ 321		[8]
$CH_3CHFCH_2CNXeF^+$	HF	−10 to −30	−1700	−186.1 (FXe) −172.1 (CHF)	^{14}N −257.8	^1J/6038	$^1J/^{14}N$ 315		[8]

Table 2 (Continued)

Noble gas species	Solvent	T (°C)	$\delta(^{129}Xe)^{a}$ (ppm)	$\delta(^{19}F)^{a,b}$ (ppm)	$\delta(L)^{a}$ (ppm)	$J(^{129}Xe-^{19}F)^{c}$ (Hz)	$J(^{129}Xe-L)^{c}$ (Hz)	$J(^{19}F\text{-}L)^{c}$ (Hz)	Ref.
$C_4H_9CNXeF^+$	HF	−10 to −30	−1720	−183.2	^{14}N −247.1	^{1}J/6022	$^{1}J/^{14}N$ 309		[8]
$CH_2FC_3H_7CNXeF^+$	HF	−10 to −30	−1703	−184.6 (FXe)		^{1}J/6027	$^{1}J/^{14}N$ 311		[8]
$CH_3CHFC_2H_4CNXeF^+$	HF	−10 to −30	ca. −1705	−185.1 (FXe) −175.9 (CHF)		^{1}J/6015			[8]
$(CH_3)_2CHCNXeF^+$	HF	−10 to −30	−1721	−184.5	^{14}N −251.4	^{1}J/6016	$^{1}J/^{14}N$ 309		[8]
$(CH_3)_3CCNXeF^+$	HF	−10 to −30	−1721	−184.3	^{14}N −251.4	^{1}J/6024	$^{1}J/^{14}N$ 309		[8]
$CH_2Cl(CH_3)CHCNXeF^+$	HF	−10 to −30	−1703	−198.7		^{1}J/6027	$^{1}J/^{14}N$ 314		[8]
$CH_2F(CH_3)CHCNXeF^+$	HF	−10 to −30	−1669	−187.9 (FXe) −235.3 (CH_2F)	^{14}N 243.8	^{1}J/6027	$^{1}J/^{14}N$ 301		[8]
$HCNXeF^{+m}$	BrF_5	−50	−1570	−193.1	^{15}N 230.2 ^{1}H 6.01	^{1}J/6176	$^{1}J/^{15}N$ 483 $^{3}J/^{1}H$ 26.8	$^{2}J/^{15}N$ 23.9 $^{4}J/^{1}H$ 2.7	[84]
$HCNXeF^{+n}$	HF	−10	−1552	−198.7	^{14}N −235.1 ^{15}N −234.5 ^{13}C 104.1 ^{1}H 4.70	^{1}J/6161	$^{1}J/^{14}N$ 332 $^{1}J/^{15}N$ 471 $^{2}J/^{13}C$ 84 $^{3}J/^{1}H$ 24.7	$^{2}J/^{15}N$ 23.9 $^{3}J/^{13}C$ 18 $^{4}J/^{1}H$ 2.6	[84]
$CH_2FCNXeF^+$	HF	−10	−1541	−198.4 (FXe) −241.7 (CH_2F)	^{14}N −229.2 ^{1}H 5.44	^{1}J/6163	$^{1}J/^{14}N$ 333	$^{2}J/^{1}H$ 44	[81]
$C_6H_5CNXeF^+$	HF	−10	−1426			^{1}J/6610			[81]
CF_3CNXeF^+	BrF_5	−63	−1337.1	−210.4 (FXe) −54.8 (CF_3)		^{1}J/6397			[83]
$C_2F_5CNXeF^+$	BrF_5	−63	−1293.7	−212.9 (FXe) −83.9 (CF_3) −109.3 (CF_2)		^{1}J/6437			[83]
n-$C_3F_7CNXeF^+$	BrF_5	−63	−1294.2	−213.2 (FXe) −81.9 (CF_3) −106.6 (CF_2) −125.2 (CF_2CN)		^{1}J/6430			[83]
$CF_3C(OXeF)NH_2$	BrF_5	−53	−1578			^{1}J/5991			[85]
$CF_3C(OXeF)NH_2$	BrF_5	−54		−183.1 (FXe) 74.4 (CF_3)		^{1}J/6012			[85]

Table 2 (Continued)

Noble gas species	Solvent	T (°C)	$\delta(^{129}Xe)^a$ (ppm)	$\delta(^{19}F)^{a,b}$ (ppm)	$\delta(L)^a$ (ppm)	$J(^{129}Xe-^{19}F)^c$ (Hz)	$J(^{129}Xe-L)^c$ (Hz)	$J(^{19}F\text{-}L)^c$ (Hz)	Ref.
$CF_3C(OXeF)NH_2$	BrF_5	−59.4			^{13}C −165.7 (CO) ^{13}C −113.7 (CF_3)			$^2J/^{13}C$ 42 $^1J/^{13}C$ 285	[85]
$CF_3C(OXeF)NH_2$	BrF_5	−55			^1H 7.88 ^1H 7.71				[85]
$XeOSeF_5^+$	BrF_5	−56	−1438	62.4 (F_{ax}) 73.3 (F_{eq})					[87]
$XeOTeF_5^+$	SbF_5	5	−1481.9						[74]
$XeOTeF_5^+$	SbF_5	25	−1472	−54.6 (F_{ax}) −41.0 (F_{eq})	^{125}Te −134.9	^3J/18.5		$^1J/^{125}Te$ 3802 $^1J/^{125}Te$ 3814 $^2J/^{19}F$ 172.2	[67]
$XeOTeF_5^+$	HSO_3F	−80		−49.6 (F_{ax}) −42.5 (F_{eq})				$^1J/^{125}Te$ 3658 $^1J/^{125}Te$ 3766 $^2J/^{19}F$ 176.7	[67]
$XeOTeF_5^+$ (AsF_5)	HSO_3F	−78		−51.5 (F_{ax}) −42.9 (F_{eq})				$^1J/^{125}Te$ 3684 $^1J/^{125}Te$ 3777 $^2J/^{19}F$ 171.0	[67]
$XeOTeF_5^+$ (AsF_5)	HSO_3F	3	−1608						[67]
$XeOTeF_5^+$ (AsF_5)	HSO_3F	−94.6	−1521						[67]
$Xe(SO_3F)_2$	HSO_3F	−84	−1613						[55]
$Xe(SO_3F)_2$	HSO_3F	−90	−1572						[55]
$Xe(SO_3F)_2$	HSO_3F	−80		42.6					[16]
$FXeSO_3F$	SO_2ClF	−5	−1725	−170.9 (FXe)		^1J/5837			[92]
$FXeSO_3F$	HSO_3F	−100	−1407			^1J/6051			[62]
$FXeSO_3F$	HSO_3F	−90	−1416			^1J/6021			[62]
$FXeSO_3F$	HSO_3F	−90	−1416			^1J/6012			[55]
$FXeSO_3F$	HSO_3F	−84	−1467			^1J/5975			[55]
$FXeSO_3F$	HSO_3F	−90		−196.9 (FXe) 40.2 (SO_3F)		^1J/5942			[62]

Table 2 (Continued)

Noble gas species	Solvent	T (°C)	$\delta(^{129}Xe)^{a}$ (ppm)	$\delta(^{19}F)^{a,b}$ (ppm)	$\delta(L)^{a}$ (ppm)	$J(^{129}Xe-^{19}F)^{c}$ (Hz)	$J(^{129}Xe-L)^{c}$ (Hz)	$J(^{19}F\text{-}L)^{c}$ (Hz)	Ref.
$FXeSO_3F$	HSO_3F	−97		−194.5 (FXe) 40.1 (SO_3F)		^{1}J/5924			[62]
$FXeSO_3F$	BrF_5	−40	−1666			^{1}J/5830			[55]
$FXeSO_3F$	BrF_5	−77	−1613			^{1}J/5848			[55]
$FXeSO_3F$	HSO_3F	−80		−193.3 (FXe) 40.2 (SO_3F)		^{1}J/6025			[16]
$FXeSO_3F$	Melt	40		−172.1 (FXe) 42.1 (SO_3F)		^{1}J/5835			[16]
$FXeSO_3F$	HF	−68		−196.9 (FXe) 37 0 (SO_3F)		^{1}J/6025			[16]
$(FXe)_2SO_3F^+$	BrF_5	−77	−1258			^{1}J/6428			[55]
$(FXe)_2SO_3F^+$	HSO_3F	−91		−220.7 (FXe) 44.6 (SO_3F)		^{1}J/6330			[23]
$(FXe)_2SO_3F^+$	BrF_5	−59		−221.9 (FXe) 44.4 (SO_3F)		^{1}J/6470			[23]
$FXeSO_3FMoOF_4$	HSO_3F	−100	−1342			^{1}J/5971			[62]
$FXeSO_3FMoOF_4$	HSO_3F	−97		−201.6 (FXe) 146.8 (FMo)		^{1}J/5853			[62]
$FXeSO_3FWOF_4$	HSO_3F	−90	−1335			^{1}J/6131			[62]
$FXeSO_3FWOF_4$	HSO_3F	−90		−204.3 (FXe) 67.8 (FW)		^{1}J/5992			[62]
$FXeFBrOF_2^+$	BrF_5	−59	−1359	−163.9 (FXe) 193.9 (FBr)		^{1}J/5680			[67]
$FXeFMoOF_4$[e]	BrF_5	−84		−223.1 (F_tXe) −170.0 (XeF_b) 141.8 (F_1Mo)		^{1}J/6140 ^{1}J/5117		$^{2}J/^{19}F_b$ 264 $^{2}J/^{19}F_1$ 50	[62]
$FXeFMoOF_4$	BrF_5	−80	−1381			^{1}J/6139 ^{1}J/5117			[62]
$FXeFMoOF_4$[e]	SO_2ClF	−124		−219.6 (F_tXe)		^{1}J/6018		$^{4}J/^{19}F_b$ 267 $^{4}J/^{19}F_1$ 8	[62]
				−166.6 (XeF_b) 147.7 (F_1Mo)		^{1}J/5110		$^{2}J/^{19}F_1$ 47	

Table 2 (Continued)

Noble gas species	Solvent	T (°C)	$\delta(^{129}Xe)$[a] (ppm)	$\delta(^{19}F)$[a,b] (ppm)	$\delta(L)$[a] (ppm)	$J(^{129}Xe-^{19}F)$[c] (Hz)	$J(^{129}Xe-L)$[c] (Hz)	$J(^{19}F\text{-}L)$[c] (Hz)	Ref.
$FXeFMoOF_4$	SO_2ClF	−118	−1441			^1J/6058 ^1J/5076			[62]
$FXeF(MoOF_4)_2$[e]	SO_2ClF	−124		−229.1 (F_tXe)		^1J/5197		$^4J/^{19}F_1$ 8 $^4J/^{19}F_1'$ 8	[62]
				−167.1 (XeF_b)		^1J/5110		$^2J/^{19}F_1$ 46 $^2J/^{19}F_b'$ 50	
				195.1 (F_1Mo_1)				$^2J/^{19}F_1'$ 102 $^2J/^{19}F_b'$ 100	
				207.9 (F_1' Mo_1) −37.7 ($Mo_1F_b'Mo_2$) 150.1 (F_2Mo_2)				$^2J/^{19}F_b'$ 100 $^2J/^{19}F_2$ 47	
$FXeF(MoOF_4)_2$	SO_2ClF	−118	−1338			^1J/6159 ^1J/5036			[62]
$FXeF(MoOF_4)_3$[e]	SO_2ClF	−124		−230.4 (F_tXe) −167 (XeF_b)		^1J/6210 ^1J/5110		$^2J/^{19}F_b$ 266 $^2J/^{19}F_1$ 50 $^2J/^{19}F_1'$ 50 $^2J/^{19}F_b'$ 50	[62]
				−28.9 ($Mo_1F_b'Mo_2$) −62.8 ($Mo_2F_b''Mo_3$) 150 (F_3Mo_3)				$^2J/^{19}F_3$ 47	
$FXeF(MoOF_4)_3$	SO_2ClF	−118	−1321			^1J/6156 ^1J/5029			[62]
$FXeF(MoOF_4)_4$[e]	SO_2ClF	−124		−230.8 (F_tXe) −167 (XeF_b) −29 ($Mo_1F_b'Mo_2$) −55.2 ($Mo_2F_b''Mo_3$) −64.9 ($Mo_3F_b''Mo_4$) 150 (F_4Mo_4)		^1J/6200 ^1J/5000		$^2J/^{19}F_b$ 258 $^2J/^{19}F_4$ 48	[62]

Table 2 (Continued)

Noble gas species	Solvent	T (°C)	$\delta(^{129}Xe)^a$ (ppm)	$\delta(^{19}F)^{a,b}$ (ppm)	$\delta(L)^a$ (ppm)	$J(^{129}Xe-^{19}F)^c$ (Hz)	$J(^{129}Xe-L)^c$ (Hz)	$J(^{19}F\text{-}L)^c$ (Hz)	Ref.
$FXeFWOF_4$[e]	BrF_5	−62		−228.9 (F_tXe) −168.8 (XeF_b) 135.8 (F_1W)		^1J/6150 ^1J/5016		$^2J/^{19}F_b$ 275 $^2J/^{19}F_1$ 50	[62]
$FXeFWOF_4$	BrF_5	−66	−1331			^1J/6196 ^1J/5051			[62]
$FXeFWOF_4$[e]	SO_2ClF	−121		−225.7 (F_tXe) −166.8 (XeF_b) 69.7 (F_1W)		^1J/6150 ^1J/5000		$^2J/^{19}F_b$ 266 $^2J/^{19}F_1$ 55	[62]
$FXeFWOF_4$	SO_2ClF	−115	−1315			^1J/6127 ^1J/5000			[62]
$FXeF(WOF_4)_2$[e]	SO_2ClF	−121		−236.7 (F_tXe) −168.4 (XeF_b) 119 (F_1W_1) 121 (F'_1W_1) −107.8 ($W_1F'_bW_2$) 73.2 (F_2W_2)		^1J/6260 ^1J/5000		$^2J/^{19}F_b$ 267 $^2J/^{19}F_1$ 60 $^2J/^{19}F'_1$ 60 $^2J/^{19}F'_b$ 60 $^2J/^{19}F'_b$ 60 $^2J/^{19}F'_b$ 60 $^2J/^{19}F_2$ 60	[62]
$FXeF(WOF_4)_2$	SO_2ClF	−115	−1189			^1J/6268 ^1J/4964			[62]
$FXeF(WOF_4)_3$[e]	SO_2ClF	−121		−238.7 (F_tXe) −169 (XeF_b) 73 (F_3)		^1J/6300 ^1J/5000		$^2J/^{19}F_b$ 265 $^2J/^{19}F'_b$ 60	[62] [62]
$FXeF(WOF_4)_3$	SO_2ClF	−115	−1170			^1J/6304 ^1J/4996			
$FXeFXe'OTeF_5$	BrF_5	−60	−1146 (Xe) −1633 (Xe′)	−50.9 (TeF_{ax}) −43.4 (TeF_{eq})		^1J/5747			[67]
$FXeFXeF^+$	BrF_5	−57	−1051			^1J/6740 (F_t) ^1J/4865 (F_b)			[55]
$FXeFXeF^+$	BrF_5	−60	−1059			^1J/6662 (F_t) ^1J/4828(F_b)			[69]

Table 2 (Continued)

Noble gas species	Solvent	T (°C)	$\delta(^{129}Xe)$[a] (ppm)	$\delta(^{19}F)$[a,b] (ppm)	$\delta(L)$[a] (ppm)	$J(^{129}Xe-^{19}F)$[c] (Hz)	$J(^{129}Xe-L)$[c] (Hz)	$J(^{19}F-L)$[c] (Hz)	Ref.
$FXeFXeF^+$	BrF_5	−62		−252.0 (F_t) −184.7 (F_b)		^1J/6740 (F_t) ^1J/4865 (F_b)		$^2J/^{19}F$ 308	[16,43]
$FXeOWF_4WOF_4$[e]	SO_2ClF	−121		−240.2 (F_tXe) 97.1 (F_1W_1) −72.0 ($W_1F_b'W_2$) 73 (F_2W_2)		^1J/6315		$^2J/^{19}F_b'$ 64 $^2J/^{19}F_2$ 61	[62]
$FXeOWF_4WOF_4$	SO_2ClF	−115	−955			^1J/6373			[62]
$FXeO(WOF_4)_3$[e]	SO_2ClF	−121		−243.8 (F_tXe) 96.8 (F_1W_1) −72 ($W_1F_b'W_2$) −119.3 ($W_2F_b'W_3$) 72 (F_3W_3)		^1J/6330		$^2J/^{19}F_b'$ 65 $^2J/^{19}F_2$ 60 $^2J/^{19}F_2'$ 60 $^2J/^{19}F_3$ 60	[62]
$FXeO(WOF_4)_3$	SO_2ClF	−115	−906			^1J/6373			[62]
XeF^+	SbF_5	26	−574			^1J/7210			[69]
XeF^+	SbF_5	25	−574			^1J/7594			[55]
XeF^+	SbF_5	26		−289.8		^1J/7210			[16,43]
XeF^+	SbF_5	26		−291.5		^1J/7260			[33]
XeF^+	SbF_5	5		−294.5		^1J/7295			[33]
XeF^+	SbF_5	5		−289.5		^1J/7215			[33]
XeF^+ (AsF_6^-)	HSO_3F	−18	−991			^1J/6350			[67]
XeF^+ (AsF_6^-)	HSO_3F	−96		−243.5		^1J/6615			[16]
XeF^+ (SbF_6^-)	HSO_3F	−93		−242.5		^1J/6620			[16]
Xe(IV)									
XeF_5^-	CH_3CN	24	−527.0	38.1		^1J/3400			[95]
$Xe(OTeF_5)_4$	$CFCl_3$	24	−646.5			$^3J/F_{eq}$ 66	$^2J/^{125}Te$ 1008		[73]
$Xe(OTeF_5)_4$	$CFCl_3$	24	−662.8			$^3J/F_{eq}$ 63	$^2J/^{125}Te$ 988		[69]
$Xe(OTeF_5)_4$	$C_4F_9SO_2F$		−637[i]			$^3J/F_{eq}$ 67.7	$^2J/^{125}Te$ 1107		[93]

Table 2 (Continued)

Noble gas species	Solvent	T (°C)	$\delta(^{129}Xe)^{a}$ (ppm)	$\delta(^{19}F)^{a,b}$ (ppm)	$\delta(L)^{a}$ (ppm)	$J(^{129}Xe-^{19}F)^{c}$ (Hz)	$J(^{129}Xe-L)^{c}$ (Hz)	$J(^{19}F\text{-}L)^{c}$ (Hz)	Ref.
$Xe(OTeF_5)_4$	$C_4F_9SO_2F$			47.2 (F_{ax})				$^{2}J/^{19}F_{eq}$ 188	[93]
				39.4 (F_{eq})		$^{3}J/F_{eq}$ 59			
$Xe(OTeF_5)_3^{+}$	SbF_5	5	−341.9						[74]
$FXe(OTeF_5)_3$	$CFCl_3$	24	−436.5	16.36 (FXe)		^{1}J/3506	$^{2}J/^{125}$Te 1032		[73]
						$^{3}J/F_{eq}$ 66	$^{2}J/^{125}$Te 1293		
$FXe(OTeF_5)_2^{+}$	SbF_5	5	−174.4	49.3 (FXe)		^{1}J/2900			[74]
Cis-$F_2Xe(OTeF_5)_2$	$CFCl_3$	24	−242.6	−8.58 (F_2Xe)		^{1}J/3714	$^{2}J/^{125}$Te 1059		[73]
						$^{3}J/F_{eq}$ 69			
Trans-$F_2Xe(OTeF_5)_2$	$CFCl_3$	24	−215.9	10.95 (F_2Xe)		^{1}J/3503	$^{2}J/^{125}$Te 1166		[73]
						$^{3}J/F_{eq}$ 69			
$F'F_2XeOTeF_5$	$CFCl_3$	24	−25.5	5.87 (F)		^{1}J/3552	$^{2}J/^{125}$Te 1192	$^{2}J/^{19}F'$ 355	[73]
				−11.98 (F′)		^{1}J/3733			
						$^{3}J/F_{eq}$ 71			
$F_2XeOTeF_5^{+}$	SbF_5	5	22.4	26.8 (F_2Xe)		^{1}J/2893			[75]
XeF_4	$CFCl_3$	24	202.9	−15.66		^{1}J/3817			[73]
XeF_4	$CFCl_3$	24	166.1			^{1}J/3801			[69]
XeF_4	BrF_5	25	253			^{1}J/3823			[55]
XeF_4	CH_3CN	−42	335.3	−20.1		^{1}J/3913			[120]
XeF_4	CH_3CN	24	316.9	−18.7		^{1}J/3895			[95]
$XeOF_2$	CH_3CN	−42	283.5	−45.2		^{1}J/3554			[120]
$XeOF_2$	CH_3CN	−45	240.1	−48.6	^{17}O 209	^{1}J/3448			[120]
$OXeF(OTeF_5)$	CH_3CN	−42	533.6	−27.2 (FXe)		^{1}J/3374	$^{2}J/^{125}$Te 1221		[120]
						$^{3}J/F_{eq}$ 38			
$OXe(OTeF_5)_2$	CH_3CN	−42	583.3			$^{3}J/F_{eq}$ 30	$^{2}J/^{125}$Te 968		[120]
XeF_3^{+}	SbF_5	25	595			$^{1}J/F_{ax}$ 2609			[55]
						$^{1}J/F_{eq}$ 2384			
XeF_3^{+}	SbF_5	26		38.7 (F_{ax})		^{1}J/2620		$^{2}J/^{19}F_{eq}$ 174	[33]
				23.0 (F_{eq})		^{1}J/2440			
Xe(VI)									
XeF_7^{-o}	CH_3CN	−40	−169.3			^{1}J/2724			[124]
$XeOF_5^{-}$	CH_3CN	30	−357 9	118.9	^{17}O 270.8		$^{1}J/^{17}O$ 566		[96]

Table 2 (Continued)

Noble gas species	Solvent	T (°C)	$\delta(^{129}Xe)^{a}$ (ppm)	$\delta(^{19}F)^{a,b}$ (ppm)	$\delta(L)^{a}$ (ppm)	$J(^{129}Xe-^{19}F)^{c}$ (Hz)	$J(^{129}Xe-L)^{c}$ (Hz)	$J(^{19}F\text{-}L)^{c}$ (Hz)	Ref.
$OXe(OTeF_5)_4$	$CFCl_3$	24	−204.1			$^3J/F_{eq}$ 52	$^2J/^{125}Te$ 1351		[73]
$OXe(OTeF_5)_4$	$CFCl_3$	24	−211.8			$^3J/F_{eq}$ 54	$^2J/^{125}Te$ 1304		[69]
$OXeF(OTeF_5)_3$	$CFCl_3$	24	−157.0	111.27		^1J/1206 $^3J/F_{eq}$ 52			[73]
Trans-$OXeF_2(OTeF_5)_2$	$CFCl_3$	24	−106.4	108.24		^1J/984 $^3J/F_{eq}$ 53	$^2J/^{125}Te$ 1535		[73]
cis-$OXeF_2(OTeF_5)_2$	$CFCl_3$	24	−117.8	112.59		^1J/1074 $^3J/F_{eq}$ 51	$^2J/^{125}Te$ 1536		[73]
$OXeF'F_2(OTeF_5)$	$CFCl_3$	24	−66.3	106.78 (F′) 103.00 (F)		^1J/1148 ^1J/931 $^3J/F_{eq}$ 53	$^2J/^{125}Te$ 1364		[73]
$OXe(OTeF_5)_3^+$	SO_2ClF	−78	−1.9				$^2J/^{125}Te$ 1245		[74]
$OXeF(OTeF_5)_2^+$	SbF_5	5	60.6	129.2 (FXe)		^1J/1089			[74]
$OXeF_2(OTeF_5)^+$	SbF_5	5	121.3	136.9 (F_2Xe) −60.5 (TeF_{ax}) −21.2 (TeF_{eq})		^1J/796			[74]
$(XeF_6)_4$	SO_2ClF/CF_2Cl_2	−145	−60.8			^1J/331.7			[55]
$(XeF_6)_4$	SO_2ClF/CF_3Cl	−140		109.3		^1J/325			[58]
$(XeF_6)_4$	$O(SF_5)_2$	25	−35						[56]
$(XeF_6)_4$	$O(SF_5)_2$	−118	−39			^1J/330			[56]
XeF_5^+	SbF_5	35		231.7 (F_{ax}) 108.8 (F_{eq})		^1J/1512 ^1J/143.1		$^2J/^{19}F$ 175.5	[17]
XeF_5^+	HF	25	12.7			^1J/1400 ^1J/159			[55]
XeF_5^+ (xs SbF_5)	HF	26		226.2 (F_{ax}) 108.5 (F_{eq})		^1J/1381 ^1J/158.8		$^2J/^{19}F$ 176.0	[17]
XeF_5^+ (xs SbF_5)	HF	−40		229.1 (F_{ax}) 108.1 (F_{eq})		^1J/1380 ^1J/180.7		$^2J/^{19}F$ 180.4	[17]
XeF_5^+ (SbF_6^-)	HF	26		233.2 (F_{ax}) 109.6 (F_{eq})		^1J/1409 ^1J/156.1		$^2J/^{19}F$ 177.1	[17]

Table 2 (Continued)

Noble gas species	Solvent	T (°C)	$\delta(^{129}Xe)^a$ (ppm)	$\delta(^{19}F)^{a,b}$ (ppm)	$\delta(L)^a$ (ppm)	$J(^{129}Xe-^{19}F)^c$ (Hz)	$J(^{129}Xe-L)^c$ (Hz)	$J(^{19}F\text{-}L)^c$ (Hz)	Ref.
XeF_5^+	HF	−10		231.5 (F_{ax})		^1J/1409		$^2J/^{19}F$ 178.8	[17]
(AsF_6^-)				108.5 (F_{eq})		^1J/176.0			
XeF_5^+	HF	−80		228.2 (F_{ax})		^1J/1348		$^2J/^{19}F$ 182.0	[17]
(BF_4^-)				106.2 (F_{eq})		^1J/182.8			
XeF_5^+	BrF_5	26		231.7 (F_{ax})		^1J/1512		$^2J/^{19}F$ 175.7	[17]
($Sb_2F_{11}^-$)				108.8 (F_{eq})		^1J/143.1			
XeF_5^+	HSO_3F	−80	−23.9			^1J/1377			[55]
						^1J/165			
XeF_5^+	HSO_3F	−80		225.4 (F_{ax})		^1J/1425		$^2J/^{19}F$ 183.0	[17]
(xs SbF_5)				108.2 (F_{eq})		^1J/193.8			
XeF_5^+	HSO_3F	−90		226.2 (F_{ax})		^1J/1357		$^2J/^{19}F$ 178.5	[17]
				108.2 (F_{eq})		^1J/175.0			
XeF_5^+	HSO_3F	−81		228.3 (F_{ax})		^1J/1389		$^2J/^{19}F$ 178.5	[17]
				108.9 (F_{eq})		^1J/179.6			
$OXeF_4$	$CFCl_3$	24	−29.9	101.59		^1J/1131			[73]
$OXeF_4$	HF	−50	23.7			^1J/1146			[73]
$OXeF_4$	HF	24			^{17}O 316.3		$^1J/^{17}O$ 704		[73]
$OXeF_4$	HF				^{17}O 313		$^1J/^{17}O$ 692		[125]
$OXeF_4$[p]	Neat	24	0	100.3		^1J/1128			[69,103]
$OXeF_4$	SO_2ClF/ CF_2Cl_2	−145	−0.1			^1J/1127			[55]
$XeOF_4{\cdot}CH_3CN$	CH_3CN	30		92.5		^1J/1570			[96]
$XeOF_4{\cdot}CH_3CN$	CH_3CN	−40	164.7	93.3		^1J/1540			[103]
$XeOF_3^+$	SbF_5	25	238			^1J/1018			[55]
						^1J/434			
$XeOF_3^+$	SbF_5	5	242.8	189.6 (F_{eq})		^1J/1021		$^2J/^{19}F$ 88	[74]
				143.9 (F_{ax})		^1J/496			
$XeOF_3^+$	SbF_5	5		195.1 (F_{eq})		$^1J/F_{eq}$ 983		$^2J/^{19}F$ 103	[33]
				147.1 (F_{ax})		$^1J/F_{ax}$ 434			
$XeOF_3^+$	HF	30	200.8		^{17}O 333.7		$^1J/^{17}O$ 619		[38]

Table 2 (Continued)

Noble gas species	Solvent	T (°C)	$\delta(^{129}Xe)^{a}$ (ppm)	$\delta(^{19}F)^{a,b}$ (ppm)	$\delta(L)^{a}$ (ppm)	$J(^{129}Xe-^{19}F)^{c}$ (Hz)	$J(^{129}Xe-L)^{c}$ (Hz)	$J(^{19}F\text{-}L)^{c}$ (Hz)	Ref.
$XeOF_3^+$	SbF_5	30	237.4		^{17}O 342	$^{1}J/F_{eq}$ 1012 $^{1}J/F_{ax}$ 464			[38]
$O_2Xe(OTeF_5)_2$	SO_2ClF	−74	131.0			$^{3}J/F_{eq}$ 34	$^{2}J/^{125}Te$ 1684		[73]
$O_2XeF(OTeF_5)$	SO_2ClF	−74	154 1			^{1}J/1046 $^{3}J/F_{eq}$ 37	$^{2}J/^{125}Te$ 1856		[73]
$O_2XeOTeF_5^+$	SbF_5	5	543.0						[74]
XeO_2F_2	HF	−50	171.0	105.1		^{1}J/1213			[73,103]
XeO_2F_2	HF	25	173.2			^{1}J/1217			[55]
XeO_2F_2	HF	24			^{17}O 302.5		$^{1}J/^{17}O$ 521		[73]
$XeO_2F_2{\cdot}CH_3CN$	CH_3CN	−40	263.0	86.5		^{1}J/1425			[103]
XeO_2F^+	SbF_5	25	600			^{1}J/95			[55]
XeO_2F^+	SbF_5	5		199.4		^{1}J/80			[33]
XeO_2F^+	SbF_5	5	704.3	195.7		^{1}J/95			[74]
XeO_3	H_2O	25	217.0						[56,103]
$XeO_3{\cdot}CH_3CN$	CH_3CN	−40	218.1						[103]
Xe(VIII)									
XeO_6^{4-}	H_2O	30	−748[q]						[99]
XeO_6^{4-}	Solid Na_4XeO_6	25	*ca.* −720[q]						[99]
XeO_3F_2	HF	−75	−412.9	223.9		^{1}J/1015			[99]
XeO_3F_2	SO_2ClF	−80	−414.5	229.5		^{1}J/991			[99]
XeO_3F_2	BrF_5	−50	−413.5			^{1}J/994			[99]
XeO_4	HF	−75	−85.8						[99]
XeO_4	SO_2ClF	−80	−92.9						[99]

Table 2 (Continued)

Noble gas species	Solvent	T (°C)	$\delta(^{129}Xe)$[a] (ppm)	$\delta(^{19}F)$[a,b] (ppm)	$\delta(L)$[a] (ppm)	$J(^{129}Xe-^{19}F)$[c] (Hz)	$J(^{129}Xe-L)$[c] (Hz)	$J(^{19}F\text{-}L)$[c] (Hz)	Ref.
XeO_4	BrF_5	−50	−94.7						[99]
$XeO_4 \cdot CH_3CN$	CH_3CN	−40	224.9						[99]

[a] Samples were referenced externally at 30°C with respect to the neat liquid references; $XeOF_4$ (^{129}Xe), $(CH_3)_2Te$ (^{125}Te), $CFCl_3$ (^{19}F), H_2O (^{17}O), CH_3NO_2 (^{15}N and ^{14}N), and $(CH_3)_4Si$ (^{13}C and ^{1}H). A positive chemical shift denotes a resonance occurring to high frequency of the reference compound.

[b] F_t, F_b, F_o, F_m, and F_p denote terminal and bridging fluorines and fluorines in the *ortho*, *meta*, and *para* positions, respectively.

[c] Only the magnitude of the coupling constant is given.

[d] $^1J(^{13}C–^{15}N) = 312$ Hz, $^2J(^{15}N–^1H) = 12.2$ Hz.

[e] The numerical subscript, x, of the metal atom, M (M = Mo, W), and the fluorines, F_x, attached to MX in the compounds $FNgF(MOF_4)_n$ (Ng = Kr, Xe; $x = 1$ to n) increases with distance from the noble gas atom. In the case of M_1, where the fluorines *cis* to the oxygen atom are non-equivalent, these atoms are denoted F_1, and F'_1, and are *cis* and *trans* to the Ng–F_b–M_1 fluorine bridge, respectively.

[f] $^1J(^{15}N–^1H) = 62$ Hz.

[g] $^1J(^{15}N–^1H) = 62$ Hz.

[h] The two axial fluorines on sulfur and the xenon atom in $XeN{=}SF_4^+$ are *anti* and *syn* to each other and are denoted F_{ax} and F'_{ax}, respectively.

[i] The ^{129}Xe chemical shift was originally referenced to a sample of Xe in *n*-C_6F_{14}, $\delta(^{129}Xe) = -5331$ ppm.

[j] In *cis*-$OIOF_4$, F_1, F_2, and F_3 denote the fluorine *trans* to the Xe–O–I bridge, the fluorine *trans* to the doubly bonded oxygen, and the two fluorines *cis* to the doubly bonded oxygen and the bridging oxygen, respectively.

[k] $^3J(^1H–^1H) = 7.5$ Hz.

[l] $^1J(^{13}C–^1H) = 141$ Hz.

[m] $^2J(^{15}N–^1H) = 13.0$ Hz.

[n] $^1J(^{14}N–^{13}C) = 22$ Hz, $^1J(^{13}C–^1H) = 308$ Hz.

[o] Fluxionality on the NMR timeseale averages the fluorine environments.

[p] The absolute frequency of neat $XeOF_4$ at 24°C is given as 27.810184 MHz, quoted relative to a ^1H frequency of exactly 100 MHz for neat $(CH_3)_4Si$ at 24°C.

[q] The previously reported ^{129}Xe chemical shift for Na_4XeO_6 (2077 ppm) [55] is erroneous.

$XeO_3 \cdot CH_3CN$, $XeO_2F_2 \cdot CH_3CN$, and $XeOF_4 \cdot CH_3CN$ having the isotopic composition, 35.4% ^{16}O, 21.9% ^{17}O, and 42.7% ^{18}O [103].

All ^{19}F and ^{129}Xe chemical shifts of the various isotopomers of these molecules exhibit strict proportionality to the mass factor, $(m' - m)/m'$. The magnitude of the secondary isotopic shift decreases with the increasing oxygen content in the xenon oxide fluorides, which is paralleled by a decrease in $^1J(^{129}Xe-^{17}O)$ on going from $XeOF_4$ to XeO_2F_2.

Acknowledgements

The authors thank the Canada Council for a Killam Research Fellowship (G.J.S.) and the Natural Sciences and Engineering Research Council of Canada for past and continuing support of this work in the form of research and equipment grants.

Appendix A

All multi-NMR spectroscopic data cited in this review are summarized in the comprehensive table included.

References

[1] N. Bartlett, Proc. Chem. Soc. (1962) 218.
[2] R.J. Gillespie, in: H.H. Hyman (Ed.), Noble-Gas Compounds, University of Chicago Press, Chicago, 1963, pp. 333–339.
[3] G.J. Schrobilgen, in: R.K. Harris, B.E. Mann (Eds.), NMR and the Periodic Table, Academic Press, London, 1978, pp. 439–454.
[4] C.J. Jameson, in: J. Mason (Ed.), Multinuclear NMR, Plenum Press, London, 1987, pp. 463–477.
[5] G.J Schrobilgen, in: D.M. Grant, R.K. Harris (Eds.), The Encyclopedia of Nuclear Magnetic Resonance, Wiley, New York, 1996, pp. 3251–3262.
[6] C.I. Ratcliffe, Annu. Rep. NMR Spectrosc. 36 (1998) 123.
[7] S. Braun, H.-O. Kalinowski, S. Berger, NMR-Spektroskopie von Nichtmetallen: ^{19}F-NMR-Spektroskopie, vol. 4, Thieme, Stuttgart, 1994.
[8] G.J. Schrobilgen, in: G.A. Olah, G.K.S. Prakash, R.D. Chambers (Eds.), Synthetic Fluorine Chemisty, Wiley, New York, 1992, pp. 1–30.
[9] J.C. Hindman, A. Svirmickas, in: H.H. Hyman (Ed.), Noble-Gas Compounds, University of Chicago Press, Chicago, 1963, pp. 251–262.
[10] T.H. Brown, E.B. Whipple, P.H. Verdier, in: H.H. Hyman (Ed.), Noble-Gas Compounds, University of Chicago Press, Chicago, 1963, pp. 263–269.
[11] T.H. Brown, E.B. Whipple, P.H. Verdier, J. Chem. Phys. 38 (1963) 3029.
[12] B. Cohen, R.D. Peacock, J. Inorg. Nucl. Chem. 28 (1966) 3056.
[13] A.J. Edwards, J.H. Holloway, R.D. Peacock, Proc. Chem. Soc. (1963) 275.
[14] V.M. McRae, R.D. Peacock, D.R. Russel, J. Chem. Soc. Chem. Commun. (1969) 62.
[15] H.D. Frame, Chem. Phys. Lett. 3 (1969) 182.
[16] R.J. Gillespie, A. Netzer, G.J. Schrobilgen, Inorg. Chem. 13 (1974) 1455.
[17] R.J. Gillespie, G.J. Schrobilgen, Inorg. Chem. 13 (1974) 765.

[18] R.J. Gillespie, I. Hargittai, The VSEPR Model of Molecular Geometry, Allyn and Bacon, Needham Heights, MA, 1991.
[19] N. Bartlett, M. Wechsberg, F.O. Sladky, P.A. Bulliner, G.R. Jones, R.D. Burbank, J. Chem. Soc. Chem. Commun. (1969) 703.
[20] N. Bartlett, M. Wechsberg, G.R. Jones, R.D. Burbank, Inorg. Chem. 11 (1972) 1124.
[21] F.O. Sladky, P.A. Bulliner, N. Bartlett, B.G. DeBoer, A. Zalkin, J. Chem. Soc. Chem. Commun. (1968) 1048.
[22] N. Bartlett, B.G. DeBoer, F.J. Hollander, F.O. Sladky, D.H. Templeton, A. Zalkin, Inorg. Chem. 13 (1974) 780.
[23] R.J. Gillespie, G.J. Schrobilgen, Inorg. Chem. 13 (1974) 1694.
[24] M. Wechsberg, P.A. Bulliner, F.O. Sladky, R. Mews, N. Bartlett, Inorg. Chem. 11 (1972) 3063.
[25] R.J. Gillespie, G.J. Schrobilgen, D.R. Slim, J. Chem. Soc. Dalton Trans. (1977) 1003.
[26] N. Bartlett, F. Einstein, D.F. Stewart, J. Trotter, J. Chem. Soc. Chem. Commun. (1966) 550.
[27] N. Bartlett, F. Einstein, D.F. Stewart, J. Trotter, J. Chem. Soc. A (1967) 1190.
[28] N. Bartlett, M. Gennis, D.D. Gibler, B.K. Morrell, A. Zalkin, Inorg. Chem. 12 (1973) 1717.
[29] K. Leary, D.H. Templeton, A. Zalkin, N. Bartlett, Inorg. Chem. 12 (1973) 1726.
[30] R.J. Gillespie, G.J. Schrobilgen, Inorg. Chem. 13 (1974) 765.
[31] D.D. DesMarteau, M. Eisenberg, Inorg. Chem. 11 (1972) 2641.
[32] R.J. Gillespie, B. Landa, G.J. Schrobilgen, J. Chem. Soc. Chem. Commun. (1971) 1543.
[33] R.J. Gillespie, G.J. Schrobilgen, Inorg. Chem. 13 (1974) 2370.
[34] P. Boldrini, R.J. Gillespie, P.R. Ireland, G.J. Schrobligen, Inorg. Chem. 13 (1974) 1690.
[35] D.E. McKee, C.J. Adams, A. Zalkin, N. Bartlett, J. Chem. Soc. Chem. Commun. (1973) 26.
[36] D.E. McKee, A. Zalkin, N. Bartlett, Inorg. Chem. 12 (1973) 1713.
[37] R.J. Gillespie, B. Landa, G.J. Schrobilgen, J. Chem. Soc. Chem. Commun. (1972) 607.
[38] H.P.A. Mercier, J.C.P. Sanders, G.J. Schrobilgen, S.S. Tsai, Inorg. Chem. 32 (1993) 386.
[39] N. Bartlett, F. Sladky Jr., in: J.C. Bailar Jr., H.J. Emeléus, R. Nyholm, A.F. Trotman-Dickenson (Eds.), Comprehensive Inorganic Chemistry, vol. 1, Pergamon, Oxford, 1973, p. 245.
[40] A.G. Sharpe, in: V. Gutmann (Ed.), Halogen Chemistry, vol. 1, Academic Press, New York, 1967, p. 3.
[41] F. Schreiner, J.G. Malm, J.C. Hindman, J. Am. Chem. Soc. 87 (1965) 25.
[42] R.J. Gillespie, G.J. Schrobilgen, J. Chem. Soc. Chem. Commun. (1974) 90.
[43] R.J. Gillespie, G.J. Schrobilgen, Inorg. Chem. 15 (1976) 22.
[44] F.Q. Roberto, Inorg. Nucl. Chem. Lett. 8 (1972) 737.
[45] K.O. Christe, Inorg. Nucl. Chem. Lett. 8 (1972) 741.
[46] K.O. Christe, Inorg. Chem. 12 (1973) 1580.
[47] K.O. Christe, W. Sawodny, Inorg. Chem. 6 (1967) 1783.
[48] R.J. Gillespie, G.J. Schrobilgen, Inorg. Chem. 13 (1974) 1230.
[49] E.H. Appelman, Inorg. Synth. 13 (1972) 1.
[50] E.H. Appelman, M.H. Studier, J. Am. Chem. Soc. 91 (1969) 4561.
[51] K.O. Christe, D.A. Dixon, J. Am. Chem. Soc. 114 (1992) 2978.
[52] D.E. McKee, C.J. Adams, A. Zalkin, N. Bartlett, J. Chem. Soc. Chem. Commun. (1973) 26
[53] J.H. Holloway, G.J. Schrobilgen, J. Chem. Soc. Chem. Commun. (1975) 623.
[54] J.H. Holloway, G.J. Schrobilgen, P. Granger, C. Brevard, C.R. Acad. Sci. Paris 282 (1976) 519.
[55] G.J. Schrobilgen, J.H. Holloway, P. Granger, C. Brevard, Inorg. Chem. 17 (1978) 980.
[56] K. Seppelt, H.H. Rupp, Z. Anorg. Allg. Chem. 409 (1974) 331.
[57] K. Seppelt, H.H. Rupp, Z. Anorg. Allg. Chem. 409 (1974) 338.
[58] K. Seppelt, N. Bartlett, Z. Anorg. Allg. Chem. 436 (1977) 122.
[59] A. Zalkin, D.L. Ward, R.N. Biagione, D.H. Templeton, N. Bartlett, Inorg. Chem. 17 (1978) 1318.
[60] B. Frlec, J.H. Holloway, J. Chem. Soc. Dalton Trans. (1975) 535.
[61] J.H. Holloway, G.J. Schrobilgen, P. Taylor, J. Chem. Soc. Chem. Commun. (1975) 40.
[62] J.H. Holloway, G.J. Schrobilgen, Inorg. Chem. 19 (1980) 2632.
[63] P.A. Tucker, P.A. Taylor, J.H. Holloway, D.R. Russell, Acta Crystallogr. B 31 (1975) 906.
[64] J.H. Holloway, G.J. Schrobilgen, Inorg. Chem. 20 (1981) 3363.
[65] J.C.P. Sanders, G.J. Schrobilgen, J. Chem. Soc. Chem. Commun. (1989) 1576.

[66] F. Sladky, Monatsh. Chem. 101 (1970) 1578.
[67] N. Keller, G.J. Schrobilgen, Inorg. Chem. 20 (1981) 2118.
[68] D. Lentz, K. Seppelt, Angew. Chem. 90 (1978) 390; Angew. Chem. Int. Ed. Engl. 17 (1978) 355.
[69] T. Birchall, R.D. Myers, H. de Waard, G.J. Schrobilgen, Inorg. Chem. 21 (1982) 1068.
[70] A.L. Allred, J. Inorg. Nucl. Chem. 17 (1961) 215.
[71] B.P. Dailey, J.N. Shoolery, J. Am. Chem. Soc. 77 (1955) 3977.
[72] F. Sladky, H. Kropshofer, Inorg. Nucl. Chem. Lett. 8 (1972) 195.
[73] G.A. Schumacher, G.J. Schrobilgen, Inorg. Chem. 23 (1984) 2923.
[74] R.G. Syvret, K.M. Mitchell, J.C.P. Sanders, G.J. Schrobilgen, Inorg. Chem. 31 (1992) 3381.
[75] R.D. LeBlond, D.D. DesMarteau, J. Chem. Soc. Chem. Commun. (1974) 555.
[76] J.F. Sawyer, G.J. Schrobilgen, S.J. Sutherland, J. Chem. Soc. Chem. Commun. (1982) 210.
[77] J.F. Sawyer, G.J. Schrobilgen, S.J. Sutherland, Inorg. Chem. 21 (1982) 4064.
[78] D.D. DesMarteau, J. Am. Chem. Soc. 100 (1978) 6270.
[79] G.A. Schumacher, G.J. Schrobilgen, Inorg. Chem. 22 (1983) 2178.
[80] R. Faggiani, D.K. Kennepohl, C.J.L. Lock, G.J. Schrobilgen, Inorg. Chem. 25 (1986) 563.
[81] A.A.A. Emara, G.J. Schrobilgen, J. Chem. Soc. Chem. Commun. (1987) 1644.
[82] A.A.A. Emara, G.J. Schrobilgen, J. Chem. Soc. Chem. Commun. (1988) 257.
[83] G.J. Schrobilgen, J. Chem. Soc. Chem. Commun. (1988) 1506.
[84] A.A.A. Emara, G.J. Schrobilgen, Inorg. Chem. 31 (1992) 1323.
[85] G.J. Schrobilgen, J.M. Whalen, Inorg. Chem. 33 (1994) 5207.
[86] G.J. Schrobilgen, Final Technical Report No. PL-TR-93-3007, Aug. 1993, Contract F04611-91-K-0004, Phillips Laboratory, Propulsion Directorate, USAF Systems Command, Edwards Air Force Base, CA, vol. 1, part III, pp. 1–87.
[87] G.J. Schrobilgen, Final Technical Report No. PL-TR-91-3108, Feb. 1992, Contract F49620-87-C-0049, Phillips Laboratory, Propulsion Directorate, USAF Systems Command, Edwards Air Force Base, CA, vol. 2, part V, pp. 22–103.
[88] G.J. Schrobilgen, J. Chem. Soc. Chem. Commun. (1988) 862.
[89] J.P. Jokisaari, L.P. Ingman, G.J. Schrobilgen, J.C.P. Sanders, Magn. Res. Chem. 32 (1994) 242.
[90] D.D. DesMarteau, R.D. LeBlond, S.F. Hossain, D. Nothe, J. Am. Chem. Soc. 103 (1981) 7734.
[91] R.G. Syvret, G.J. Schrobilgen, J. Chem. Soc. Chem. Commun. (1985) 1529.
[92] R.G. Syvret, G.J. Schrobilgen, Inorg. Chem. 28 (1989) 1564.
[93] E. Jacob, D. Lentz, K. Seppelt, A. Simon, Z. Anorg. Allg. Chem. 472 (1981) 7.
[94] K.O. Christe, W.W. Wilson, R.D. Wilson, R. Bau, J. Feng, J. Am. Chem. Soc. 112 (1990) 7619.
[95] K.O. Christe, E.C. Curtis, D.A. Dixon, H.P.A. Mercier, J.C.P. Sanders, G.J. Schrobilgen, J. Am. Chem. Soc. 113 (1991) 3351.
[96] K.O. Christe, D.A. Dixon, J.C.P. Sanders, G.J. Schrobilgen, S.S. Tsai, W.W. Wilson, Inorg. Chem. 34 (1995) 1868.
[97] J.H. Holloway, V. Kaučič, D. Martin-Rovet, D.R. Russell, G.J. Schrobilgen, H. Selig, Inorg. Chem. 24 (1985) 678.
[98] A. Ellern, K. Seppelt, Angew. Chem. 107 (1995) 1772; Angew. Chem. Int. Ed. Engl. 34 (1995) 1586.
[99] M. Gerken, G.J. Schrobilgen, unpublished results.
[100] B. Jaselskis, T.M. Spittler, J.L. Huston, J. Am. Chem. Soc. 88 (1966) 2149.
[101] E.H. Appelman, Inorg. Synth. 11 (1968) 210.
[102] J.L. Huston, M.H. Studier, E.N. Sloth, Science 143 (1964) 1161.
[103] Ref. [86], part IA, pp. 4–11.
[104] C.J. Jameson, H.S. Gutowsky, J. Chem. Phys. 40 (1964) 1714.
[105] (a) N.F. Ramsey, Phys. Rev. 77 (1950) 567. (b) N.F. Ramsey, Phys. Rev. 78 (1950) 699. (c) N.F. Ramsey, Phys. Rev. 83 (1951) 540. (d) N.F. Ramsey, Phys. Rev. 86 (1952) 243.
[106] C.J. Jameson, H.S. Gutowsky, J. Chem. Phys. 40 (1964) 2285.
[107] N. Bartlett, F. Sladky Jr., in: J.C. Bailar Jr., H.J. Emeléus, R. Nyholm, A.F. Trotman-Dickenson (Eds.), Comprehensive Inorganic Chemistry, vol. 1, Pergamon, Oxford, 1973, pp. 223–228.
[108] A. Saika, C.P. Slichter, J. Chem. Phys. 22 (1954) 26.
[109] M. Karplus, T.P. Das, J. Chem. Phys. 34 (1961) 1683.

[110] L.G. Alexakos, C.D. Cornwell, J. Chem. Phys. 41 (1964) 2098.
[111] K.O. Christe, J.F. Hon, D. Philipovich, Inorg. Chem. 12 (1973) 84.
[112] C.D. Cornwell, J. Chem. Phys. 44 (1966) 874.
[113] K.O. Christe, D.A. Dixon, A.R. Mahjoub, H.P.A. Mercier, J.C.P. Sanders, K. Seppelt, G.J. Schrobilgen, W.W. Wilson, J. Am. Chem. Soc. 115 (1993) 2696.
[114] P. Pyykkö, L. Wiesenfeld, Mol. Phys. 43 (1981) 557.
[115] J.A. Pople, D.P. Santry, Mol. Phys. 8 (1964) 1.
[116] G.A. Webb, in: R.K. Harris, B.E. Mann (Eds.), NMR and the Periodic Table, Academic Press, London, 1978, pp. 49–86.
[117] R.C. Burns, L.A. Devereux, P. Granger, G.J. Schrobilgen, Inorg. Chem. 24 (1985) 2615.
[118] J. Feeney, R. Haque, L.W. Reeves, C.P. Yue, Can. J. Chem. 46 (1968) 1389.
[119] C.J. Jameson, J. Mason, in: J. Mason (Ed.), Multinuclear NMR, Plenum Press, London, 1987, pp. 51–88.
[120] Ref. [86], part IV, pp. 1–11.
[121] H.-J. Frohn, A. Klose, T. Schroer, G. Henkel, V. Buss, D. Opitz, R. Vahrenhorst, Inorg. Chem. 37 (1998) 4884.
[122] G.J. Schrobilgen, Final Technical Report No. PL-TR-93-3007, Feb. 1993, Contract F04611-91-K-0004, Phillips Laboratory, Propulsion Directorate, USAF Systems Command, Edwards Air Force Base, CA, vol. 2, part VII, pp. 1–67.
[123] Ref. [87], vol. 1, part I, pp. 7–51.
[124] J.C.P. Sanders, G.J. Schrobilgen, unpublished results.
[125] J. Shamir, H. Selig, D. Samuel, J. Reuben, J. Am. Chem. Soc. 87 (1965) 2359.